INDUCED RESPONSE OF VEHICLE DURING ANTI—SKID BRAKING

by

C. Vinay Kumar Singh

DEPARTMENT OF AEROSPACE ENGINEERING

INDIAN INSTITUTE OF TECHNOLOGY KANPUR

AUGUST, 1991

INDUCED RESPONSE OF VEHICLE DURING ANTI–SKID BRAKING

A Thesis Submitted

in Partial Fulfillment of the Requirements

for the Degree of

Master of Technology

by

C. Vinay Kumar Singh

to the

DEPARTMENT OF AEROSPACE ENGINEERING

INDIAN INSTITUTE OF TECHNOLOGY KANPUR

AUGUST 1991

CERTIFICATE

It is certified that the work contained in this thesis entitled *"Induced Response of Vehicle during Anti-skid Breaking"*, by *"C. Vinay Kumar Singh"*, has been carried out under my supervision and that this work has not been submitted elsewhere for a degree.

Dayanand Yadav

Dayanand Yadav
Assistant Professor
Department of Aerospace Engineering
Indian Institute of Technology
Kanpur

August 1991

TO

DR. DAYANAND YADAV

AND

DR. RAM KISHORE SINGH RATHORE

Abstract

Skidding is one of the most dangerous instabilities which a vehicle might encounter while braking. This phenomenon becomes all the more critical in adverse conditions like flooded roads, roads covered with sheet ice etc. The importance of anti-skid landing gear is also highlighted by the stringent operational requirements of the defence forces.

In the present work a simple anti-skid system has been presented. The equations are for a general case of the vehicle problem but the numerical solution has been carried out for a single wheel heave-degrees-of-freedom vehicle model on a linear spring and linear damper shock absorber. The dynamics of the vehicle during anti-skid braking have been presented.

The anti-skid system has been implemented by taking into consideration the stochastic properties of the road. The braking force is predicted one step ahead in time with the help of an auto-regressive or an all poles filter. The road is modelled as the combination of a deterministic variable mean process and a random zero mean process. The road is modelled in the space domain, and transformed into the time-domain with the help of an integral space-time equation. The road is simulated in terms of the sum of cosine functions with random frequencies and random phase angles.

Acknowledgements

To acknowledge the help and affection of all the people known to me would perhaps be impossible, nor would it be in any way a measure of my gratitude for them. However as a duty it is sacred.

I am rightly indebted to my guide Dr. Yadav, who stood by me in the most trying of situations and guided me ever upwards. But for his sheer perseverance and kind attentions, neither me nor this thesis would be in this present state.

Among the many close friends, Jatinder and Rinky will always be special, for having always boosted my morale from unimaginable depths to unbelievable heights. Chojar, Narendra, Onkar, Rajji, Siddhu, Subir, Sudhir, Sujay, Umesh, and the inimitable Prabhu will always haunt my fondest thoughts for having provided many moments of blissful companionship, even in the most depressing of conditions. Shreesh and Prakash, my partners on endless nights in front of the boob-tube and on night-long hacks, are and will always be special friends.

Dr. R. K. S. Rathore, a special person, will always be revered and maintained in high esteem.

C . V . K . Singh

Contents

Abstract iv

Acknowledgements v

List of Tables ix

List of Figures x

1 Introduction and Literature Survey 1

1.1 Introduction 1

1.2 Dynamics of Braking 2

1.2.1 The Limitation on Maximum Braking Force 2

1.2.2 Variation of Maximum Friction Force with Time 3

1.2.3 Variation of Frictional Coefficient 3

1.3 The Control Problem 4

1.4 Literature Survey 5

1.4.1 Input Models 5

1.4.2 Vehicle Models and Solution Schemes 7

1.5 Present Work 10

1.5.1 Mathematical Models Used 11

2 Models Chosen **14**

2.1 The Vehicle Model 14

2.1.1 Forces on The Vehicle 15

2.2 The Input Process 15

2.2.1 The Deterministic Variable Mean Process 16

2.2.2 The Random Zero Mean Process 16

3 Equations of Motion **18**

3.1 The Generalised Equation of Motion 18

3.2 Solution for The Equation of Motion 19

3.3 Present Model 21

3.4 Forces on The Model 22

3.4.1 Lift Force on The Aircraft 22

3.4.2 Drag Force on The Aircraft 22

3.4.3 Reaction of The Ground 23

3.4.4 Braking Force Applied on The Aircraft 23

3.5 Domain of The Equations of Motion 24

3.5.1 Equations for Tyre Bottoming 24

3.5.2 Equations for Shock Absorber Locking 25

3.5.3 Equation for Aircraft Ballooning 25

3.6 Space–Time Realationship 26

3.7 Skid–Time Relationship 26

4 The Track Profile Generation and Prediction **27**

4.1 Generation of The Track Profile 27

4.1.1 Generation of The Uniform Deviate 29

4.2 Prediction of The Track Profile 29

4.2.1 Optimisation of The Prediction Coefficients 30

5 Presentation of Results 32
5.1 The Model Parameters 32
5.2 Track Parameters 32
5.3 Presentation of Results and Discussion 35
5.3.1 Ground Reaction 37
5.3.2 Friction Force 37
5.3.3 Sprung Mass Displacement 38
5.3.4 Sprung Mass Velocity 39
5.3.5 Sprung Mass Acceleration 39
5.3.6 Unsprung Mass Displacement 39
5.3.7 Unsprung Mass Acceleration 40
5.3.8 Braking Torque and Skid 40
5.3.9 Ground Velocity 41
5.3.10 Braking Distance 41

6 Conclusions and Scope for Future Work 107
6.1 Conclusions 107
6.2 Scope for Future Work 108

References 110

List of Tables

5.1 Model Parameters 33

5.2 List of trial runs 35

5.3 Output for Landing Run on a Flat Runway,
aircraft glide velocity = 75.56 $\frac{m}{s}$ aircraft sink velocity = 1.0 $\frac{m}{s}$ 36

List of Figures

1.1 Variation of friction coefficient μ with tyre skid 4

1.2 The vehicle model 12

5.1 Predicted and actual ground reaction for flat runway ,
glide velocity = 75.56 $\frac{m}{s}$, sink velocity = 1.0 $\frac{m}{s}$ 43

5.2 Predicted and actual ground reaction for flat runway ,
glide velocity = 75.56 $\frac{m}{s}$, sink velocity = 2.0 $\frac{m}{s}$ 44

5.3 Predicted and actual ground reaction for flat runway ,
glide velocity = 75.56 $\frac{m}{s}$, sink velocity = 3.0 $\frac{m}{s}$ 45

5.4 Predicted and actual ground reaction for flat runway ,
glide velocity = 76.32 $\frac{m}{s}$, sink velocity = 1.0 $\frac{m}{s}$ 46

5.5 Predicted and actual ground reaction for flat runway ,
glide velocity = 77.00 $\frac{m}{s}$, sink velocity = 1.0 $\frac{m}{s}$ 47

5.6 Predicted and actual ground reaction for inclined runway ,
glide velocity = 75.56 $\frac{m}{s}$, sink velocity = 1.0 $\frac{m}{s}$ 48

5.7 Predicted and actual ground reaction for sinusoidal runway ,
glide velocity = 75.56 $\frac{m}{s}$, sink velocity = 1.0 $\frac{m}{s}$ 49

5.8 Predicted and actual ground reaction for stepped runway ,
glide velocity = 75.56 $\frac{m}{s}$, sink velocity = 1.0 $\frac{m}{s}$ 50

5.9 Predicted and actual retarding friction for flat runway ,
glide velocity = 75.56 $\frac{m}{s}$, sink velocity = 1.0 $\frac{m}{s}$ 51

5.10 Predicted and actual retarding friction for flat runway ,
glide velocity = 75.56 $\frac{m}{s}$, sink velocity = 2.0 $\frac{m}{s}$ 52
5.11 Predicted and actual retarding friction for flat runway ,
glide velocity = 75.56 $\frac{m}{s}$, sink velocity = 3.0 $\frac{m}{s}$ 53
5.12 Predicted and actual retarding friction for flat runway ,
glide velocity = 76.32 $\frac{m}{s}$, sink velocity = 1.0 $\frac{m}{s}$ 54
5.13 Predicted and actual retarding friction for flat runway ,
glide velocity = 77.00 $\frac{m}{s}$, sink velocity = 1.0 $\frac{m}{s}$ 55
5.14 Predicted and actual retarding friction for inclined runway ,
glide velocity = 75.56 $\frac{m}{s}$, sink velocity = 1.0 $\frac{m}{s}$ 56
5.15 Predicted and actual retarding friction for sinusoidal runway ,
glide velocity = 75.56 $\frac{m}{s}$, sink velocity = 1.0 $\frac{m}{s}$ 57
5.16 Predicted and actual retarding friction for stepped runway ,
glide velocity = 75.56 $\frac{m}{s}$, sink velocity = 1.0 $\frac{m}{s}$ 58
5.17 Sprung mass displacement for flat runway ,
glide velocity = 75.56 $\frac{m}{s}$, sink velocity = 1.0 $\frac{m}{s}$ 59
5.18 Sprung mass displacement for flat runway ,
glide velocity = 75.56 $\frac{m}{s}$, sink velocity = 2.0 $\frac{m}{s}$ 60
5.19 Sprung mass displacement for flat runway ,
glide velocity = 75.56 $\frac{m}{s}$, sink velocity = 3.0 $\frac{m}{s}$ 61
5.20 Sprung mass displacement for flat runway ,
glide velocity = 76.32 $\frac{m}{s}$, sink velocity = 1.0 $\frac{m}{s}$ 62
5.21 Sprung mass displacement for flat runway ,
glide velocity = 77.00 $\frac{m}{s}$, sink velocity = 1.0 $\frac{m}{s}$ 63
5.22 Sprung mass displacement for inclined runway ,
glide velocity = 75.56 $\frac{m}{s}$, sink velocity = 1.0 $\frac{m}{s}$ 64

5.23 Sprung mass displacement for sinusoidal runway ,
glide velocity = 75.56 $\frac{m}{s}$, sink velocity = 1.0 $\frac{m}{s}$ 65
5.24 Sprung mass displacement for stepped runway ,
glide velocity = 75.56 $\frac{m}{s}$, sink velocity = 1.0 $\frac{m}{s}$ 66
5.25 Sprung mass velocity for flat runway ,
glide velocity = 75.56 $\frac{m}{s}$, sink velocity = 1.0 $\frac{m}{s}$ 67
5.26 Sprung mass velocity for flat runway ,
glide velocity = 75.56 $\frac{m}{s}$, sink velocity = 2.0 $\frac{m}{s}$ 68
5.27 Sprung mass velocity for flat runway ,
glide velocity = 75.56 $\frac{m}{s}$, sink velocity = 3.0 $\frac{m}{s}$ 69
5.28 Sprung mass velocity for flat runway ,
glide velocity = 76.32 $\frac{m}{s}$, sink velocity = 1.0 $\frac{m}{s}$ 70
5.29 Sprung mass velocity for flat runway ,
glide velocity = 77.00 $\frac{m}{s}$, sink velocity = 1.0 $\frac{m}{s}$ 71
5.30 Sprung mass velocity for inclined runway ,
glide velocity = 75.56 $\frac{m}{s}$, sink velocity = 1.0 $\frac{m}{s}$ 72
5.31 Sprung mass velocity for sinusoidal runway ,
glide velocity = 75.56 $\frac{m}{s}$, sink velocity = 1.0 $\frac{m}{s}$ 73
5.32 Sprung mass velocity for stepped runway ,
glide velocity = 75.56 $\frac{m}{s}$, sink velocity = 1.0 $\frac{m}{s}$ 74
5.33 Sprung mass acceleration for flat runway ,
glide velocity = 75.56 $\frac{m}{s}$, sink velocity = 1.0 $\frac{m}{s}$ 75
5.34 Sprung mass acceleration for flat runway ,
glide velocity = 75.56 $\frac{m}{s}$, sink velocity = 2.0 $\frac{m}{s}$ 76
5.35 Sprung mass acceleration for flat runway ,
glide velocity = 75.56 $\frac{m}{s}$, sink velocity = 3.0 $\frac{m}{s}$ 77

5.36 Sprung mass acceleration for flat runway ,
glide velocity = 76.32 $\frac{m}{s}$, sink velocity = 1.0 $\frac{m}{s}$ 78
5.37 Sprung mass acceleration for flat runway ,
glide velocity = 77.00 $\frac{m}{s}$, sink velocity = 1.0 $\frac{m}{s}$ 79
5.38 Sprung mass acceleration for inclined runway ,
glide velocity = 75.56 $\frac{m}{s}$, sink velocity = 1.0 $\frac{m}{s}$ 80
5.39 Sprung mass acceleration for sinusoidal runway ,
glide velocity = 75.56 $\frac{m}{s}$, sink velocity = 1.0 $\frac{m}{s}$ 81
5.40 Sprung mass acceleration for stepped runway ,
glide velocity = 75.56 $\frac{m}{s}$, sink velocity = 1.0 $\frac{m}{s}$ 82
5.41 Unsprung mass displacement for flat runway ,
glide velocity = 75.56 $\frac{m}{s}$, sink velocity = 1.0 $\frac{m}{s}$ 83
5.42 Unsprung mass displacement for flat runway ,
glide velocity = 75.56 $\frac{m}{s}$, sink velocity = 2.0 $\frac{m}{s}$ 84
5.43 Unsprung mass displacement for flat runway ,
glide velocity = 75.56 $\frac{m}{s}$, sink velocity = 3.0 $\frac{m}{s}$ 85
5.44 Unsprung mass displacement for flat runway ,
glide velocity = 76.32 $\frac{m}{s}$, sink velocity = 1.0 $\frac{m}{s}$ 86
5.45 Unsprung mass displacement for flat runway ,
glide velocity = 77.00 $\frac{m}{s}$, sink velocity = 1.0 $\frac{m}{s}$ 87
5.46 Unsprung mass displacement for inclined runway ,
glide velocity = 75.56 $\frac{m}{s}$, sink velocity = 1.0 $\frac{m}{s}$ 88
5.47 Unsprung mass displacement for sinusoidal runway ,
glide velocity = 75.56 $\frac{m}{s}$, sink velocity = 1.0 $\frac{m}{s}$ 89
5.48 Unsprung mass displacement for stepped runway ,
glide velocity = 75.56 $\frac{m}{s}$, sink velocity = 1.0 $\frac{m}{s}$ 90

5.49 Unsprung mass acceleration for flat runway ,
glide velocity = 75.56 $\frac{m}{s}$, sink velocity = 1.0 $\frac{m}{s}$ 91
5.50 Unsprung mass acceleration for flat runway ,
glide velocity = 75.56 $\frac{m}{s}$, sink velocity = 2.0 $\frac{m}{s}$ 92
5.51 Unsprung mass acceleration for flat runway ,
glide velocity = 75.56 $\frac{m}{s}$, sink velocity = 3.0 $\frac{m}{s}$ 93
5.52 Unsprung mass acceleration for flat runway ,
glide velocity = 76.32 $\frac{m}{s}$, sink velocity = 1.0 $\frac{m}{s}$ 94
5.53 Unsprung mass acceleration for flat runway ,
glide velocity = 77.00 $\frac{m}{s}$, sink velocity = 1.0 $\frac{m}{s}$ 95
5.54 Unsprung mass acceleration for inclined runway ,
glide velocity = 75.56 $\frac{m}{s}$, sink velocity = 1.0 $\frac{m}{s}$ 96
5.55 Unsprung mass acceleration for sinusoidal runway ,
glide velocity = 75.56 $\frac{m}{s}$, sink velocity = 1.0 $\frac{m}{s}$ 97
5.56 Unsprung mass acceleration for stepped runway ,
glide velocity = 75.56 $\frac{m}{s}$, sink velocity = 1.0 $\frac{m}{s}$ 98
5.57 Braking torque and skid for flat runway ,
glide velocity = 75.56 $\frac{m}{s}$, sink velocity = 1.0 $\frac{m}{s}$ 99
5.58 Braking torque and skid for flat runway ,
glide velocity = 75.56 $\frac{m}{s}$, sink velocity = 2.0 $\frac{m}{s}$ 100
5.59 Braking torque and skid for flat runway ,
glide velocity = 75.56 $\frac{m}{s}$, sink velocity = 3.0 $\frac{m}{s}$ 101
5.60 Braking torque and skid for flat runway ,
glide velocity = 76.32 $\frac{m}{s}$, sink velocity = 1.0 $\frac{m}{s}$ 102
5.61 Braking torque and skid for flat runway ,
glide velocity = 77.00 $\frac{m}{s}$, sink velocity = 1.0 $\frac{m}{s}$ 103

5.62 Braking torque and skid for inclined runway ,
glide velocity = 75.56 $\frac{m}{s}$, sink velocity = 1.0 $\frac{m}{s}$ 104
5.63 Braking torque and skid for sinusoidal runway ,
glide velocity = 75.56 $\frac{m}{s}$, sink velocity = 1.0 $\frac{m}{s}$ 105
5.64 Braking torque and skid for stepped runway ,
glide velocity = 75.56 $\frac{m}{s}$, sink velocity = 1.0 $\frac{m}{s}$ 106

Chapter 1

Introduction and Literature Survey

The present work deals with the optimal braking of aircraft landing gears during the landing run. An attempt has been made to achieve some amount of anti-skid behaviour in the braking system by using some basic tenets of control theory and theory of stochastic processes. The salient aspects of this problem, review of the available literature, and the approach adopted in the present study, follow in the subsequent sections of this chapter.

1.1 Introduction

In the modern world, the transportation sector, and therefore, vehicles play a major role in the day-to-day life. The two principal requirements from a transportation system, other than its obvious requirement to carry goods or passengers, are the ability to accelerate/decelerate at will, and the ability to change its direction of motion at will. The acceleration is provided by complex propulsion mechanisms, where as the deceleration is carried out by relatively simplistic mechanisms.

The research on driving mechanisms with its obvious economic implications has been extensive, however, that on the braking mechanisms has languished to some

extent. Though this is true to a certain extent for land vehicles, for aircrafts, the braking mechanisms have indirect economic implications due to their ability to dictate operational requirements pertaining to landing. Stark examples of this are the present day *"jumbo jets"*, which require large and well prepared runway surfaces and are therefore restricted to operating between major airports. It can be easily seen that the present trend of growth in air traffic will lead, in the future, to requirements of larger aircrafts landing on smaller landing strips.

In the case of the military, the requirements from a landing system are much more severe and diverse. The military aircrafts often have to takeoff and land on badly prepared small runways. This necessitates extremely sturdy and specialised landing gears and brakes. On aircraft carriers the landing deck is often slippery due to the shipping of green seas in rough weather, and the runway length quite limited. This necessitates specialised mechanisms to effectively halt the aircraft.

For land vehicles, the design of a braking system is often dictated by stringent safety requirements which require a minimum braking distance and time. However as can be seen in §1.2 the braking distance can not be reduced arbitrarily, as doing so would have implications on the general dynamics of the vehicle and it's safety. The main danger, specially on bad roads like those covered with sheet-ice, snow, water, etc., is skidding.

The above scenario points to the needs of an *"intelligent"* braking gear capable of reducing braking distances drastically on any kind of surface.

1.2 Dynamics of Braking

1.2.1 The Limitation on Maximum Braking Force

In a wheeled vehicle the process of braking involves a change in the dynamics of the moving body which if not checked could proceed into unstable regions.

Any rolling body like a wheel has inherent stability due to the stabilising gyroscopic forces set up due to its motion. These forces tend to oppose the effects of any destabilising moments that may exist due to unbalanced or misaligned forces on the body.

The rolling motion of the free rolling wheel is guaranteed by the frictional force between the wheel and the track. Thus if a braking force greater than the maximum frictional force sustainable by the road is applied on the wheel, it stops rolling and starts skidding on the surface. In the case of total skid the stabilising gyroscopic forces are lost and the destabilising forces come in full play. This leads to a loss of control on the vehicle and may eventually lead to an accident. Further, any corrective measures other than the release of brakes may be to no avail, as they may not be sufficient in magnitude to overcome the destabilising moments on the vehicle.

1.2.2 Variation of Maximum Friction Force with Time

As the vehicle moves over the track the effect of its weight passed on to the track, filtered through the landing gear, varies due to the dynamics of the vehicle. The vehicle oscillations induced by the random unevenness depend on the vehicle suspension characteristics, its forward velocity and the nature of the track profile. The temporal variation in the filtering of the weight through the landing gear naturally results in variation of the reaction force by the track on the wheel, and a corresponding variation in the maximum sustainable friction force. Both these forces are random in nature due to the randomness of the track profile.

1.2.3 Variation of Frictional Coefficient

The frictional coefficient for a rolling tyre and the road is not uniform but varies as in Figure 1.1 [1], with the skid. It has a maxima somewhere between 0.05 and 0.3s

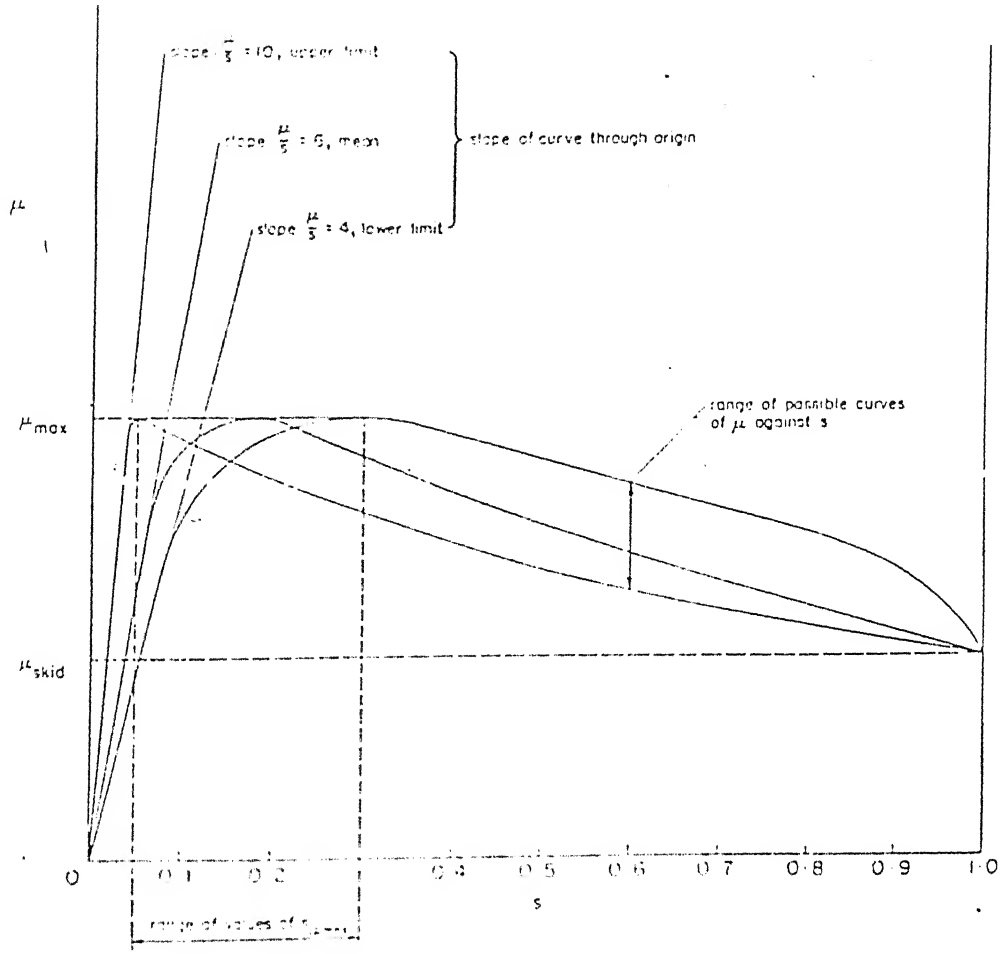

Figure 1.1: Variation of friction coefficient μ with tyre skid

where slip s is defined as [1] :

$$s = 1 - \frac{\omega}{\omega_a} \tag{1.1}$$

where ω is the angular velocity of the wheel and ω_a the free roll angular velocity at that speed. This implies that in order to have better braking characteristics, the vehicle has to continuously vary either the braking force or the vehicle parameters so as to change the filtering characteristics for the better, and maintain itself in the range of optimal skid.

1.3 The Control Problem

The generalised vehicle control problem may be summed up as the modelling of the vehicle, its input disturbances or forces (track parameters, the drag and driving forces)

and its response to these forces. Control on the response is effected by varying either the model parameters or the force parameters, whichever may be controllable. It is also possible to optimise for the model parameters for some suitable optimality criterion. The optimisation (say of the mean square response) can be carried out for a statistical description (spatial or temporal) of the disturbance parameters. This will give an optimised response for a probable range of disturbances the vehicle might encounter in reality. Such optimisations lead to better and more economic designs of the vehicles.

1.4 Literature Survey

As described in §1.3 the control problem of a vehicle deals with 3 major modelling tasks namely

- modelling of the input process,
- modelling of the system, and
- the control mechanism

Extensive work has been done on each of the above, and considerable literature is therefore available, some of which is detailed below. However literature on anti–skid braking was not discovered. Two such systems are commercially available, developed by *Messrs.* Goodyear and Dunlop. This problem has also been studied by various defence establishments. The lack of literature is perhaps due to the strategic nature of this work.

1.4.1 Input Models

The inputs in a vehicle problem are chiefly the track undulations, therefore the modelling of the input is modelling of the track. The track is usually modelled as a

discrete or continuous random process. Initially the track profile was taken directly from observations on roads, runways or rail tracks. Tung *et al.* [32] have measured undulations of runway profiles for their input models. The track can also be completely described by its statistical properties like the auto-correlation and power spectral density (PSD) functions to the second degree. Lindgren [20] cites that the PSD can be given as

$$S_{\tilde{q}}(\omega) = \begin{cases} \frac{S_r \omega_{ref}^2}{\omega^2} & if\ \omega_{min} \leq \omega \leq \omega_{max} \\ 0 & otherwise \end{cases} \tag{1.2}$$

where ω is the temporal frequency, $\omega_{ref} = 2\pi$, ω_{min} and ω_{max} are the cut-off frequencies. He has modelled the track as an auto-regressive process of order 3 given as

$$\tilde{q}(s+h) = a_1\tilde{q}(s) + a_2\tilde{q}(s-2h) + a_3\tilde{q}(s-2h) + \epsilon(s) \tag{1.3}$$

$$S_{\tilde{q}}^h(\omega) = \left(\frac{h\sigma_h^2}{2\pi}\right) \frac{1}{|1 - a_1 e^{-j\omega h} - a_2 e^{-2j\omega h} - a_3 e^{-3j\omega h}|^2} \tag{1.4}$$

Yadav and Nigam [35] have modelled the track profile as a homogeneous process with zero mean and the single sided spatial PSD function

$$\Phi(\Omega) = \begin{cases} \frac{C}{\Omega^2 + \nu^2} & if\ \Omega \leq \Omega_0 \\ 0 & otherwise \end{cases} \tag{1.5}$$

where Ω_0 is the cut-off frequency and ν is the correlation constant. The track was then generated as the output of a cosine filter to white noise. ElMadany [6] has used a single sided temporal PSD given as

$$\phi(\omega) = \begin{cases} \left(\frac{2\alpha v \sigma^2}{\pi}\right) \frac{1}{\omega^2 + \alpha^2 v^2} & if\ \omega \leq \omega_0 \\ 0 & otherwise \end{cases} \tag{1.6}$$

where v is the vehicle forward speed, σ^2 is the variance and α a coefficient depending on the road irregularities. The excitation model was then obtained by a shaping filter to white noise

$$\dot{\lambda}(t) = -\alpha v \lambda(t) + \xi(t) \tag{1.7}$$

Narayanan and Raju [21] have described their track by the auto-correlation function

$$R(\xi) = \sigma^2 e^{-(\alpha|\xi|)} \tag{1.8}$$

where $\xi = s_2 - s_1$, is the spatial lag with $\alpha > 0$. The effect of the rolling contact of the tyre has been considered as an additional filter in cascade [15].

$$h''(s) + (\alpha + \beta)h'(s) + \alpha\beta h(s) = k\omega(s) \tag{1.9}$$

expressed in the time domain this is,

$$h_1' = -(\alpha + \beta)\dot{s}(t)h_1' - \alpha\beta\dot{s}(t)h_1 + \frac{k}{\sigma}\dot{s}(t)\omega\{s(t)\} \tag{1.10}$$

where α is the cut-off wave number of the road profile spectrum, β is the cut-off wave number of the rolling contact filter, $k = \beta\sigma\sqrt{2\alpha}$ is a factor to ensure the desired variance, and $\omega\{s(t)\}$ is a white noise process transformed in time domain. Freymann [10] in his experimental investigation has described the runway as a series of bumps and has devised a bump factor

$$M_\Delta = \sqrt{1 + E_\Delta^2 + 2E_\Delta C_\Delta} \tag{1.11}$$

where $E_\Delta = e^{-\xi\omega_\Delta^*}$,

$C_\Delta = \cos\omega_\Delta^*\sqrt{1-\xi^2}$, and

$\omega_\Delta^* = \omega_0\Delta/V$

where Δ is the bump spacing, ξ the damping ratio, ω_0 the natural frequency of the landing gear, and V the vehicles forward speed. He has gone on to investigate the most critical bump factor.

1.4.2 Vehicle Models and Solution Schemes

The increasing demand for safety and ride comfort, especially at high speeds, has led to the development of new types of suspension systems for road and rail vehicles.

Sharp and Crolla [25] have reviewed different concepts in road vehicle suspension system design, and have compared relative merits and demerits of passive, active, semi-active, and slow-active suspensions from the view-point of ride comfort and control of wheel load variations. In recent years a lot of research work has been carried out in the analysis and design of active suspension systems. Tomizuka [30] has studied the preview control of vehicle suspension from the viewpoint of discrete optimal control. Hac [11, 12] has used stochastic optimal control theory in the suspension optimisation of a two-degree-of-freedom vehicle model and a vehicle with an elastic body, traversing a rough road, for better ride comfort and road holding characteristics. Yoshimura *et al.* [36] have considered a cascade arrangement of a Kalman filter and optimal controller, to formulate and solve the problem of designing an active suspension to control the vertical vibrations of railway track vehicle. He has performed measurements in a noisy environment and estimated unknown state variables from this data by using a Kalman filter. Yoshimura and Sugimoto [38] have continued the same work for a vehicle travelling on a flexible beam with an irregular surface. The vehicle is modelled as a four degrees-of-freedom system. The beam deflection itself is described by a set of modal functions. The measurement of track inputs is done by means of a pre-view arrangement. ElMadany [6] used stochastic optimal control and estimation theories to design active suspension system for a cab ride in a tractor-semitrailer vehicle. Sharp and Hassan [26] have shown that a pneumatic air-pump based automobile suspension system has very good ride performance properties over a wide range of workspace-road roughness ratios. Lindgren [20] has analysed the response of a single-degree-of-freedom system for the case of vehicle jump or take-off while traversing a rough road. He has presented a switching stochastic differential equation for the system. Thompson [29] has optimised the tuning and damping ratio for a two-degrees-of-freedom system, to minimise wheel bounce on a random road. Freymann [10] has carried out experimental investigations for aircraft taxi ground

loads alleviation of landing gear. In these studies, the vehicle was assumed to be traversing the rough road/track with a constant velocity. The stationary response of the vehicle was found to be superior in comparison to that of a passive system in terms of ride comfort and road–holding.

Non-stationarity is inherent to most vehicle problems. The vehicle response is non-stationary

- for variable velocity traverse over rough roads with spatial homogeneity,
- when the vehicle traversing a smooth surface (zero initial conditions) at constant velocity suddenly encounters a spatially homogeneous rough terrain and continues to move — in this case the response becomes stationary after a lapse of time,
- for traverse over a partially non-homogeneous terrain with constant or variable velocity.

Non-stationary vehicle response due to variable velocity has been treated in a time–domain formulation by Virchis and Robson [33] and by Sobczyk and Macvean [28]. A space–domain formulation admitting a evolutionary spectral form in the wavenumber has been presented by Yadav and Nigam [35]. In their paper the knowledge of the exact nature of the time space relation was a pre-requisite. They transformed their temporal equations into the space domain assuming the time space relation to conform to a power law. Hammond and Harrison [13, 15] adopted linear state–space techniques, yielding a set of matrix differential equations for the determination of the non-stationary response covariance. In the works mentioned above, a single–degree–of–freedom vehicle model with passive suspension was assumed, and the different analyses involved evaluation of multiple integrals in the time–domain, contour integration in the wavenumber domain, and numerical integration for the covariance response.

1.5 Present Work

The present work is an attempt to design an anti-skid algorithm for an optimal braking problem.

In aircraft braking systems during landing there already exist two types of anti-skid methods.

1. Pulsed braking system :

   In this system the braking force is applied in discrete pulses. The wheel is braked for a short period of time with no concessions to skidding, and then released. During the period of free roll the wheel recovers from any skid it might have entered. This process is repeated until the aircraft is brought to a halt. This is a rugged design even though very sub-optimal.

2. Skid monitoring system :

   In this type of landing gear the motion of the aircraft is monitored to detect any skidding during braking, with the help of sensors. When a skid is sensed, the wheel is released to roll freely and come out of the skid. This process is repeated until the aircraft is brought to a halt.

In both the above methods the braking force is either switched on or off but not varied continuously. The present work attempts to optimise the braking by varying the braking force with time.

It is physically impossible for any device to react instantaneously to a stimulus. This is mainly due to the time taken :

- to detect the stimulus and its nature.
- to calculate the response.

- by the device to activate it's sensors and achieve fully the response, due to the inherent physical inertia of the servo–mechanism.

Thus a continually varying braking force will lag behind the impulse by a small time interval. Therefore to achieve optimality it is not sufficient to just find out the braking force and apply it, but to do it with a view to the future. That is, the brakes have to be applied so that, the events, namely the vehicle encountering the impulse and the brakes achieving the calculated optimal braking force, should be simultaneous. This requires the prediction of the impulse one step ahead in time. The prediction of the impulse can be done by using a pre-view arrangement as suggested by Yoshimura [37, 38] or by using statistical and/or probabilistic methods.

In this study the surface is assumed to be a random process with a given PSD. The surface characteristics are predicted one step ahead in time by using the statistical properties of random processes, with the help of an auto regressive filter.

1.5.1 Mathematical Models Used

This study is computational in nature and deals with mathematical modelling of the vehicle and the track surface.

The Vehicle Model

The vehicle is modelled as a rigid body, single wheel, heave degrees of freedom model, supported on a linear shock absorber consisting of a spring and a damper. The tyre is modelled as an equivalent linear spring and damper as in Figure 1.2

The Surface Model

The surface is modelled as a zero mean random process superimposed over a variable deterministic mean. The PSD of the zero mean random process has been found to

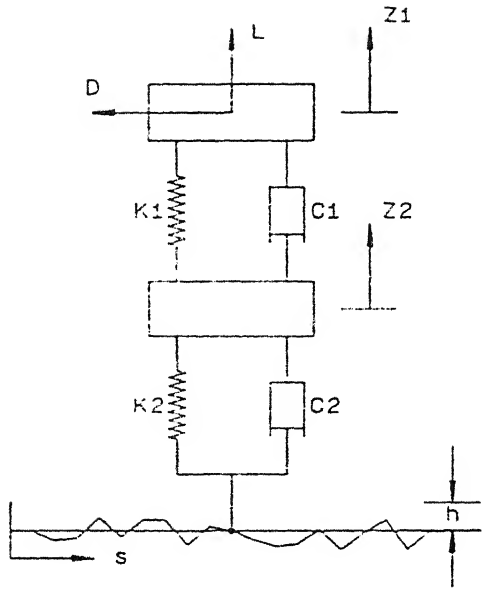

Figure 1.2: The vehicle model

conform to a *"flat bell shape"* . Various approximations to this shape have been used to describe the PSD distribution, depending on the primary variable chosen, namely velocity or distance. In this work the PSD is described by equation 2.5 [22] :

$$\Phi(\Omega) = \begin{cases} \frac{\sigma^2}{2\sqrt{\pi}} e^{-\frac{\Omega^2}{4\alpha_1^2}} & \text{if } |\Omega| \leq \Omega_0 \\ 0 & \text{otherwise} \end{cases}$$

Here Φ is the PSD, Ω the spatial frequency, Ω_0 the cut-off frequency, σ is the standard deviation of the sample track from the zero mean, and α_1 is a correlation constant describing the roughness of the track.

The random process is generated using a cosine filter [27] to a uniform deviate, described in §4.1. The uniform deviate is generated using the modulo, and the data encryption standard (DES) algorithm [24]. The track heights generated from this, as a function of distance, are added to the corresponding deterministic means which

were taken as simple algebraic or transcendental functions of distance.

Prediction Algorithm

The auto–regressive algorithm was used for predicting the track profile one step ahead in time. In this algorithm the predicted value is taken to be a weighted average of the time series' history, as in equation 4.9 [34].

$$x_n^* = \sum_{k=1}^{p} a_k x_{n-k} \tag{1.12}$$

Where x_n^* is the predicted value at the present instant, a_k the weighting factor, and x_{n-k} the actual value of the time series at an instant k time steps in the past. Here a_k are calculated such that the mean square error in prediction is a minimum. Error is defined as the difference between the actual value of the time series, and it's corresponding predicted value at any instant of time.

The equations of motion are solved in the time–domain using the impulse response method. This method calculates the response at the present time due to a unit impulse disturbance in the past. This response is convolved with the disturbance history to arrive at the present response of the system.

The programmes are developed in FORTRAN–77 on the HP–9000 series 850 computer systems with a UNIX operating system, at I. I. T. Kanpur.

Chapter 2

Models Chosen

The vehicle considered for the present work is a light fighter / trainer. Only a single wheel landing gear has been considered. The models for the aircraft and the runway profile chosen for the present work are detailed in the subsequent sections of this chapter.

2.1 The Vehicle Model

The vehicle is modelled as a rigid body, single wheel, heave degrees of freedom system, suspended on a linear spring and damper shock absorber. The weight of the landing gear is considered to be partially sprung and partially unsprung. The sprung mass of the landing gear is considered along with the vehicle mass. The wheel and the tyre are modelled as an unsprung mass. The damping and spring effects of the tyre are modelled as an equivalent linear spring and damper. The model is as presented in Figure 1.2.

2.1.1 Forces on The Vehicle

The forces acting on the system which are considered in this work, other then the track undulations, are

1. Lift force on the aircraft,
2. Drag on the aircraft,
3. Gravitational force, in the form of weights of the sprung and the unsprung masses of the aircraft and landing gear,
4. Braking force being applied on the aircraft, and
5. Reaction of the ground as visible to the tyre.

Gyroscopic moments/forces on the wheel are neglected, as they do not have a direct bearing on this problem. Loss of energy in the shock absorber due to heating, secondary vibrations such as; vibrations of the shock absorber wall, emission of sound etc., are assumed not to effect the damping and spring behaviour of the shock absorber, and are neglected. Loss of energy due to bearing friction and other such secondary phenomenon is also neglected. The system is assumed to be isolated and adiabatic.

2.2 The Input Process

The input disturbance to the vehicle model is the track unevenness, which gets filtered successively through the tyre and the shock absorber. The track unevenness is modelled as a random process in the space domain, as described below.

The track is assumed to consist of two distinct processes namely,

- a deterministic variable mean process, and

- a random zero mean process described by it's statistical properties.

The track height is the algebraic sum of the two sub-processes.

2.2.1 The Deterministic Variable Mean Process

This process can be described by infinitely many combinations, over distance, of simple algebraic or transcendental functions, to satisfy some physical properties of a given runway like

- differential settlement of concrete slabs,
- bomb craters covered with repair mats,
- inclined runways,
- parabolic or curved runway surfaces,
- unevenness in landing decks of aircraft carriers due to buckling, etc.

In this study three cases of the runway profile have been considered namely

- a stepped runway, namely a crater covered with a repair mat,
- an inclined runway, and
- a sinusoidal runway.

2.2.2 The Random Zero Mean Process

This process can be described either by it's auto-correlation function or the Power Spectral Density [PSD] function.

In the literature surveyed most of the work has been done using the following approximation for the auto-correlation function for the road or it's corresponding PSD function [22].

$$R(\tau) = \sigma^2 e^{-\alpha|\tau|} \tag{2.1}$$

$$\phi(\omega) = \frac{\sigma^2}{\pi}\frac{\alpha}{\omega^2+\alpha^2} \tag{2.2}$$

However as can be easily seen, the auto-correlation function is not differentiable at $\tau = 0$, therefore $X(t)$, the corresponding random process, is also not differentiable. The following alternative approximation function for the auto-correlation, however is differentiable for all τ [22].

$$R(\tau) = \sigma^2 e^{-\alpha\tau^2} \tag{2.3}$$

The corresponding PSD function for the auto-correlation equation is

$$\phi(\omega) = \frac{\sigma^2}{2\sqrt{\pi}\alpha} e^{-\frac{\omega^2}{4\alpha^2}} \tag{2.4}$$

Narayanan and Raju [21] pointed out that the road may be treated as a homogeneous random process only in the space domain. Therefore in this study the runway has been generated in the space domain and then converted to the time domain via a space–time relation. For generating the random process therefore the spatial PSD and the spatial frequency have been used. Also since a discrete process is generated, the sampling theorem dictates a cut-off frequency, within which region only the PSD need be integrated. Thus equation 2.4 becomes

$$\Phi(\Omega) = \begin{cases} \frac{\sigma^2}{2\sqrt{\pi}} e^{-\frac{\Omega^2}{4\alpha_1^2}} & \text{if } |\Omega| \leq \Omega_0 \\ 0 & \text{otherwise} \end{cases} \tag{2.5}$$

where Ω_0 is the cut-off frequency given by [24]

$$\Omega_0 = \frac{1}{2\Delta} \tag{2.6}$$

where Δ is the sampling interval. In this study however, Ω_0 was chosen so that $\Phi(\Omega)$ was sufficiently small. Δ was calculated for this value of Ω_0.

Chapter 3

Equations of Motion

The equations of motion for the model described in the previous chapter, forces acting on it, and the physical restrictions imposed by the shock absorber and the tyre, are detailed in the subsequent sections of this chapter. A detailed description of the changes in the model due to the tire/shock absorber locking during their operation is also presented.

3.1 The Generalised Equation of Motion

The dynamics of a rigid body can be described adequately by the following system of ordinary differential equations.

$$\mathbf{M}\ddot{\mathbf{Z}} + \mathbf{C}\dot{\mathbf{Z}} + \mathbf{K}\mathbf{Z} = \mathbf{F} \tag{3.1}$$

Where **M** is the inertia matrix, **C** is the damping matrix, and **K** is the stiffness matrix. **F** is the vector of external forcing functions, and **Z** the state vector or the displacement vector.

3.2 Solution for The Equation of Motion

The solution of equation 3.1 is got by using the impulse response method [5, 19, 22, 31].

Defining a vector $\mathbf{Y} = \begin{bmatrix} \mathbf{Z} \\ \dot{\mathbf{Z}} \end{bmatrix}$ equation 3.1 can be rewritten as

$$\dot{\mathbf{Y}} + \mathbf{A}\mathbf{Y} = \mathbf{P} \tag{3.2}$$

Where

$$\mathbf{A} = \begin{bmatrix} \mathbf{M}^{-1}\mathbf{C} & \mathbf{M}^{-1}\mathbf{K} \\ -\mathbf{I} & \mathbf{0} \end{bmatrix}$$

$$\mathbf{P} = \begin{bmatrix} \mathbf{M}^{-1}\mathbf{F} \\ \mathbf{0} \end{bmatrix}$$

Where $\mathbf{I}$ is the identity matrix, and $\mathbf{0}$ is the zero matrix/vector.

Equation 3.2 is in the standard form of the Bernaulli equation [17]. Thus it's solution can be written as [17] :

$$\mathbf{Y}e^{\int \mathbf{A}\,dt} = \int \mathbf{P}e^{\int \mathbf{A}\,dt}\,d\tau + \mathbf{C}_1 \tag{3.3}$$

Here $\mathbf{Y}$, $\mathbf{A}$, and $\mathbf{P}$ can be time dependent and $\mathbf{C}_1$ is a constant depending on the initial conditions. However for a linear system $\mathbf{A}$ is a constant with time. Thus for a linear system, within the integral limits of t_0 and t, equation 3.3 becomes :

$$\mathbf{Y}e^{\int_{t_0}^{t} \mathbf{A}\,dt} = \int_{t_0}^{t} \mathbf{P}(\tau)e^{\int_{t_0}^{\tau} \mathbf{A}\,dt}\,d\tau + \mathbf{C}_1$$

$$\mathbf{Y}e^{\mathbf{A}\cdot(t-t_0)} = \int_{t_0}^{t} \mathbf{P}(\tau)e^{\mathbf{A}\cdot(\tau-t_0)}\,d\tau + \mathbf{C}_1$$

$$\mathbf{Y} = \int_{t_0}^{t} \mathbf{P}(\tau)e^{\mathbf{A}\cdot(\tau-t)}\,d\tau + \mathbf{C}_1 \cdot e^{-\mathbf{A}\cdot(t-t_0)} \tag{3.4}$$

At $t = t_0$ equation 3.4 gives

$$\mathbf{Y}|_{t=t_0} = \mathbf{C}_1 \tag{3.5}$$

Substituting equation 3.5 in 3.4 and defining the impulse response function

$$\mathrm{h}(t) = \mathrm{e}^{-\mathrm{A}t} \tag{3.6}$$

We can write

$$\mathrm{Y}(t) = \mathrm{Y}(t_0)\mathrm{h}(t - t_0) + \int_{t_0}^{t} \mathrm{h}(t - \tau)\mathrm{P}(\tau)\, d\tau \tag{3.7}$$

The evaluation of the exponential in equation 3.6 can be done as follows : A can be expressed as

$$\mathrm{A} = \mathrm{UEU}^{-1} \tag{3.8}$$

where U is the modal matrix of A, and E is a diagonal matrix whose diagonal elements correspond to the eigen values of A.

It is easily seen from 3.8 that

$$\begin{aligned}
\mathrm{A}^2 &= \mathrm{UEU}^{-1}\mathrm{UEU}^{-1} \\
&= \mathrm{UE}^2\mathrm{U}^{-1} \\
\mathrm{A}^3 &= \mathrm{UE}^2\mathrm{U}^{-1}\mathrm{UEU}^{-1} \\
&= \mathrm{UE}^3\mathrm{U}^{-1} \\
&\vdots \quad \vdots \quad \vdots \\
\mathrm{A}^n &= \mathrm{UE}^{n-1}\mathrm{U}^{-1}\mathrm{UEU}^{-1} \\
&= \mathrm{UE}^n\mathrm{U}^{-1}
\end{aligned} \tag{3.9}$$

Expanding the exponential in it's power series and substituting equation 3.9 we have

$$\begin{aligned}
\mathrm{e}^{\mathrm{A}t} &= 1 + \mathrm{A}t + \frac{\mathrm{A}^2t^2}{2!} + \cdots + \frac{\mathrm{A}^nt^n}{n!} \\
&= 1 + \mathrm{UEU}^{-1}t + \frac{\mathrm{UE}^2\mathrm{U}^{-1}t^2}{2!} + \cdots + \frac{\mathrm{UE}^n\mathrm{U}^{-1}t^n}{n!} \\
&= \mathrm{U}\left[1 + \mathrm{E}t + \frac{\mathrm{E}^2t^2}{2!} + \cdots + \frac{\mathrm{E}^nt^n}{n!}\right]\mathrm{U}^{-1} \\
&= \mathrm{Ue}^{\mathrm{E}t}\mathrm{U}^{-1}
\end{aligned} \tag{3.10}$$

From 3.10 and 3.6 we get

$$\mathrm{h}(t) = \mathbf{UVU}^{-1} \tag{3.11}$$

Where **U** is the modal matrix of **A**, and

$$\mathbf{V} = \begin{cases} e^{-\alpha_j t} & \forall \quad i = j \\ 0 & \forall \quad i \neq j \end{cases}$$

where α_j are the eigen values of **A**.

3.3 Present Model

For the present model the matrices **M**, **C**, **K**, **F**, and **Z** are as follows

$$\mathrm{M} = \begin{bmatrix} m_1 & 0 \\ 0 & m_2 \end{bmatrix}$$

$$\mathbf{C} = \begin{bmatrix} C_1 & -C_1 \\ -C_1 & C_1 + C_2 \end{bmatrix}$$

$$\mathbf{K} = \begin{bmatrix} K_1 & -K_1 \\ -K_1 & K_1 + K_2 \end{bmatrix}$$

$$\mathbf{F} = \begin{bmatrix} L(t) \\ C_2\dot{h} + K_2 h \end{bmatrix}$$

$$\mathbf{Z} = \begin{bmatrix} Z_1 \\ Z_2 \end{bmatrix}$$

The sign conventions are as shown in Figure 1.2. Z_1, Z_2, h, and t are assumed to be zero at touch down.

3.4 Forces on The Model

As enumerated in §2.1.1 the external forces acting on the aircraft are Lift, Drag, Gravity, Reaction, and Braking. The action of gravity is incorporated in the general equation via the mass of the vehicle. The expressions for the other forces for the free rolling case are as below.

3.4.1 Lift Force on The Aircraft

The Lift on the aircraft can be represented by the following cardinal form [3] :

$$L = \frac{1}{2}\rho V^2 S C_L \tag{3.12}$$

where ρ is the density of air, V is the speed of the aircraft, S is the lifting surface area or the area of the wing, and C_L is the co-efficient of lift given by

$$C_L = \begin{cases} C_{L_0} + \alpha C_{L_\alpha} & \forall \quad \alpha \leq \alpha_{stall} \\ 0 & \forall \quad \alpha > \alpha_{stall} \end{cases} \tag{3.13}$$

where α is the angle of attack, α_{stall} is the angle of stall, C_{L_0} is the lift coefficient at zero angle of attack, and C_{L_α} is the lift curve slope. For most aircraft wings the lift varies linearly with the angle of attack, and so the lift curve slope is a constant for the operation range. The angle of attack varies as the aircraft taxiis due to the heave of the wings. The effective angle of attack is got as

$$\alpha_{eff} = \alpha_0 + \tan^{-1}\left(\frac{\dot{Z}_1}{V}\right) \tag{3.14}$$

where α_0 is the pre-set angle of attack of the wing.

3.4.2 Drag Force on The Aircraft

The Drag on the aircraft is also expressed in a cardinal form similar to 3.12 as follows

$$D = \frac{1}{2}\rho V^2 S C_D \tag{3.15}$$

where C_D is the drag coefficient, which is usually described by the *"drag polar"* below

$$C_D = C_{D_0} + kC_L^2 \tag{3.16}$$

The total drag is got by summing up the drags of individual elements like the wing, fuselage, tail plane, etc. Each of these individual drag forces can be represented in the form of equation 3.15.

3.4.3 Reaction of The Ground

The weight of the aircraft is filtered through the tyre, and the landing gear. The weight as visible to the track is

$$R = C_2(\dot{h} - \dot{Z}_2) + K_2(h - Z_2) \tag{3.17}$$

This weight manifests itself in the form of the reaction of the ground on the vehicle.

3.4.4 Braking Force Applied on The Aircraft

The braking force on the aircraft is limited by the dynamics of the vehicle as shown in §1.2.1. The maximum applicable braking force can be given as

$$B = \mu_{max} R \tag{3.18}$$

where μ is given as a function of skid s, and has a maxima between 0.05 and 0.3 as shown in Figure 1.1 [1]. Skid s is defined as in equation 1.1

$$s = 1 - \frac{\omega}{\omega_a}.$$

Where ω is the angular velocity of the wheel and

$$\omega_a = \frac{V}{\text{rolling radius}} = \frac{V}{\frac{D}{2} - \frac{\delta}{3}} \tag{3.19}$$

The friction also depends on the vehicle speed, tyre inflation pressure, tread depth and ground surface conditions [1].

3.5 Domain of The Equations of Motion

The generalised equations of motion, and the corresponding equation for the reaction force are not valid for the following cases :

- tyre bottomed, that is $-T_b \leq Z_2 - h \leq T_e$,
- shock absorber locked, that is $-S_b \leq Z_1 - Z_2 \leq S_e$,
- the aircraft ballooning or jumping/bumping, that is $R \leq 0$.

3.5.1 Equations for Tyre Bottoming

Tyre bottoming occurs when the rim starts touching the ground. Even though it might be allowable for an instant, on larger periods this may result in the tyre bursting. Tyre extending is normally accompanied with the ballooning of the aircraft. Pure extension of the tyre without the aircraft is a hypothetical borderline case.

In the case of tyre locking the tyre looses it's filtering properties and the track disturbances are passed directly to the shock absorber. The system now behaves like a one-degree-of-freedom system riding on a mass which moves along the ground. The equation becomes :

$$m_1\ddot{Z}_1 + C_1(\dot{Z}_1 - \dot{Z}_2) + K_1(Z_1 - Z_2) = L - m_1 g$$

or

$$m_1\ddot{Z}_1 + C_1\dot{Z}_1 + K_1 Z_1 = L - m_1 g + K_1 Z_2 + C_1\dot{Z}_2 \tag{3.20}$$

here due to the lack of tyre filtering $Z_2 = h + \delta$, $\dot{Z}_2 = \dot{h}$, and $\ddot{Z}_2 = \ddot{h}$. δ is the displacement of the tyre at which it is locked.

The reaction on the ground is now given by the following equation :

$$R = m_2(\ddot{Z}_2 + g) + K_1(Z_2 - Z_1) + C_1(\dot{Z}_2 - \dot{Z}_1) + F_{locking} \tag{3.21}$$

where $F_{locking}$ is the force required to lock the tyre.

.5.2 Equations for Shock Absorber Locking

he locking of the shock absorber is not as critical as the locking of the tyre. In iis case the filtering characteristics of the shock absorber fail and the aircraft starts ding on the tyre, so that the tyre accelerations and displacements get transmitted to directly. This results in very high instantaneous accelerations of the aircraft, which iay be uncomfortable to the passengers. If the aircraft does not recover quickly, the ituation may lead to the locking of the tyre signifying, a total collapse of the landing ear.

The equations of motion for this case are :

$$m_2\ddot{Z}_2 + C_2(\dot{Z}_2 - \dot{h}) + K_2(Z_2 - h) = m_1\ddot{Z}_1 + (m_1 - m_2)g + F_{locking} - L$$

or

$$m_2\ddot{Z}_2 + C_2\dot{Z}_2 + K_2Z_2 = m_1\ddot{Z}_1 + (m_1 - m_2)g + C_2\dot{h} + K_2h + F_{locking} - L \quad (3.22)$$

iere due to the failure of the shock absorber $Z_1 = Z_2 + \delta$, $\dot{Z}_1 = \dot{Z}_2$, and $\ddot{Z}_1 = \ddot{Z}_2$. δ s the displacement of the shock absorber at which it is is locked.

The equation for the reaction force does not change as it depends only on the tyre parameters.

3.5.3 Equation for Aircraft Ballooning

The ballooning of the aircraft takes place when the runway is very rough and dips sharply after a peak or in the early stages when the aircraft is recovering from the impact of touch-down. The centre of gravity of the aircraft—landing-gear system follows the trajectory of a simple projectile, however the wheel and the aircraft continue to oscillate with respect to one other. The governing equation is that of the two-degree-of-freedom system with the external forcing function zero. The reaction on the ground in this case is obviously zero.

3.6 Space–Time Relationship

In this study the track has been generated in the space domain, where as the braking and the dynamics are being studied in the time domain. This necessitates the determination of the space–time relationship of the system. The relationship is not easily definable mathematically as the braking force is continually varying with time in a random fashion. However it can be stated as an integral equation which can be integrated numerically in real–time. The relationship can be stated as follows :

$$\ddot{s}(t) = -\frac{D+B}{m_1+m_2} \tag{3.23}$$

$$\dot{s}(t) = -\int_{t_0}^{t} \frac{D+B}{m_1+m_2}\,dt + \dot{s}(t_0) \tag{3.24}$$

$$s(t) = -\int_{t_0}^{t} \dot{s}(t)\,dt + s(t_0) \tag{3.25}$$

where D is the drag force and B is the brake force.

3.7 Skid–Time Relationship

The skid is defined in equation 1.1, as a function of the wheel's angular velocity. The angular velocity in turn depends on the variation of the braking torque, and the moment generated due to the shift in the centre of pressure of the radial load. The angular acceleration of the wheel is thus given as :

$$\dot{\omega} = \frac{1}{I}\left\{\left[\mu\left(\frac{D}{2}-\delta\right) - X_c\right]R - T_b\right\} \tag{3.26}$$

where D is the free outer diameter of the tyre, δ is the tyre deflection, X_c is the forward shift in centre of pressure, and T_b is the braking torque being applied.

The angular velocity can thus be got by integrating equation 3.26 in the time domain.

$$\omega = \int_{t_0}^{t} \dot{\omega}(t)\,dt + \omega(t_0) \tag{3.27}$$

Chapter 4

The Track Profile Generation and Prediction

In this chapter the method used to generate the track profile, described in chapter 2, is detailed. The prediction routine for forecasting the track height, one time step in the future, is also discussed in the subsequent sections of this chapter.

4.1 Generation of The Track Profile

The track profile is described in §2.2. The deterministic variable mean process is easily generated as it is fully described by it's equation, whereas the zero mean random process has to be generated using it's statistical properties. The random process remains homogeneous in the space-domain and becomes non-homogeneous in the time-domain. Thus it's simulation in the space-domain is simpler.

The random process is simulated in terms of the sum of cosine functions with random frequencies and random phase angles [27] as below

$$f_0(t) = \sigma \left(\frac{2}{N}\right)^{\frac{1}{2}} \sum_{k=1}^{N} \cos(\omega_k t + \psi_k). \tag{4.1}$$

where

$$\sigma = \left[\int_{-\infty}^{\infty} \phi_0(\omega)\, d\omega\right]^{\frac{1}{2}} \tag{4.2}$$

is the standard deviation of the process $f_0(t)$, ω_k $(k = 1, 2, \cdots, N)$ are independent random variables identically distributed with the density function $g(\omega) \equiv g(\omega_k)$ obtained by normalising $\phi_0(\omega)$,

$$g(\omega) = \frac{\phi_0(\omega)}{\sigma^2}, \tag{4.3}$$

and ψ_k are independent random variables identically distributed with the uniform density $1/(2\pi)$ between 0 and 2π. ω_k and $\psi_l (k, l = 1, 2, \cdots, N)$ are independent.

The random process that is generated can be easily seen to be of zero mean and the required PSD [27]. The ensemble average $E[f(t)]$ of $f(t)$ is

$$E[f(t)] = \frac{\sigma\left(\frac{2}{N}\right)^{\frac{1}{2}}}{2\pi} \int_{-\infty}^{\infty}\int_{0}^{2\pi} \cos(\omega t + \psi) g(\omega)\, d\psi\, d\omega = 0 \tag{4.4}$$

The auto-correlation function $R(\tau)$ of $f(t)$ is

$$\begin{aligned} R(\tau) &= E[f(t+\tau)f(t)] \\ &= \frac{2\sigma^2}{N} \sum_{k=1}^{N}\sum_{l=1}^{N} E\left\{\cos\left(\omega_k t + \psi_k\right)\cos\left[\omega_l(t+\tau) + \psi_l\right]\right\} \\ &= \sigma^2 \int_{-\infty}^{\infty} \cos\omega\tau\, g(\omega)\, d\omega \\ &= \int_{-\infty}^{\infty} \cos\omega\tau\, \phi_0(\omega)\, d\omega \end{aligned} \tag{4.5}$$

It is easily seen that 4.5 is identical to the auto-correlation function $R_0(\tau)$ of $f_0(t)$ because of the Wiener-Khintchine relationship:

$$R_0(\tau) = \int_{-\infty}^{\infty} \phi_0(\omega) e^{\iota\omega\tau}\, d\omega \tag{4.6}$$

$$R_0(\tau) = \int_{-\infty}^{\infty} \cos\omega\tau\, \phi_0(\omega)\, d\omega \tag{4.7}$$

where ι is the imaginary unit.

This indicates that the whenever the ensemble average is considered, the simulated process $f(t)$ possesses the auto–correlation, $R(\tau)$ and the mean square spectral density $\phi(\omega)$ which are identical, respectively, with the target auto–correlation $R_0(\tau)$ and target spectral density $\phi_0(\omega)$.

For the present model the variables corresponding to time t, process $f(t)$, and temporal frequency ω, are the corresponding spatial variables namely, distance s, track height from mean $h(t)$, and spatial frequency Ω respectively.

The normalisation of the PSD (equation 4.3) gives $g(\Omega)$ to be a gaussian distribution.

$$g(\Omega) = \begin{cases} \frac{1}{2\sqrt{\pi}} e^{-\frac{\Omega^2}{4\alpha_1^2}} & \text{if } |\Omega| \leq \Omega_0 \\ 0 & \text{otherwise} \end{cases} \tag{4.8}$$

The gaussian deviate can be generated by the transformation method [24] from a uniform deviate between 0 and 1.

4.1.1 Generation of The Uniform Deviate

The uniform deviate can be generated by many different methods. In this work two methods have been investigated, the subtractive method suggested by Donald E. Knuth [24], and the Data Encryption Standard (DES) based method [24]. The DES based method of generating pseudo–random numbers is preferred as the randomness of the result is much better than any other known algorithm, however this algorithm is much slower than the others.

4.2 Prediction of The Track Profile

The prediction of the track profile is done in the time–domain. The random process in the space–domain is sampled at discrete time steps. The distance covered by the

vehicle during a time interval is calculated using the space-time relationship 3.25. The value of the track height at this distance is got by interpolation.

The linear predictor algorithm [34] used is robust and can vary it's characteristics with time to adapt to the changing input PSD. The predictor is a auto-regressive filter defined as

$$x_n^* = \sum_{k=1}^{p} a_k x_{n-k}, \tag{4.9}$$

and it's prediction error is given as

$$e_n = x_n - x_n^*. \tag{4.10}$$

Here x_n^* is the predicted value at instant n, x_{n-k} is the value at instant $n-k$, and a_k are the weighting coefficients which have to be adjusted in order to give a good prediction. The predictive coefficients are chosen to minimise

$$\sum_{n=0}^{\infty} e_n^2,$$

the square error. If the source spectrum is not constant, it becomes necessary to re-optimise the coefficients continually.

4.2.1 Optimisation of The Prediction Coefficients

The total squared prediction error is

$$M = \sum_n e_n^2 = \sum_n (x_n - \sum_{k=1}^{p} a_k x_{n-k})^2. \tag{4.11}$$

To minimise M by choice of coefficients a_j, equation 4.11 has been differentiated with respect to the coefficients a_j,

$$\frac{dM}{da_j} = -2 \sum_n x_{n-j} \left(x_n - \sum_{k=1}^{p} a_k x_{n-k} \right) = 0 \tag{4.12}$$

so,

$$\sum_{k=1}^{p} a_k \sum_n x_{n-j} x_{n-k} = \sum_n x_n x_{n-j}, j = 1, 2, \cdots, p. \tag{4.13}$$

It can be seen that for a doubly infinite sum,

$$\sum_{n=-\infty}^{\infty} x_{n-j}x_{n-k} = \sum_{n=-\infty}^{\infty} x_{n-j+1}x_{n-k+1} = \cdots = \sum_{n=-\infty}^{\infty} x_n x_{n+j-k}$$

so now equation 4.12 transforms to

$$\begin{aligned} R_0a_1 + R_1a_2 + R_2a_3 + \cdots &= R_1 \\ R_1a_1 + R_0a_2 + R_1a_3 + \cdots &= R_2 \\ R_2a_1 + R_1a_2 + R_0a_3 + \cdots &= R_3 \\ \vdots & \quad \vdots \end{aligned} \tag{4.14}$$

where

$$R_m = \sum_n x_n x_{n+m}, m = 0, 1, 2, \cdots, p.$$

The above system of equation has to be solved for a_k. In the present study it has been solved using the Durbin and Levinson method [34] which requires much less computational effort than other methods.

Since it's impractical and undesirable to compute the infinite sums in the above equation a windowing procedure is used. The window is described as a set of weights spread over time as follows

$$x'_n = w_n x_n.$$

Here w_n is zero outside a finite range of interest. Now R_m can be redefined as

$$R^h_m = \sum_{n=h}^{h+N-1} x'_n x'_{n+m}, m = 0, 1, 2, \cdots, p.$$

The prediction co-efficients a_k are recalculated when the mean square error in prediction becomes considerable large. This results in fine tuning of the prediction coefficients with progress in time.

Chapter 5

Presentation of Results

The results of the numerical simulation of the model and the numerical values of the system parameters used for this simulation are presented in this chapter. The study was carried out for three different parameters namely landing sink velocity, landing glide velocity, and runway mean profile.

5.1 The Model Parameters

The values used are presented in table 5.1. These refer to a typical light fighter/trainer aircraft.

The actual damping and spring relations of the aircraft were non-linear. They were approximated by two straight lines which formed a crude envelope of the original curve.

5.2 Track Parameters

The track is modelled as a sum of zero mean random process and a variable mean deterministic process. The parameters used for generating these different processes

Symbol	Description	Value	Units
C_1	Damping coefficient for shock absorber	1.021×10^5	Ns/m
C_2	Damping coefficient for tyre	200.0	Ns/m
K_1	Spring coefficient for shock absorber	1.0×10^6	N/m
K_2	Spring coefficient for tyre	1.8×10^6	N/m
M_1	Sprung Mass	4133.33	Kg
M_2	Unsprung Mass	77.0	Kg
M	Landing mass of aircraft	8600.00	Kg
V	Landing velocity	75.56 – 77.0	m/s
V_{sink}	Sink velocity	1.0 – 3.0	m/s
S	Surface area of the wing	38.4	m^2
D	Diameter of the wheel	0.66	m
I	Moment of Inertia of the wheel	0.56	$Kg\ m^2$
α_a	Angle of attack at approach	13.5	deg
α_r	Set angle of attack during ground roll	6.0	deg
α_s	Stalling angle	20.0	deg
α_t	Angle of attack at touch-down	16.85	deg
$C_{D_{0_r}}$	Coefficient of friction drag during ground roll	0.1144	
$C_{D_{0_t}}$	Coefficient of friction drag at touch down	0.0614	
	Period of free roll	0.038	s

Table 5.1: Model Parameters

are as follows :

- Zero mean random process :

  The zero mean random process was generated using the Shinozuka filter. The parameters used were

  1. Correlation constant for roughness, $\alpha = 0.005$.
  2. Standard deviation of the track, $\sigma = 0.01$.
  3. Cutoff Nyquist frequency, $\Omega_l = 0.006$.
  4. Number of simulation terms for the Shinozuka filter, $N = 200$.

- Variable mean deterministic process :

  The following four different mean profiles for the runway were generated :

  1. Flat runway :

     This is equivalent to a zero mean process alone.

  2. Inclined runway :

     This runway was assumed to have an inclination of about 1 in 1000, corresponding to an angle of inclination of 0.06°

  3. Stepped runway :

     The step was assumed to be a AR–19 aluminium repair mat with a step height of 0.038 m and a length of 16.45 m, placed at a distance of 100.0 m from the point of touchdown.

  4. Sinusoidal runway :

     The sinusoidal runway was generated for a sine wave with a amplitude of 0.05 m and a wavelength of 15.23 m.

The study has been carried out for the cases listed in table 5.2

Case	Glide m/s	Sink m/s	Mean Profile	Figure Numbers
1	75.56	1.0	Flat	5.1, 5.9, 5.17, 5.25, 5.33, 5.41, 5.49, 5.57
2	75.56	2.0	Flat	5.2, 5.10, 5.18, 5.26, 5.34, 5.42, 5.50, 5.58
3	75.56	3.0	Flat	5.3, 5.11, 5.19, 5.27, 5.35, 5.43, 5.51, 5.59
4	76.32	1.0	Flat	5.4, 5.12, 5.20, 5.28, 5.36, 5.44, 5.52, 5.60
5	77.0	1.0	Flat	5.5, 5.13, 5.21, 5.29, 5.37, 5.45, 5.53, 5.61
6	75.56	1.0	Inclined	5.6, 5.14, 5.22, 5.30, 5.38, 5.46, 5.54, 5.62
7	75.56	1.0	Sinusoidal	5.7, 5.15, 5.23, 5.31, 5.39, 5.47, 5.55, 5.63
8	75.56	1.0	Stepped	5.8, 5.16, 5.24, 5.32, 5.40, 5.48, 5.56, 5.64

Table 5.2: List of trial runs

5.3 Presentation of Results and Discussion

The results are presented in figures 5.1–5.64. Points are plotted 70 milli seconds apart, whereas the programme generates output after every 0.5 milli second. This results in considerable loss of information in the presentation, specially in the early stages where the effect of the landing impact is present. In latter stages where the system has stabilised the information loss is neglegible.

The results for the following state variables are presented.

1. Ground Reaction,
2. Retarding Friction on the tyre,
3. Sprung mass vertical displacement,
4. Sprung mass vertical velocity,
5. Sprung mass vertical acceleration,
6. Unsprung mass vertical displacement,
7. Unsprung mass vertical acceleration,

Time	F	T_b	Dist	R	V	$\ddot{Z}_1$	$\ddot{Z}_2$	$\dot{Z}_1$	Z_1	Z_2	Skid
s	KN	KNm	m	KN	m/s	cm/s^2	cm/s^2	cm/s	cm	cm	
0.00	0.00	0.00	0.00	0.00	75.56	0.00	0.00	-100.00	0.00	0.00	1.000
0.70	16.83	25.88	51.18	28.90	70.65	-66.34	-12541.90	-1.15	-10.36	-1.77	0.197
1.40	25.05	7.68	98.98	43.55	65.92	5.91	2599.37	-0.29	-10.49	-1.81	0.226
2.10	49.17	17.54	143.50	86.15	61.29	526.88	29969.20	3.29	-10.43	-1.52	0.243
2.80	49.38	9.45	184.83	81.23	56.77	-310.04	68498.30	0.74	-10.58	-1.80	0.174
3.50	32.45	16.89	223.02	53.45	52.37	251.81	2258.42	-0.45	-10.41	-1.72	0.201
4.20	30.65	0.00	258.15	52.34	48.00	217.94	2635.34	0.97	-10.35	-1.61	0.247
4.90	12.26	0.00	290.25	21.48	43.73	-276.76	-10888.40	0.53	-10.46	-1.71	0.274
5.60	30.09	6.32	319.37	47.50	39.42	165.71	-846.36	-7.41	-10.76	-2.35	0.161
6.30	29.97	5.82	345.39	46.81	34.99	-28.41	8674.32	0.14	-10.87	-2.16	0.173
7.00	8.12	0.00	368.36	13.21	30.64	43.76	-38832.70	0.11	-10.89	-2.18	0.243
7.70	16.99	1.04	388.29	26.56	26.34	98.50	-24424.00	0.59	-10.83	-2.11	0.214
8.40	28.41	8.70	405.24	46.10	22.07	73.16	2307.95	0.26	-10.93	-2.22	0.264
9.10	9.98	0.49	419.19	17.90	17.86	58.91	-33557.30	-0.19	-10.85	-2.19	0.382
9.80	39.97	19.17	430.26	66.52	13.79	22.11	31570.50	-0.13	-10.87	-2.18	0.087
10.50	44.95	13.86	438.48	68.01	9.71	16.48	33807.50	0.43	-10.86	-2.14	0.239
11.20	26.08	22.19	443.95	51.30	6.22	30.76	11329.90	-0.16	-10.87	-2.19	1.000
11.90	0.00	0.00	447.28	70.26	3.13	-175.86	47046.40	-0.21	-10.88	-2.19	0.000
11.97	26.70	8.12	447.49	44.61	2.78	152.22	-3869.63	0.28	-10.89	-2.17	0.922

Table 5.3: Output for Landing Run on a Flat Runway,
aircraft glide velocity = 75.56 $\frac{m}{s}$ aircraft sink velocity = 1.0 $\frac{m}{s}$

8. Braking Torque on the wheel,

9. Skid of the wheel, and

10. the forward ground velocity of the aircraft.

The graphs are plotted as functions of time. Distance travelled by the aircraft is also plotted as an alternative scale. However this is a non-linear scale as the forward velocity changes with time.

A sample output is presented in table 5.3. This output is for the case of the aircraft landing on a flat runway with a glide velocity of 75.56 $\frac{m}{s}$, and sink velocity of 1.0 $\frac{m}{s}$.

5.3.1 Ground Reaction

Both the actual and the predicted ground reactions are plotted (figures 5.1, 5.2, 5.3, 5.4, 5.5, 5.6, 5.7, 5.8). It is observed that for all the cases the ground reaction is oscillatory in nature. A sharp peak in the initial response is present due to the landing impact. This peak is seen to increase in magnitude with increase in sink velocity, as is expected. The effect of the glide velocity (figures 5.1, 5.4, 5.5) is neglegible on the initial impact response of the vehicle. However in the latter stages the reaction stabilises much faster with increase in glide velocity. The road holding capability of the aircraft is observed to increase with increase in both sink (figures 5.1, 5.2, 5.3) and glide velocities in the latter stages.

The variation in the mean profile also affects the ground reaction. When compared to a flat track (figure 5.1) the road holding is much poorer for a sinusoidal runway (figure 5.7), where the aircraft leaves the track after almost every peak. However this is much improved in the case of inclined (figure 5.6) and the stepped runway (figure 5.8). This could be due to the faster dissipation of energy in the earlier stages.

The predicted reaction generated through an auto regressive filter, as discussed in §4.2, is found to match the actual reaction quite closely. However sometimes at peaks it is unable to follow the actual reaction exactly. The prediction is seen to get better as time progresses due to finer tuning of the prediction coefficients and stabilisation of the response.

5.3.2 Friction Force

The friction force (figures 5.9, 5.10, 5.11, 5.12, 5.13, 5.14, 5.15, 5.16) between the wheel and the ground is a function of μ the coefficient of friction and the ground reaction. The coefficient of friction itself is a function of the aircraft velocity and the skid of the wheel.

In the initial stages of the landing run the skid is maintained within a small range near the optimal skid value, corresponding to the maximum possible friction coefficient. The friction force therefore displays characteristics similar to the ground reaction (figures 5.1, 5.2, 5.3, 5.4, 5.5, 5.6, 5.7, 5.8). In the latter stages, however the skid experiences stronger oscillatory changes and consequently the friction force is not able to stabilise as in the case of the ground reaction. This unsettled behaviour is prominent at the glide velocity 75.56 m/s in lower range of the sink velocity (figures 5.9, 5.10, 5.11). For the case of increased glide velocity (figures 5.9, 5.12, 5.13) and non-zero mean track profiles (figures 5.14, 5.15, 5.16) the friction force characteristics are closer to the ground reaction characteristics.

5.3.3 Sprung Mass Displacement

The sprung mass displacement (figures 5.17, 5.18, 5.19, 5.20, 5.21, 5.22, 5.23, 5.24) stabilises after an initial peak, due to the landing impact and goes to it's static displacement value. The magnitude of the peak is observed to be dependent on the sink velocity as expected. Some kinks are visible in the graph, which are manifestations of the track profile undulations.

For the case of sinusoidal track unevenness (figure 5.23) the displacement amplitude is found to attain a maximum at 7.84 seconds after touch-down, corresponding to a velocity of 25.75 m/s, signifying resonance. The ground input frequency at this instant is found to be equal to the sprung mass frequency. After this point of resonance the displacement is seen to stabilise and go down to it's static value.

In the case of the stepped profile (figure 5.24), the effect of the step is manifest in the form of a corresponding step in the sprung mass displacement.

5.3.4 Sprung Mass Velocity

The sprung mass velocity (figures 5.25, 5.26, 5.27, 5.28, 5.29, 5.30, 5.31, 5.32) shows exactly similar nature as the sprung mass displacement (figures 5.17, 5.18, 5.19, 5.20, 5.21, 5.22, 5.23, 5.24).

5.3.5 Sprung Mass Acceleration

The sprung mass acceleration (figures 5.33, 5.34, 5.35, 5.36, 5.37, 5.38, 5.39, 5.40) shows clearly the effect of landing impact in the form of a peak with magnitude depending on the sink velocity. The variation in acceleration is seen to die down with the progress of the landing run. The effect of resonance in the case of the sinusoidal track profile (figure 5.39) is not visible, however the presence of the step in the stepped runway (figure 5.40) is clearly reflected by the acceleration graph. The effect of the inclined runway (figure 5.38) is only to damp the acceleration sooner.

5.3.6 Unsprung Mass Displacement

The unsprung mass characteristics (figures 5.41, 5.42, 5.43, 5.44, 5.45, 5.46, 5.47, 5.48) are observed to be similar to that of the sprung mass. The sprung mass displacement is plotted along with the track height so that road holding is easily visible. Road holding is seen to be poor in the case of low sink velocities (figures 5.41, 5.42, 5.43) and is very bad for the sinusoidal runway (figure 5.47). However for the sinusoidal runway the road holding improves after resonance has taken place in the sprung mass. The effect of resonance is also visible in the unsprung mass displacements as during this period the sprung mass exerts more effective weight on the unsprung mass than normal.

5.3.7 Unsprung Mass Acceleration

The unsprung mass acceleration (figures 5.49, 5.50, 5.51, 5.52, 5.53, 5.54, 5.55, 5.56) does not show the effect of landing impact clearly. This could be due to the lower resolution of the graph. Variation in acceleration is seen to die down much faster with increase in glide velocity (figures 5.49, 5.52, 5.53) and variable mean (figures 5.54, 5.55, 5.56) track profile. The effect of resonance for the sinusoidal track profile (figure 5.55) is also very small. The presence of the step in the profile (figure 5.56) is found to be not easily discernible.

5.3.8 Braking Torque and Skid

The braking torque (figures 5.57, 5.58, 5.59, 5.60, 5.61, 5.62, 5.63, 5.64) is a function of the ground reaction and μ the coefficient of friction. This torque is the control variable that is being varied so as to maintain the skid in the optimal range of 0.16 to 0.18. The brakes start acting only after the period of free roll.

At higher values of the ground velocity a small deviation in skid from the optimal range produces a large deviation in the coefficient of friction, whereas for lower values of ground velocity this deviation is much lower. Thus the range for optimal skid increases until at near zero velocity it extends up to full skid. It is seen therefore that initially the variation in skid (figures 5.57, 5.58, 5.59, 5.60, 5.61, 5.62, 5.63, 5.64) is small but as the ground velocity reduces the skid tends to go to higher values approaching full skid.

Control on the brakes is applied keeping the above variation in the friction coefficient in mind. The braking torque is varied so as to keep the angular deceleration of the wheel a constant, if as a consequence of this the wheel goes out of the optimal skid range a correction is made to the value of the braking torque. This results in a wide variation of the braking torque with time. The minimum value of the braking

torque is obviously zero corresponding to the free rolling condition. The wheel is also allowed to roll freely when the aircraft leaves the track or balloons.

Duration of continuous braking increases with increase in glide velocity (figures 5.57, 5.60, 5.61), specially in the latter stages of the landing run. Same is valid for the inclined track profile also (figure 5.62). The stepped track profile (figure 5.64) has braking characteristics similar to the flat track (figure 5.57). For the sinusoidal track (figure 5.63), however, the braking torque is discontinuous and put to zero more often as the aircraft leaves the track more often. This results in poorer braking, even though the magnitude of the braking torque is much higher than in the other cases.

5.3.9 Ground Velocity

The ground velocity (figures 5.1, 5.2, 5.3, 5.4, 5.5, 5.6, 5.7, 5.8) is seen to be almost linear except for the sinusoidal track (figure 5.7) where it is rippled. Each ripple corresponding to the period when the aircraft leaves the runway. The deceleration in aircraft ground velocity at the start of the run is seen to be higher for higher values of sink velocity. This is due to the increase in retarding friction force which is a consequence of the increased reaction due to the landing impact.

5.3.10 Braking Distance

The expected ground roll for the aircraft used in this study is 740 m during landing. In the present study the ground roll (figures 5.1 — 5.8) is found to vary from 416.6 metres for the stepped track (figure 5.8) to 493.0 metres for the inclined track (figure 5.6). This shows a marked reduction in the ground roll and the efficacy of the proposed braking system. The increased ground roll for the inclined runway is unexpected and is perhaps due to the weight component of the aircraft being neglected

in the present formulation.

The ground roll is found to vary with the track mean profile (figures 5.1, 5.6, 5.7, 5.8) and is dependent very slightly on the sink (figures 5.1, 5.2, 5.3) and glide (figures 5.1, 5.4, 5.5) velocities. It reduces marginally with increase in sink velocity and shows a small increase with the increase in glide velocity.

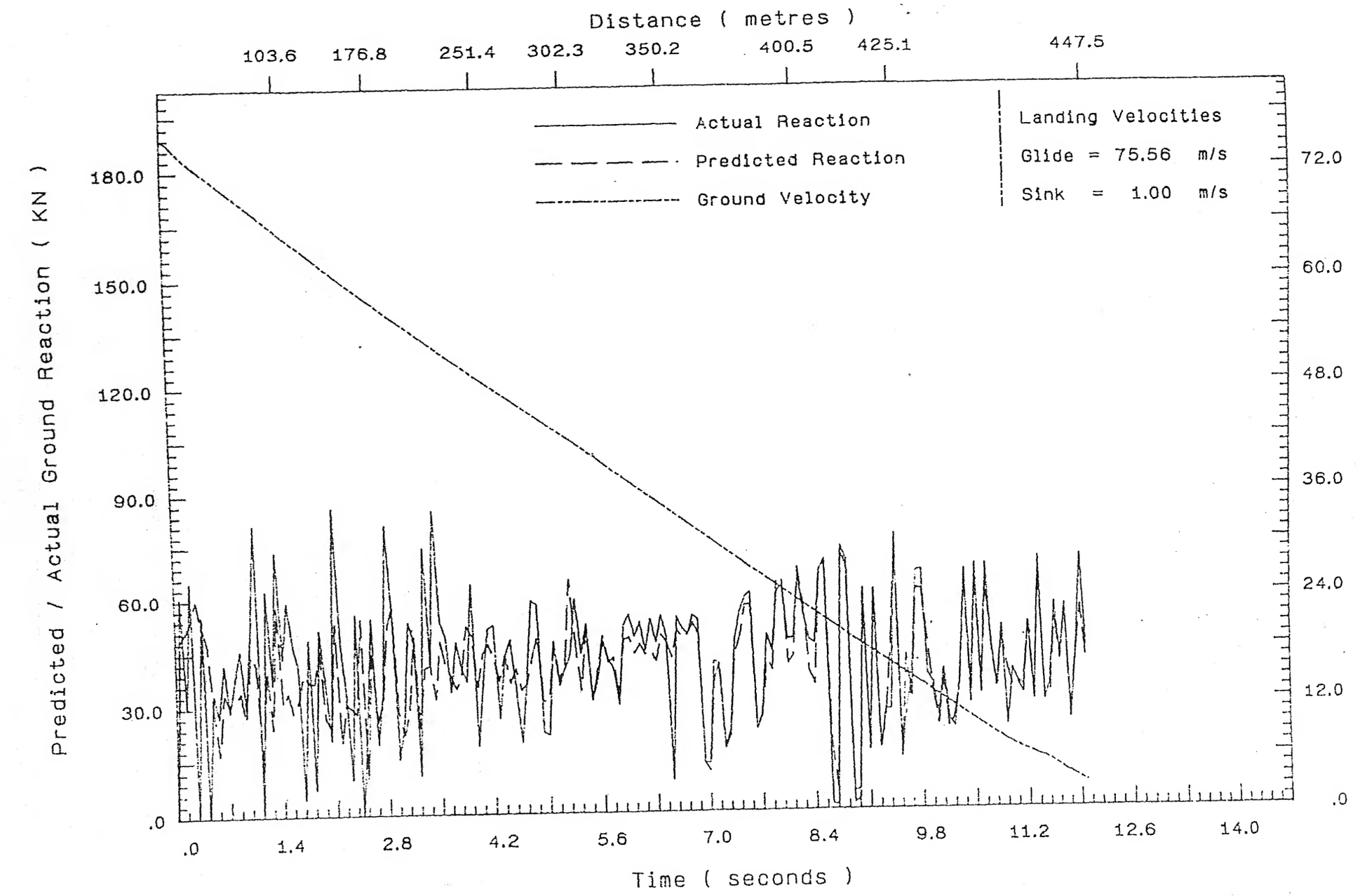

Figure 5.1: Predicted and actual ground reaction for flat runway , glide velocity = 75.56 $\frac{m}{s}$, sink velocity = 1.0 $\frac{m}{s}$

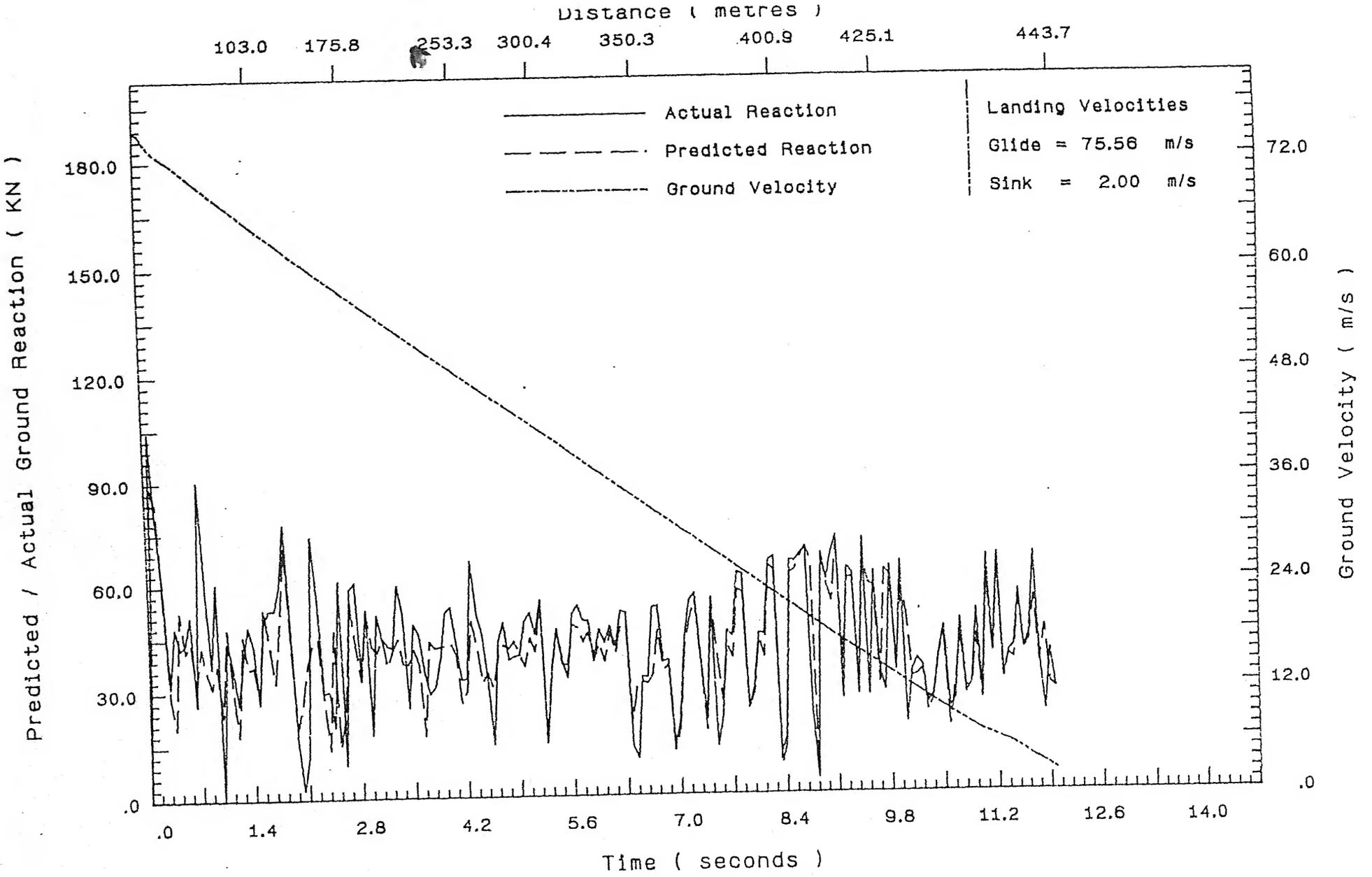

Figure 5.2: Predicted and actual ground reaction for flat runway , glide velocity = 75.56 $\frac{m}{s}$, sink velocity = 2.0 $\frac{m}{s}$

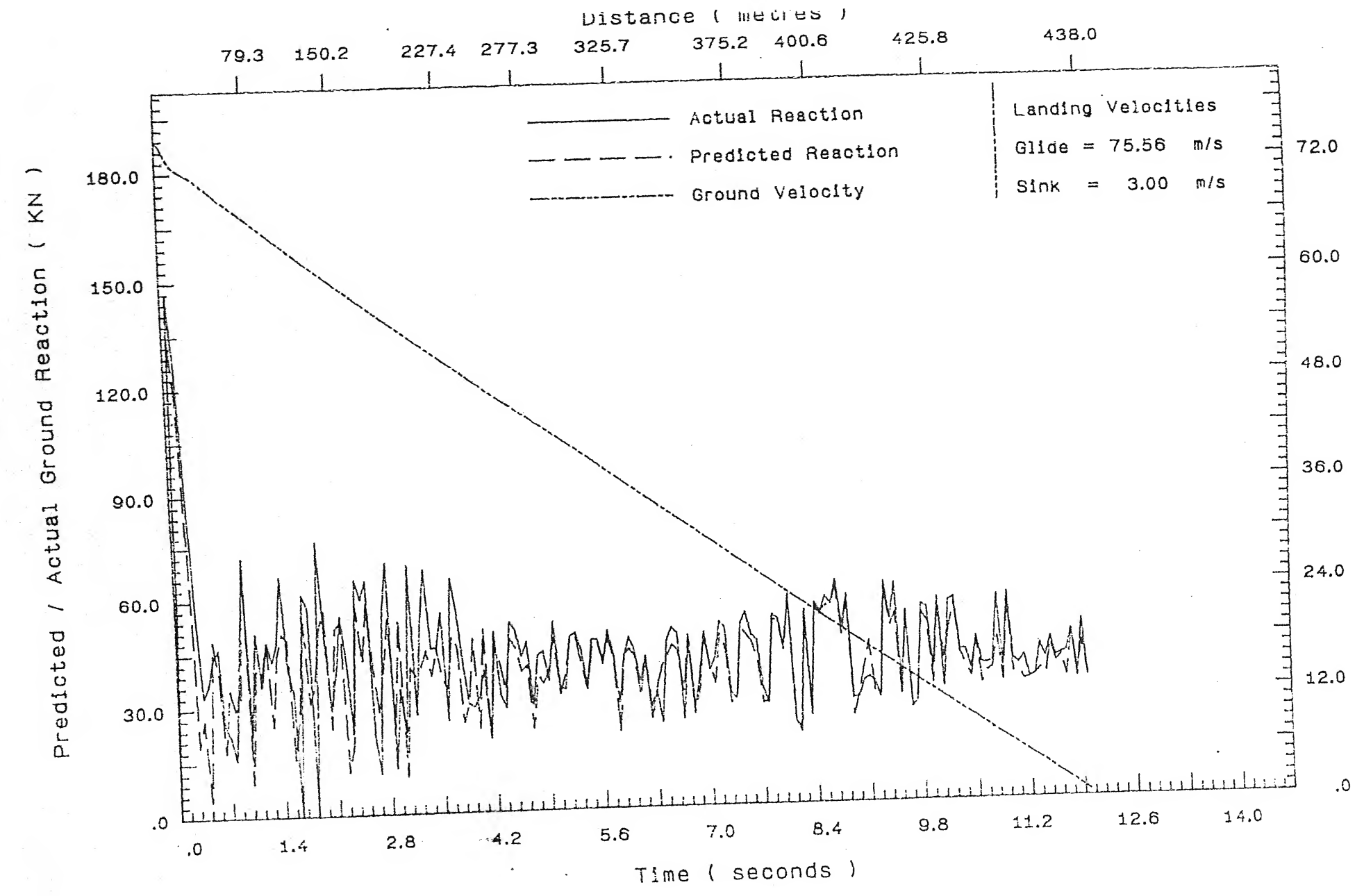

Figure 5.3: Predicted and actual ground reaction for flat runway , glide velocity = 75.56 $\frac{m}{s}$, sink velocity = 3.0 $\frac{m}{s}$

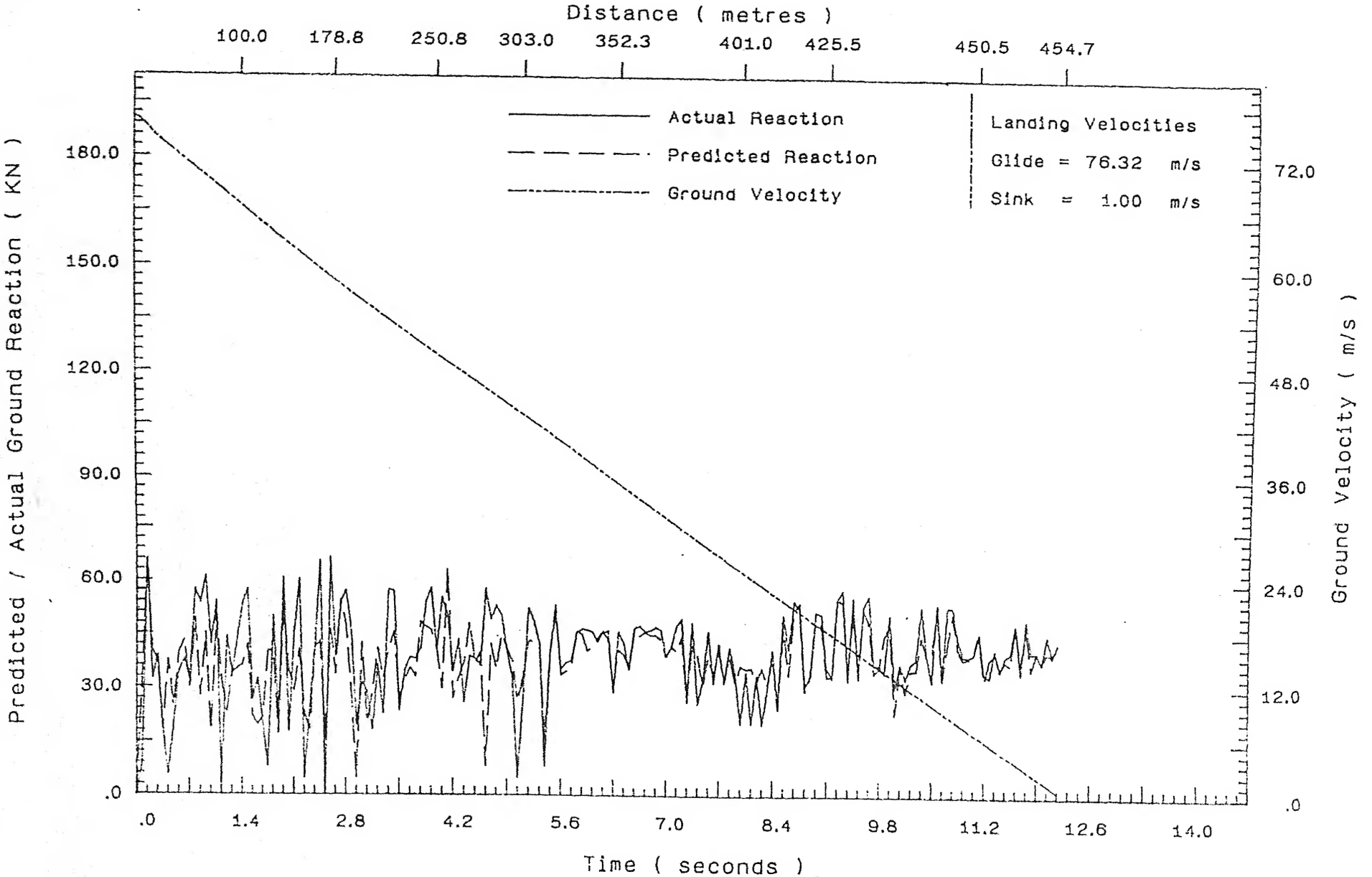

Figure 5.4: Predicted and actual ground reaction for flat runway , glide velocity = 76.32 $\frac{m}{s}$, sink velocity = 1.0 $\frac{m}{s}$

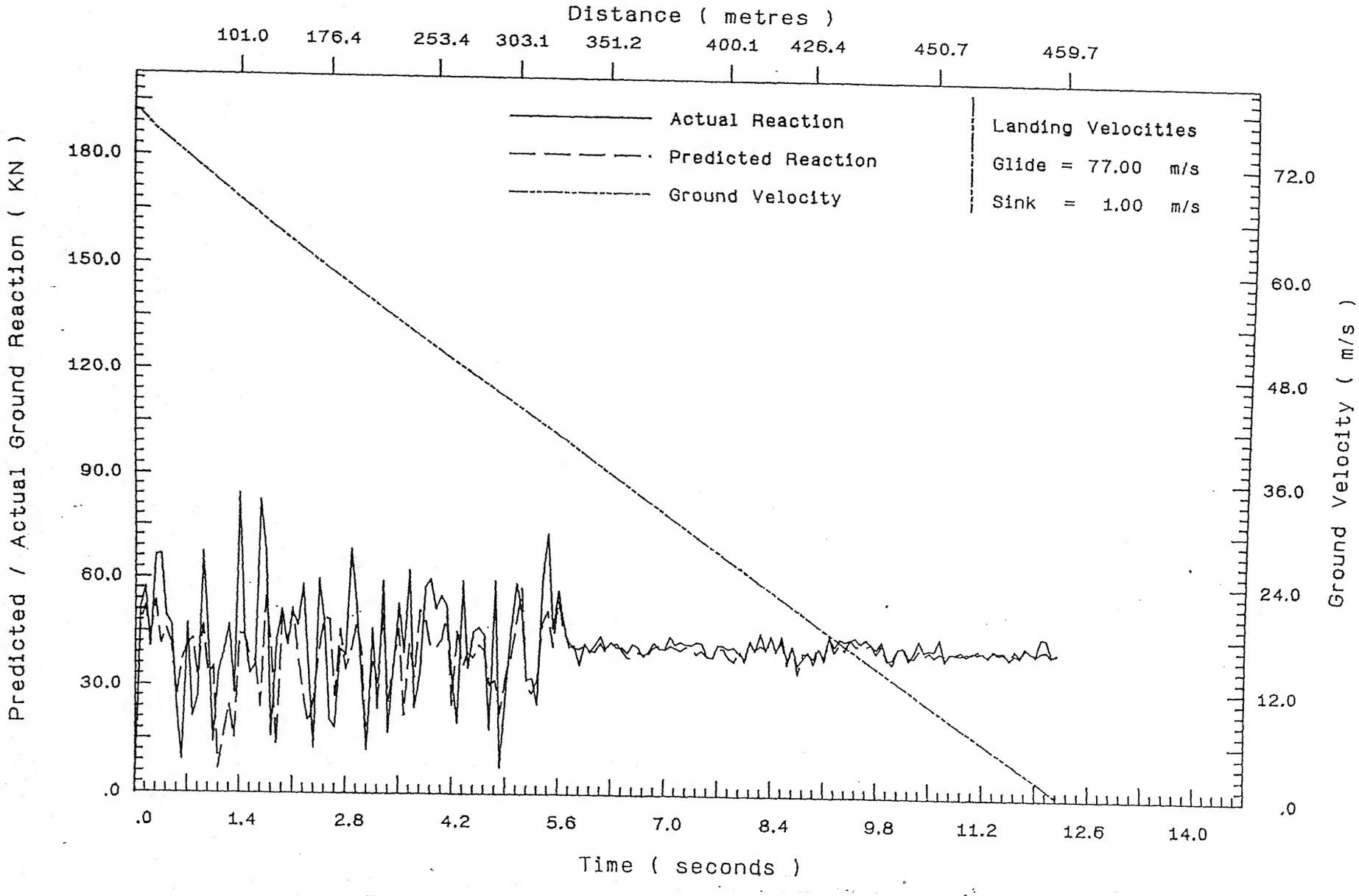

Figure 5.5: Predicted and actual ground reaction for flat runway , glide velocity = 77.00 $\frac{m}{s}$, sink velocity = 1.0 $\frac{m}{s}$

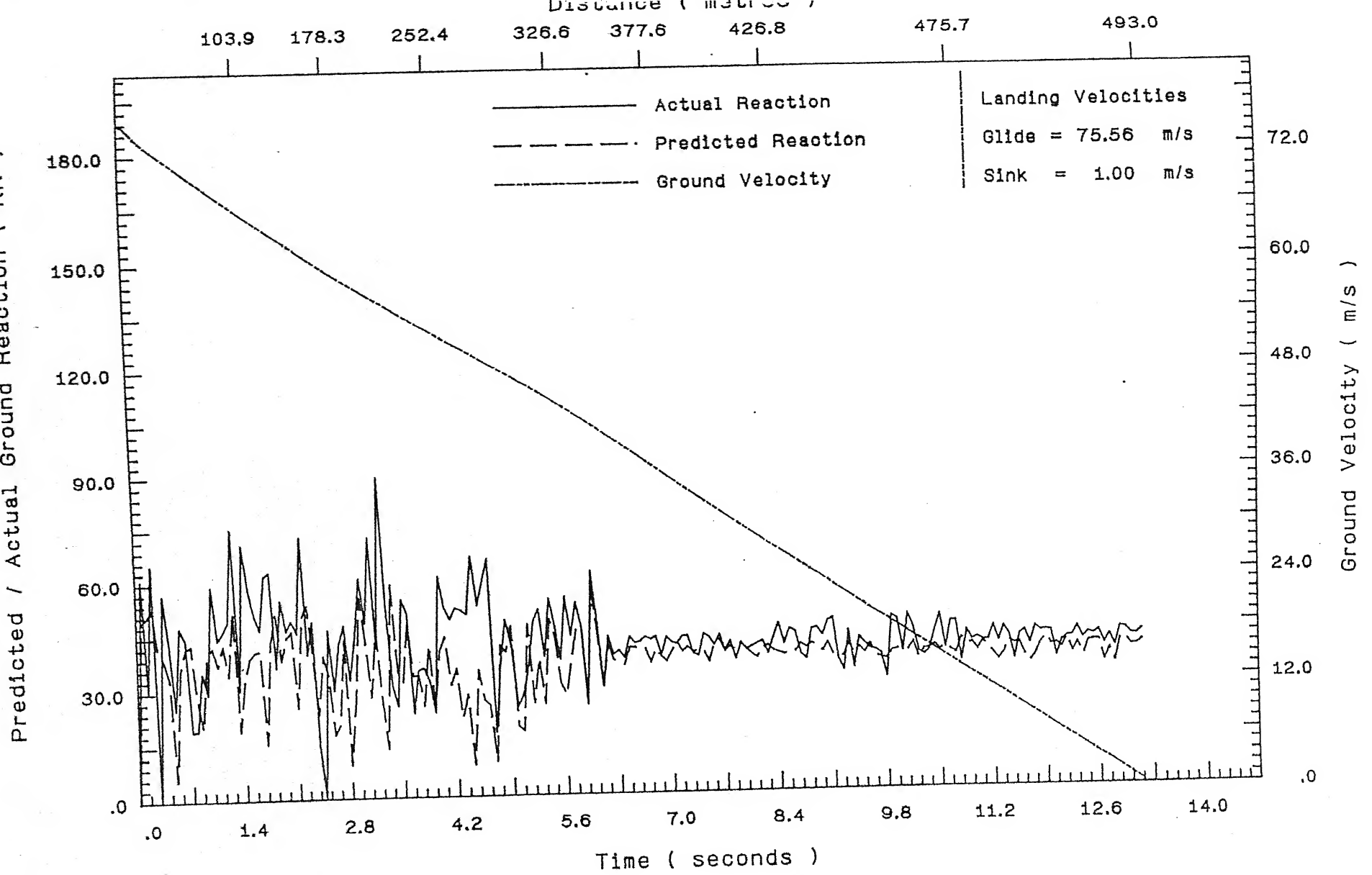

Figure 5.6: Predicted and actual ground reaction for inclined runway , glide velocity = 75.56 $\frac{m}{s}$, sink velocity = 1.0 $\frac{m}{s}$

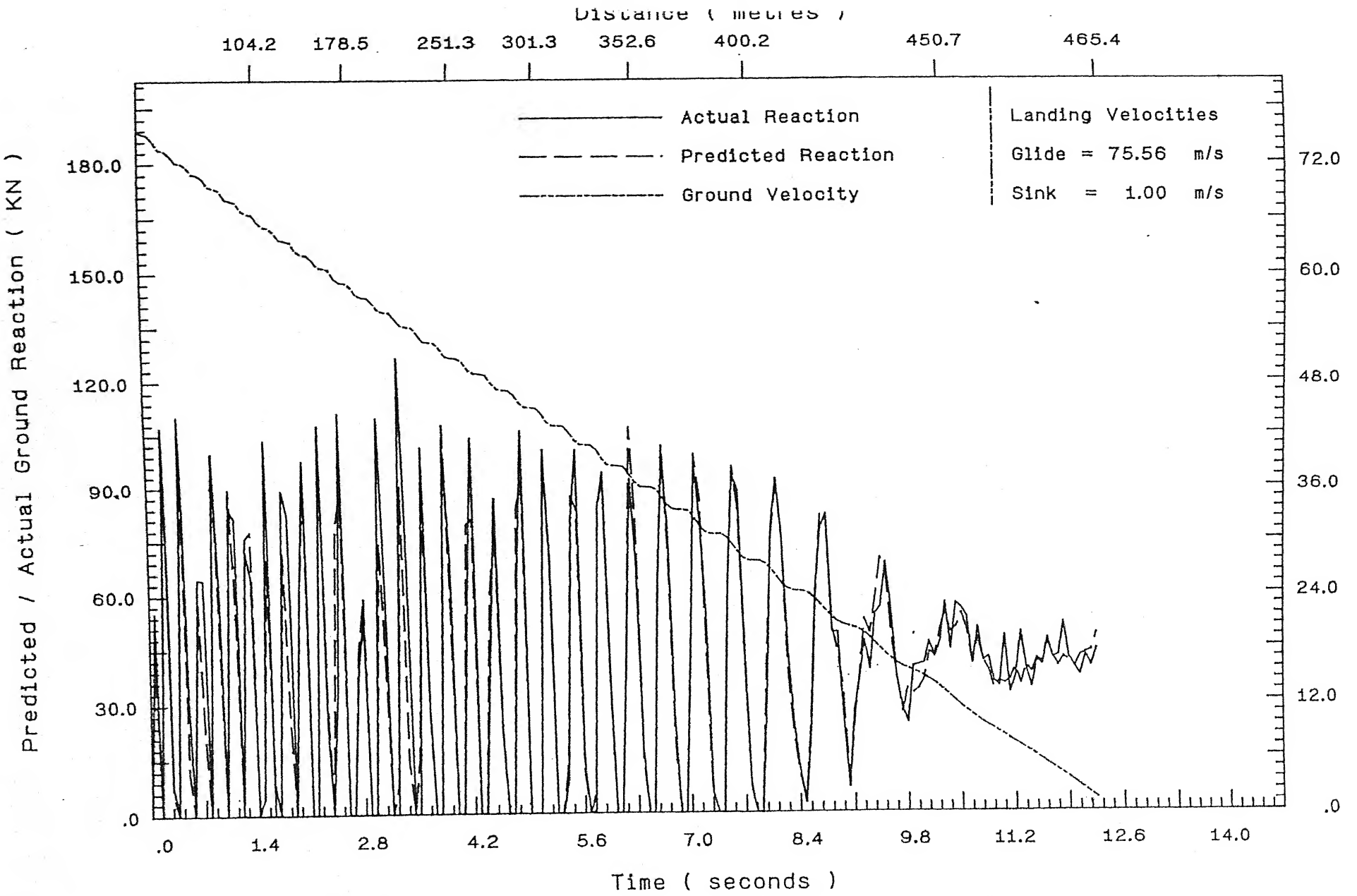

Figure 5.7: Predicted and actual ground reaction for sinusoidal runway , glide velocity = 75.56 $\frac{m}{s}$, sink velocity = 1.0 $\frac{m}{s}$

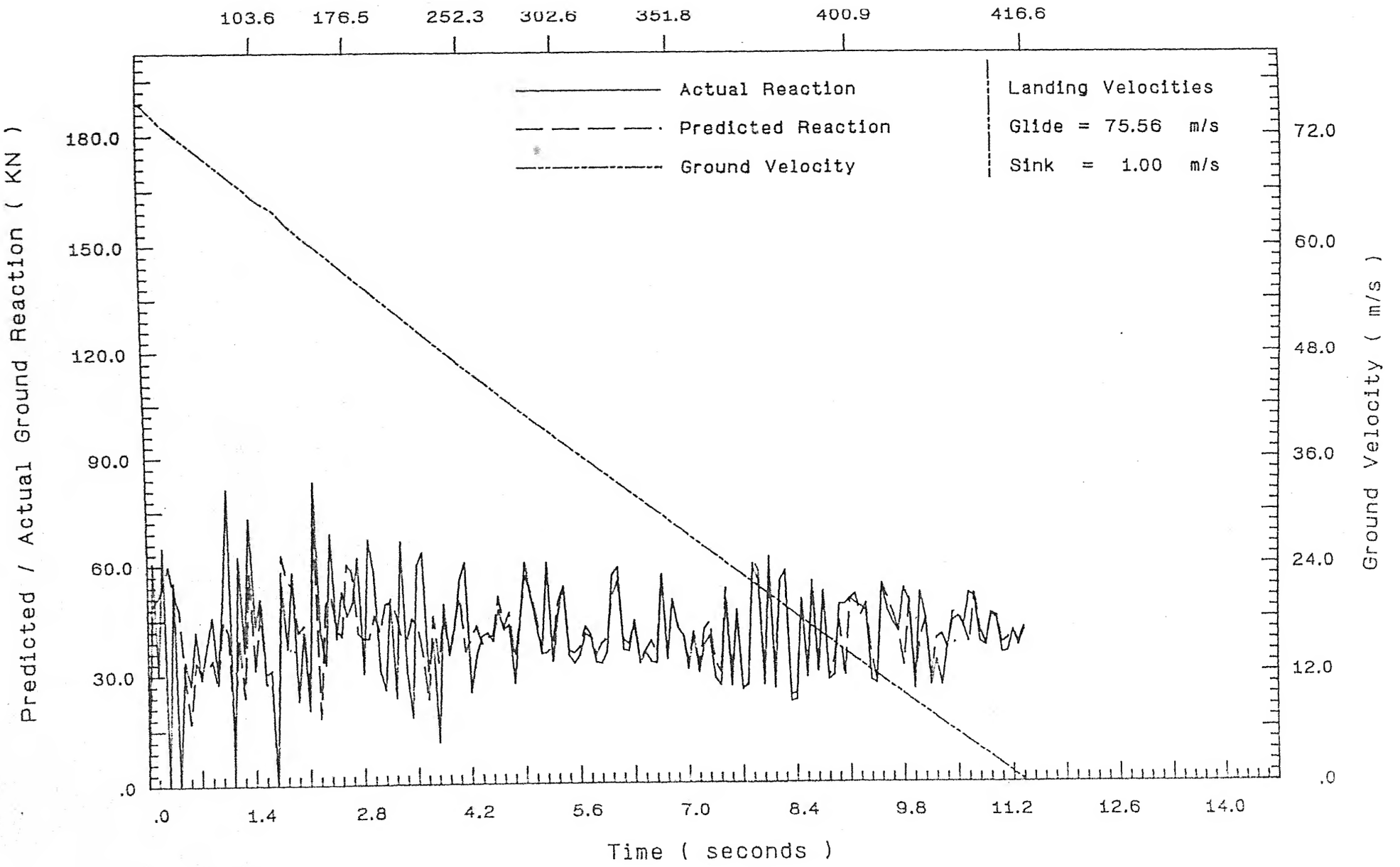

Figure 5.8: Predicted and actual ground reaction for stepped runway , glide velocity = 75.56 $\frac{m}{s}$, sink velocity = 1.0 $\frac{m}{s}$

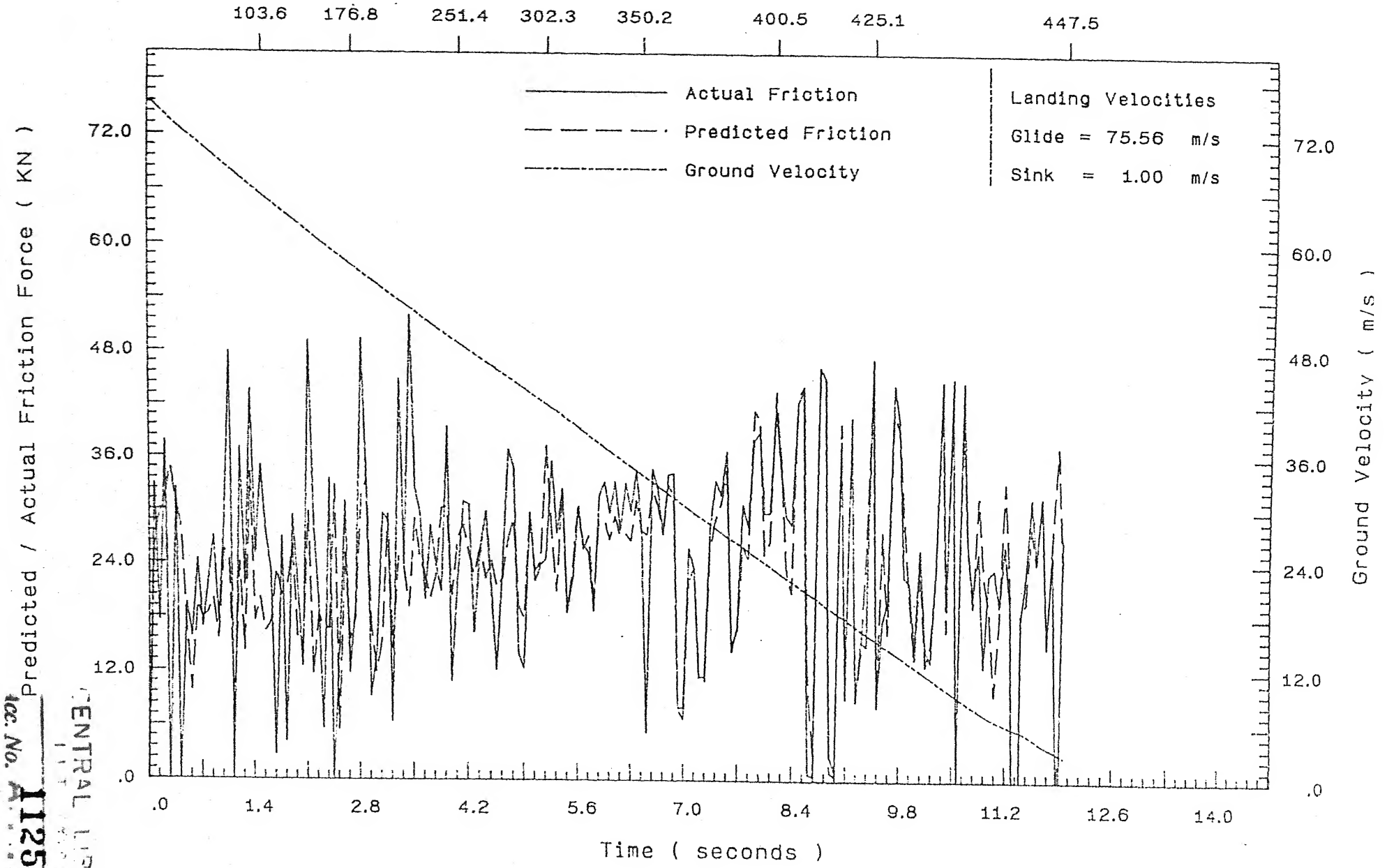

Figure 5.9: Predicted and actual retarding friction for flat runway , glide velocity = 75.56 $\frac{m}{s}$, sink velocity = 1.0 $\frac{m}{s}$

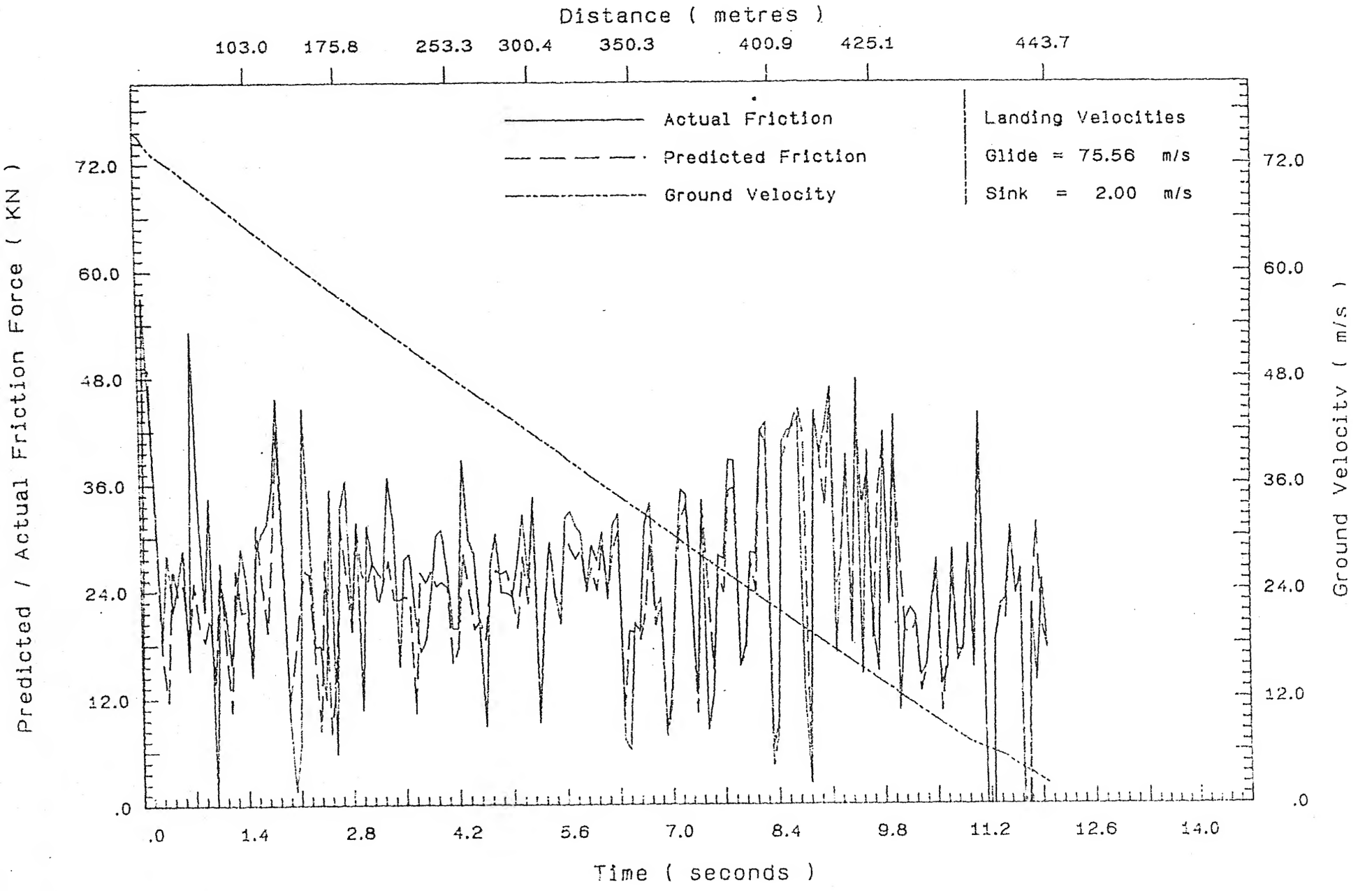

Figure 5.10: Predicted and actual retarding friction for flat runway , glide velocity = 75.56 $\frac{m}{s}$, sink velocity = 2.0 $\frac{m}{s}$

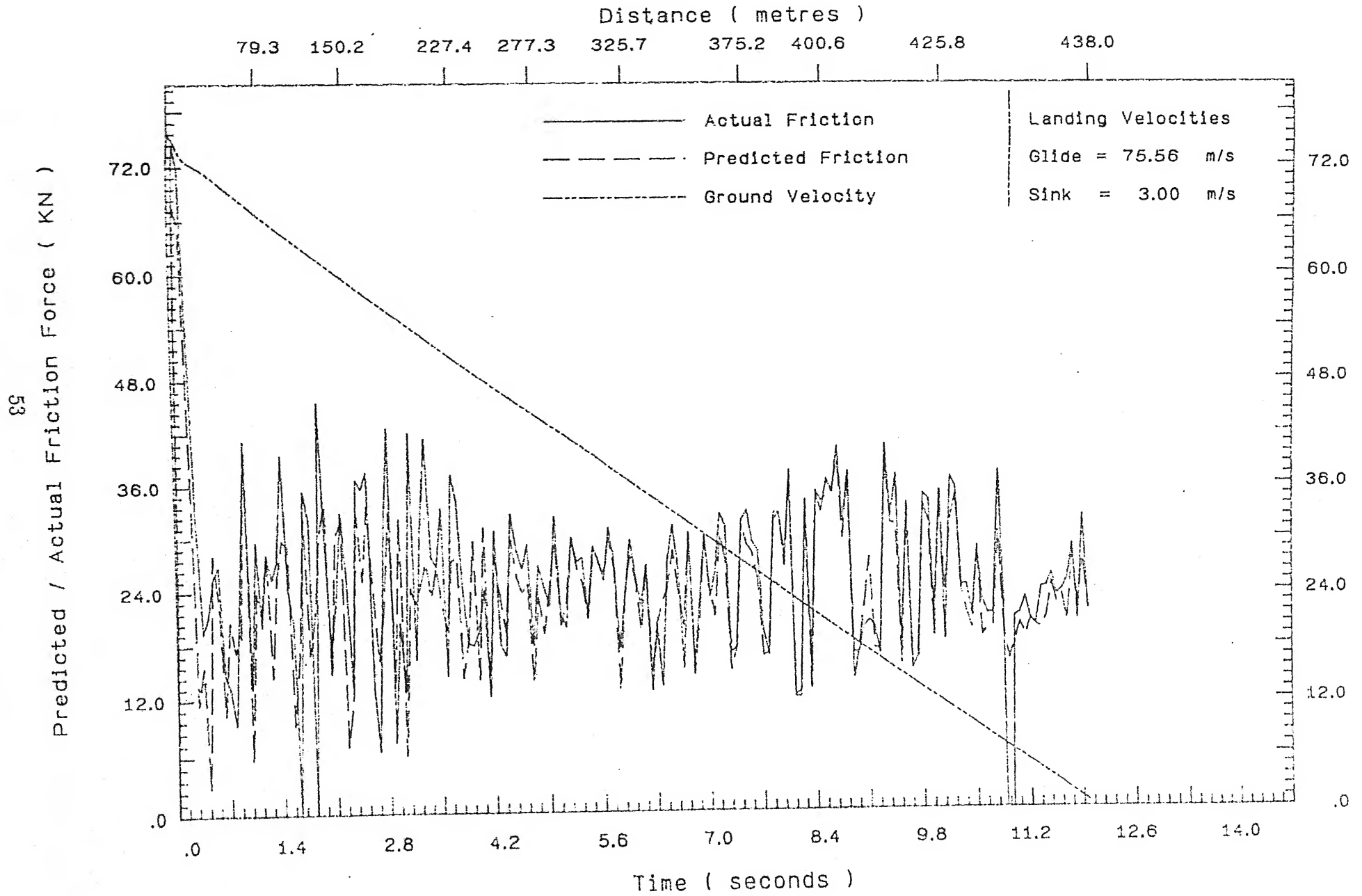

Figure 5.11: Predicted and actual retarding friction for flat runway , glide velocity = 75.56 $\frac{m}{s}$, sink velocity = 3.0 $\frac{m}{s}$

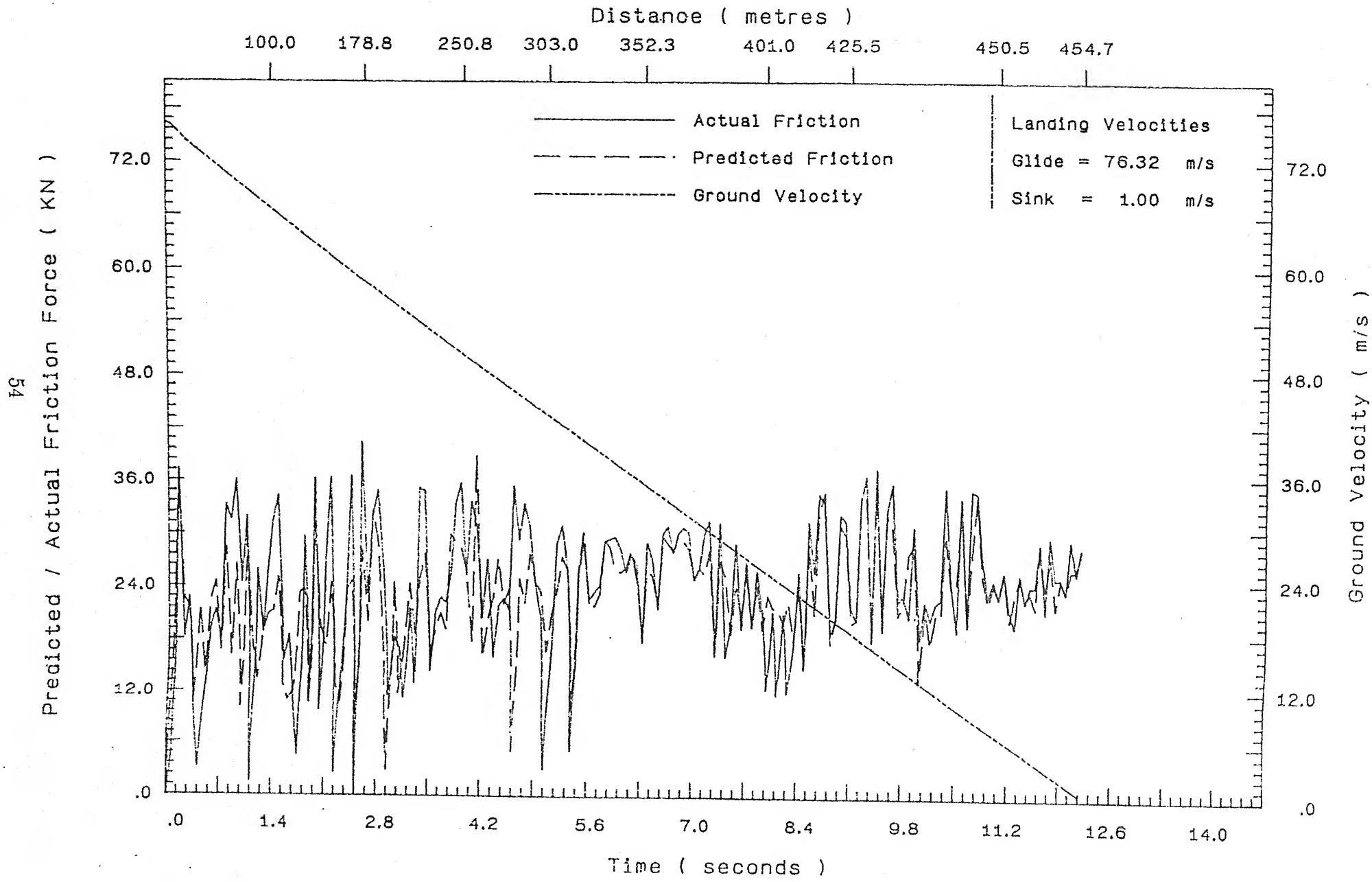

Figure 5.12: Predicted and actual retarding friction for flat runway , glide velocity = 76.32 $\frac{m}{s}$, sink velocity = 1.0 $\frac{m}{s}$

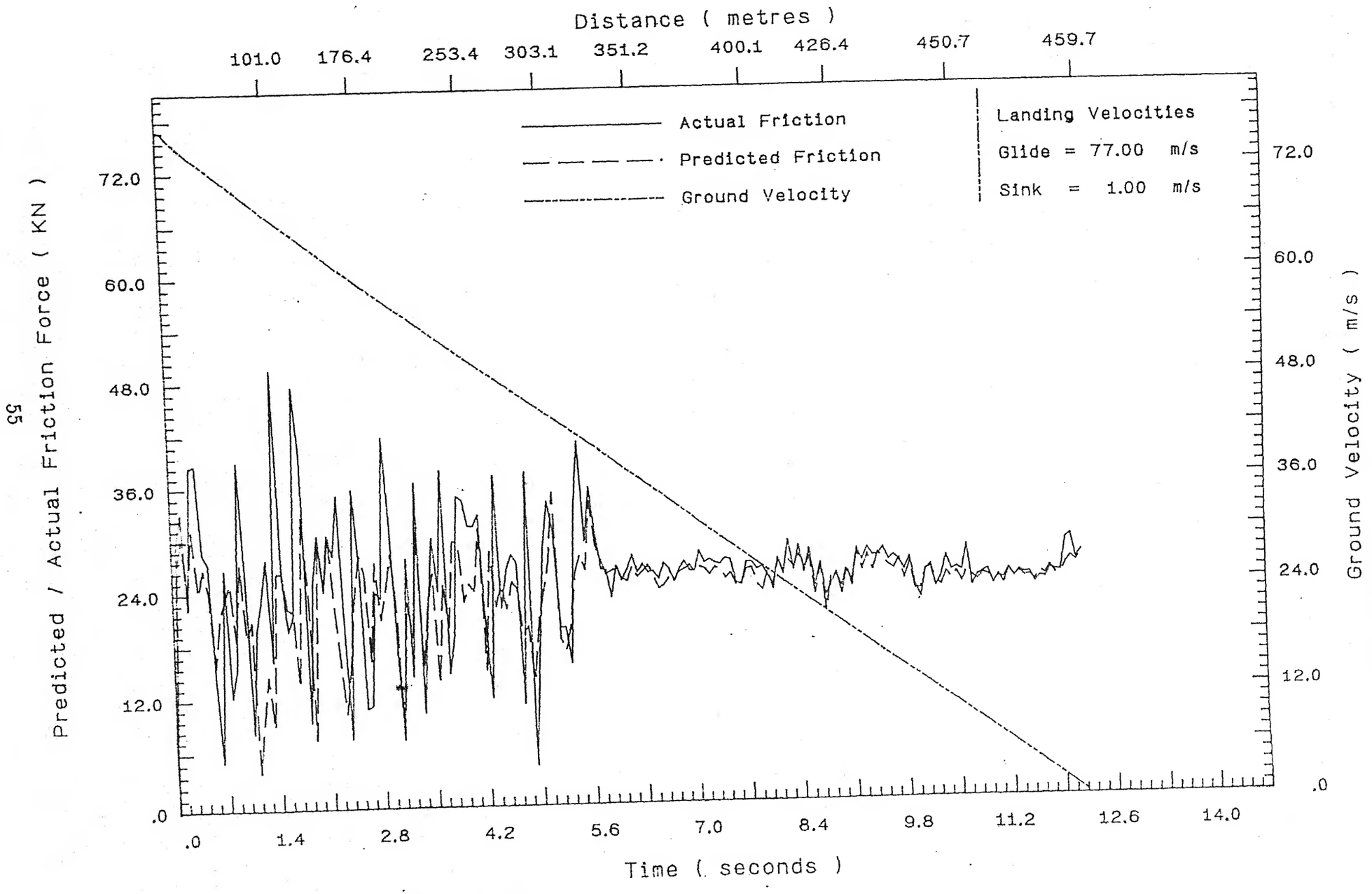

Figure 5.13: Predicted and actual retarding friction for flat runway , glide velocity = 77.00 $\frac{m}{s}$, sink velocity = 1.0 $\frac{m}{s}$

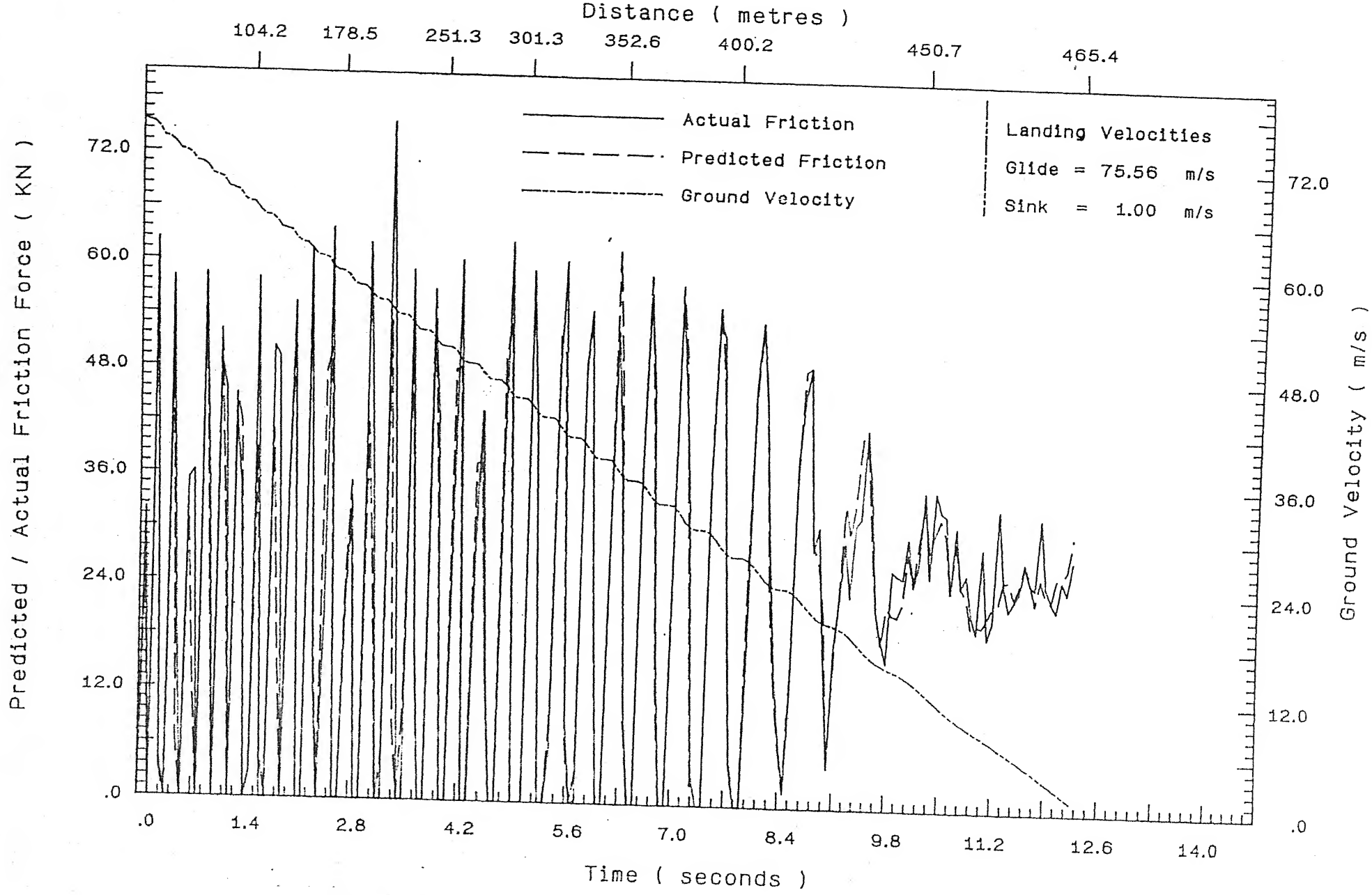

Figure 5.15: Predicted and actual retarding friction for sinusoidal runway , glide velocity = 75.56 $\frac{m}{s}$, sink velocity = 1.0 $\frac{m}{s}$

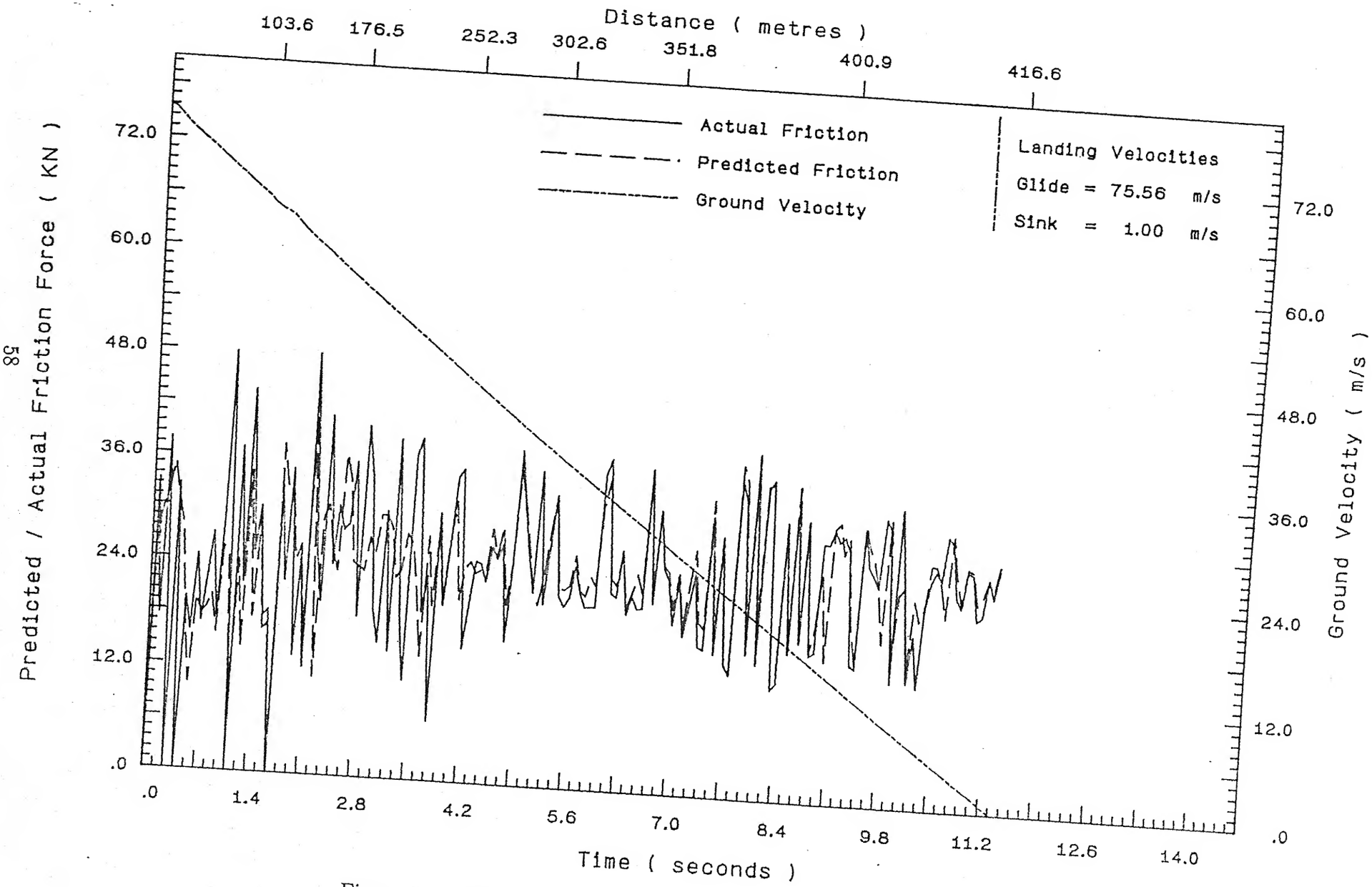

Figure 5.16: Predicted and actual retarding friction for stepped runway , glide velocity = 75.56 $\frac{m}{s}$, sink velocity = 1.0 $\frac{m}{s}$

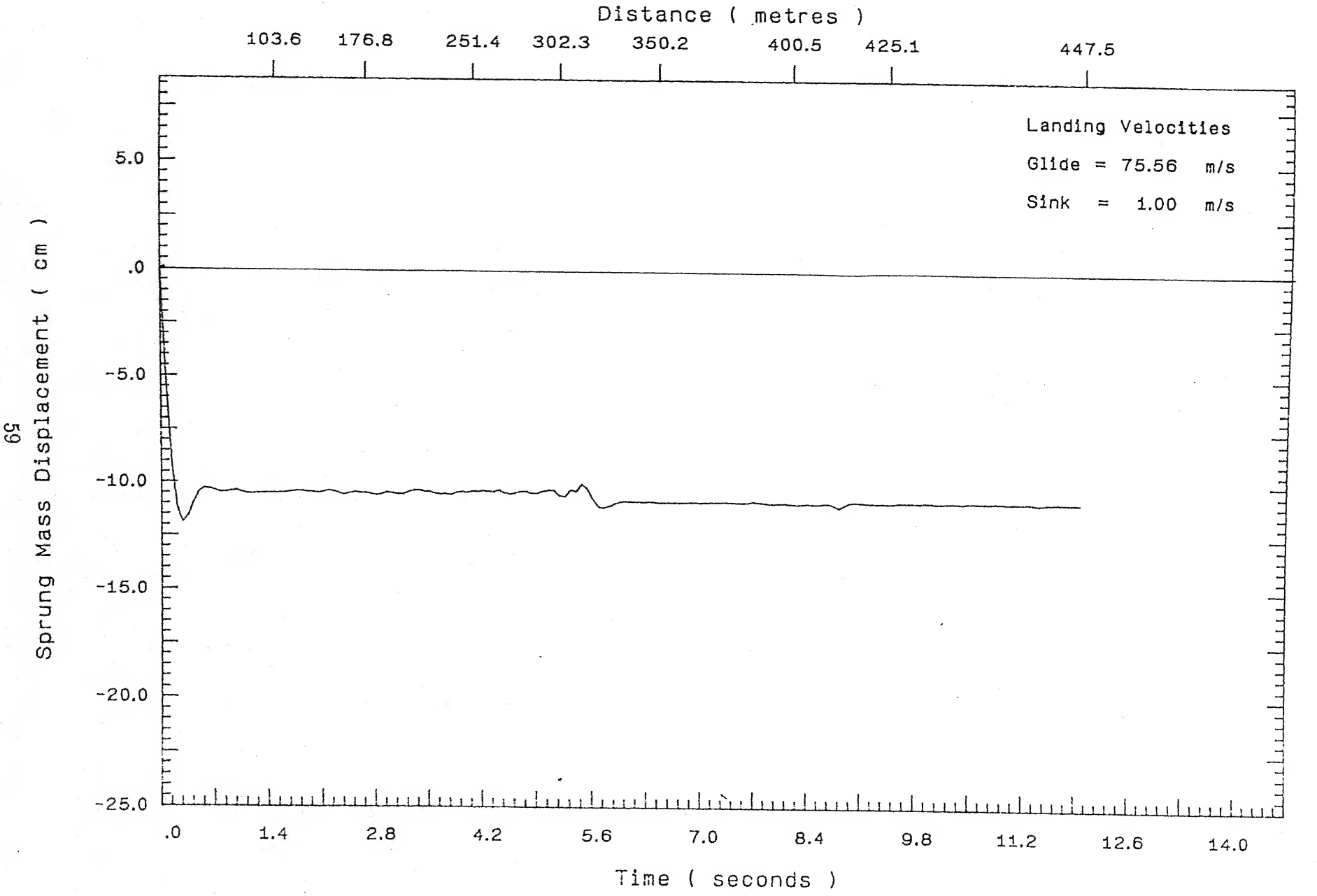

Figure 5.17: Sprung mass displacement for flat runway , glide velocity = 75.56 $\frac{m}{s}$, sink velocity = 1.0 $\frac{m}{s}$

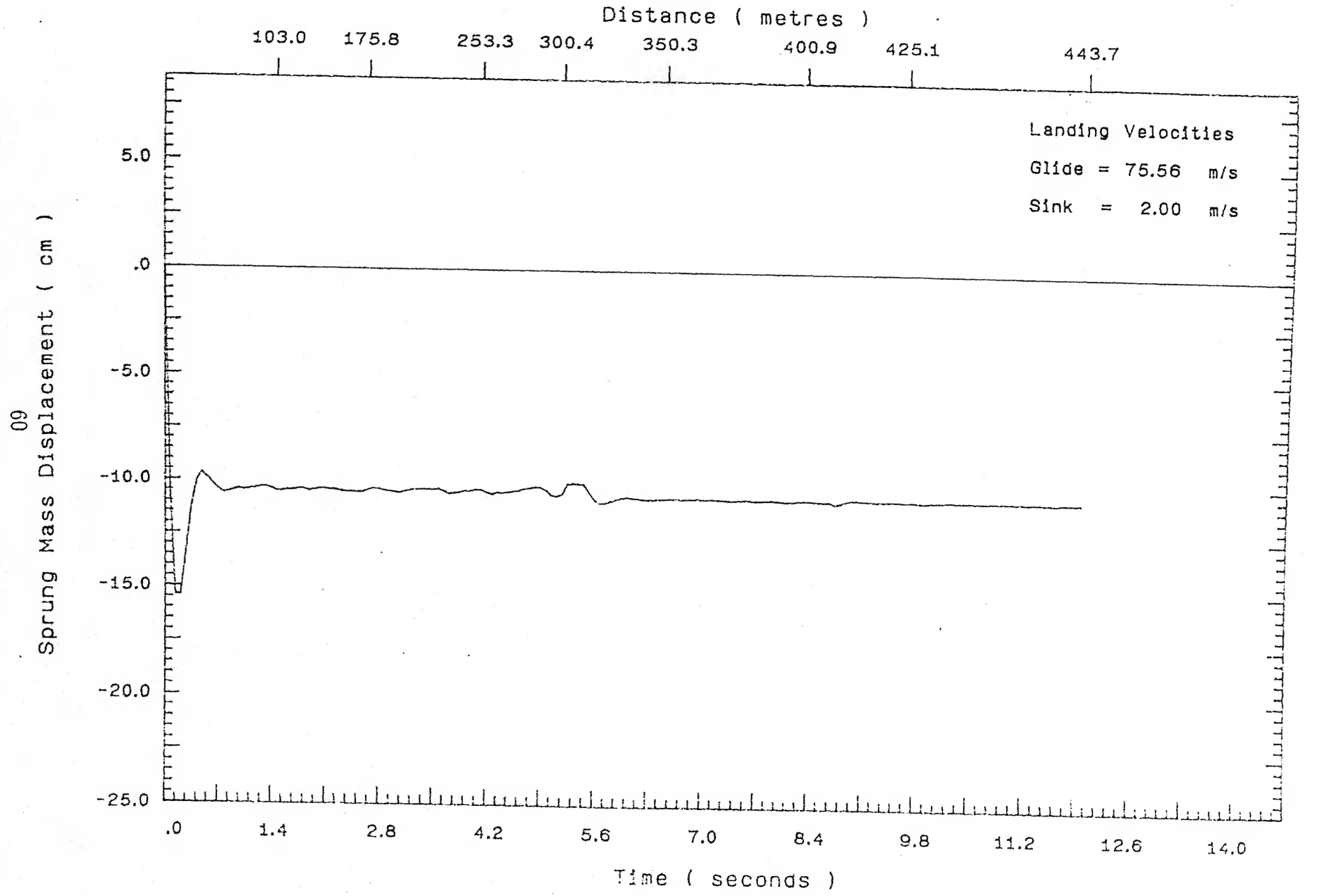

Figure 5.18: Sprung mass displacement for flat runway , glide velocity = 75.56 $\frac{m}{s}$, sink velocity = 2.0 $\frac{m}{s}$

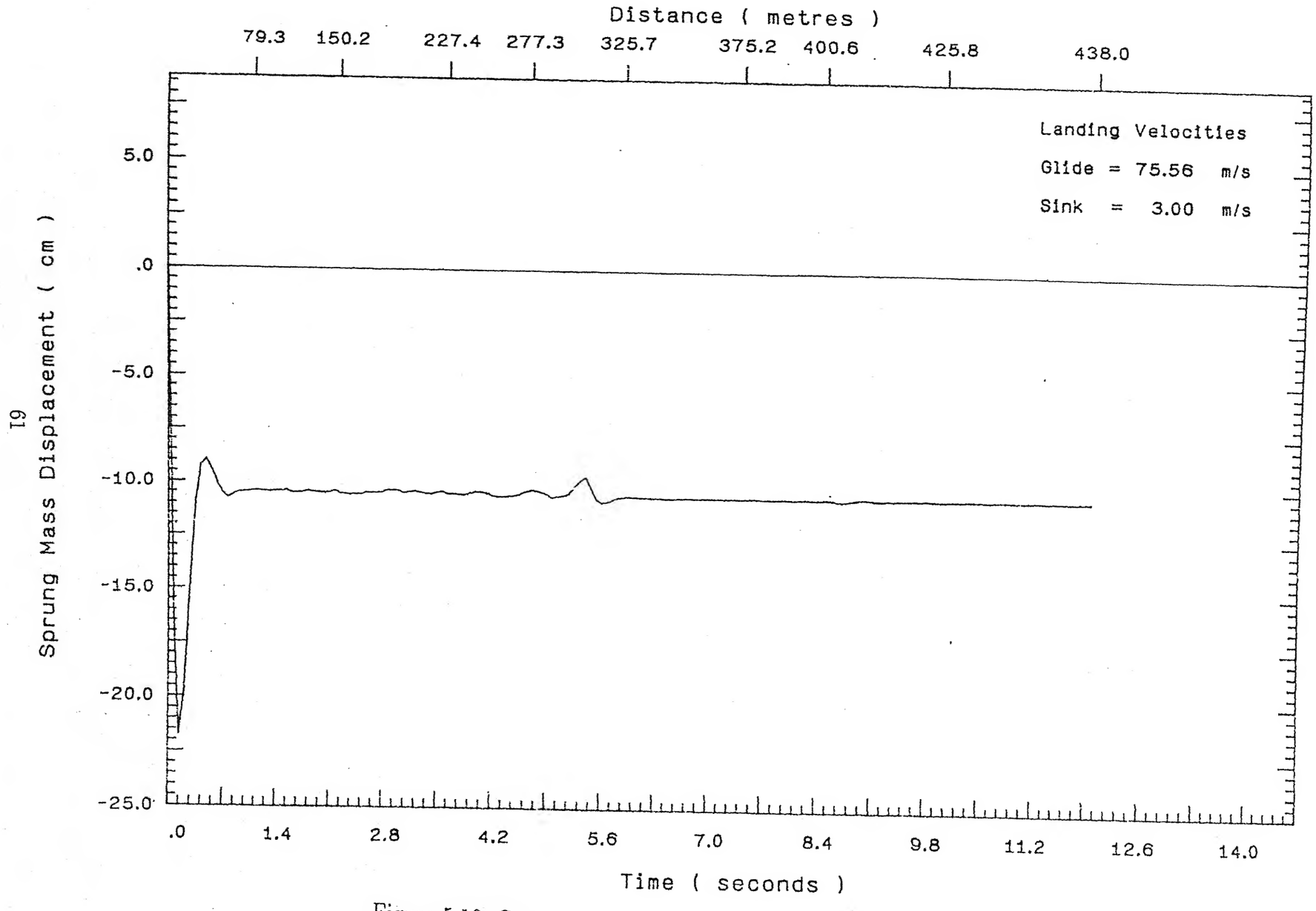

Figure 5.19: Sprung mass displacement for flat runway , glide velocity = 75.56 $\frac{m}{s}$, sink velocity = 3.0 $\frac{m}{s}$

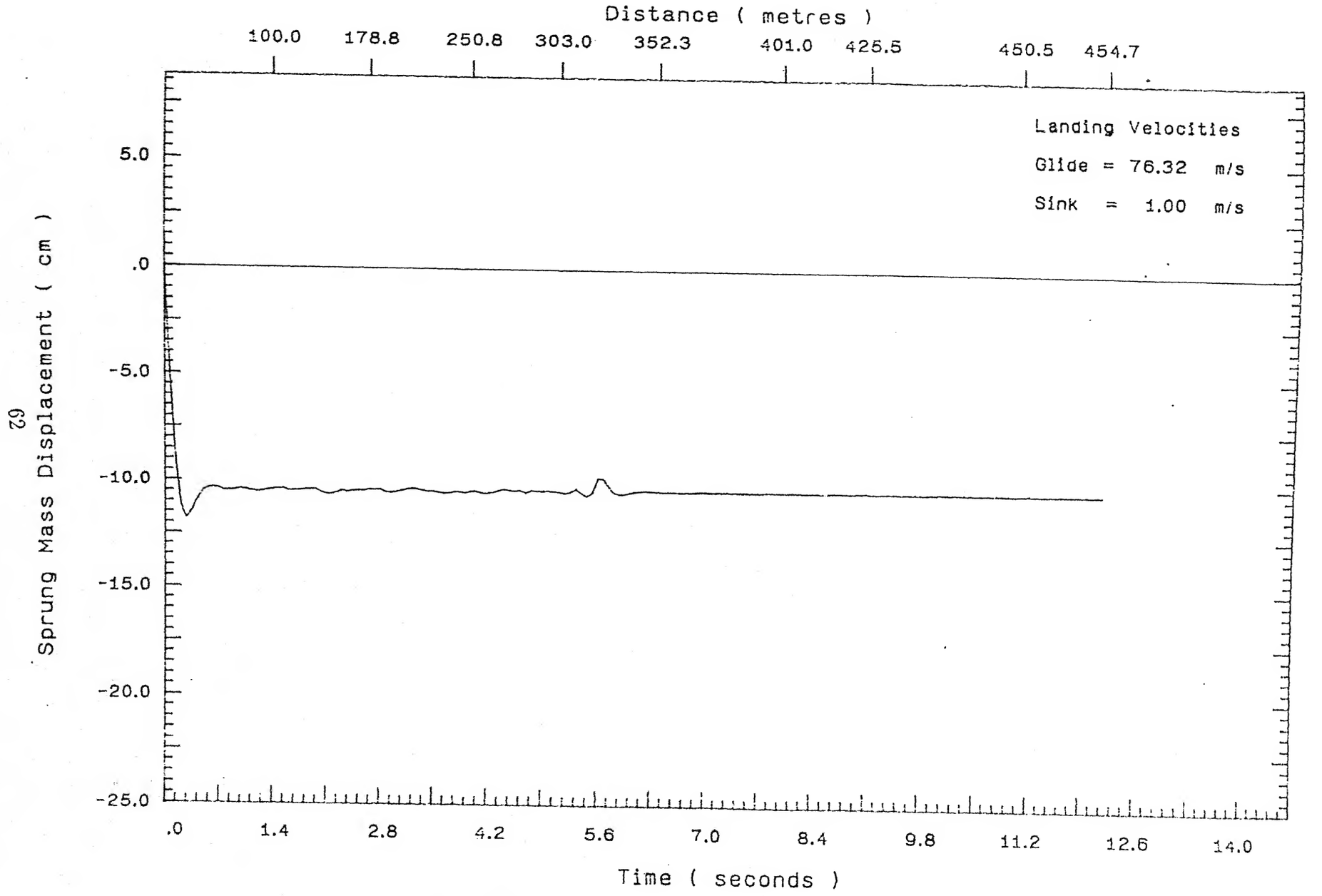

Figure 5.20: Sprung mass displacement for flat runway , glide velocity = 76.32 $\frac{m}{s}$, sink velocity = 1.0 $\frac{m}{s}$

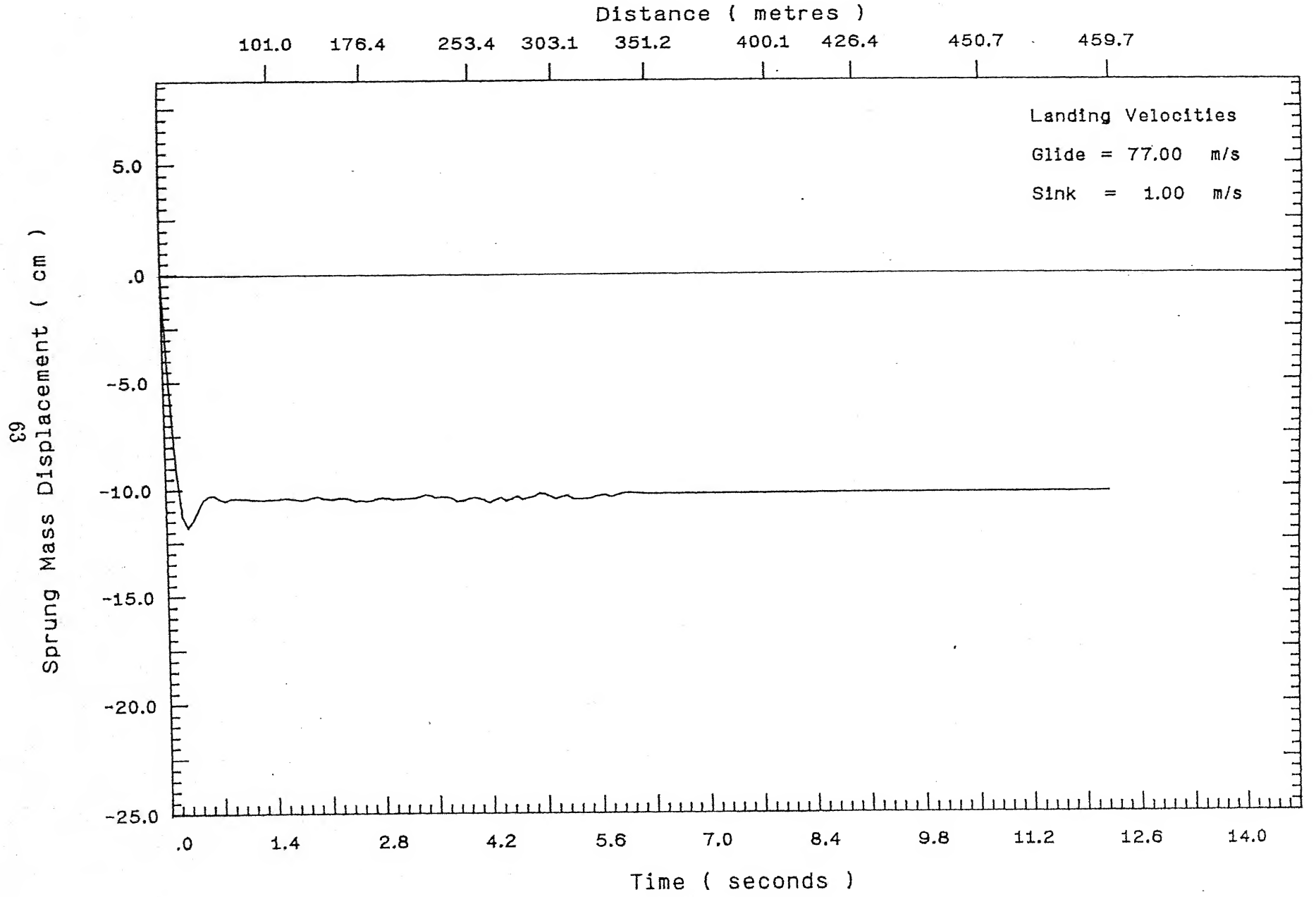

Figure 5.21: Sprung mass displacement for flat runway ,
glide velocity = 77.00 $\frac{m}{s}$, sink velocity = 1.0 $\frac{m}{s}$

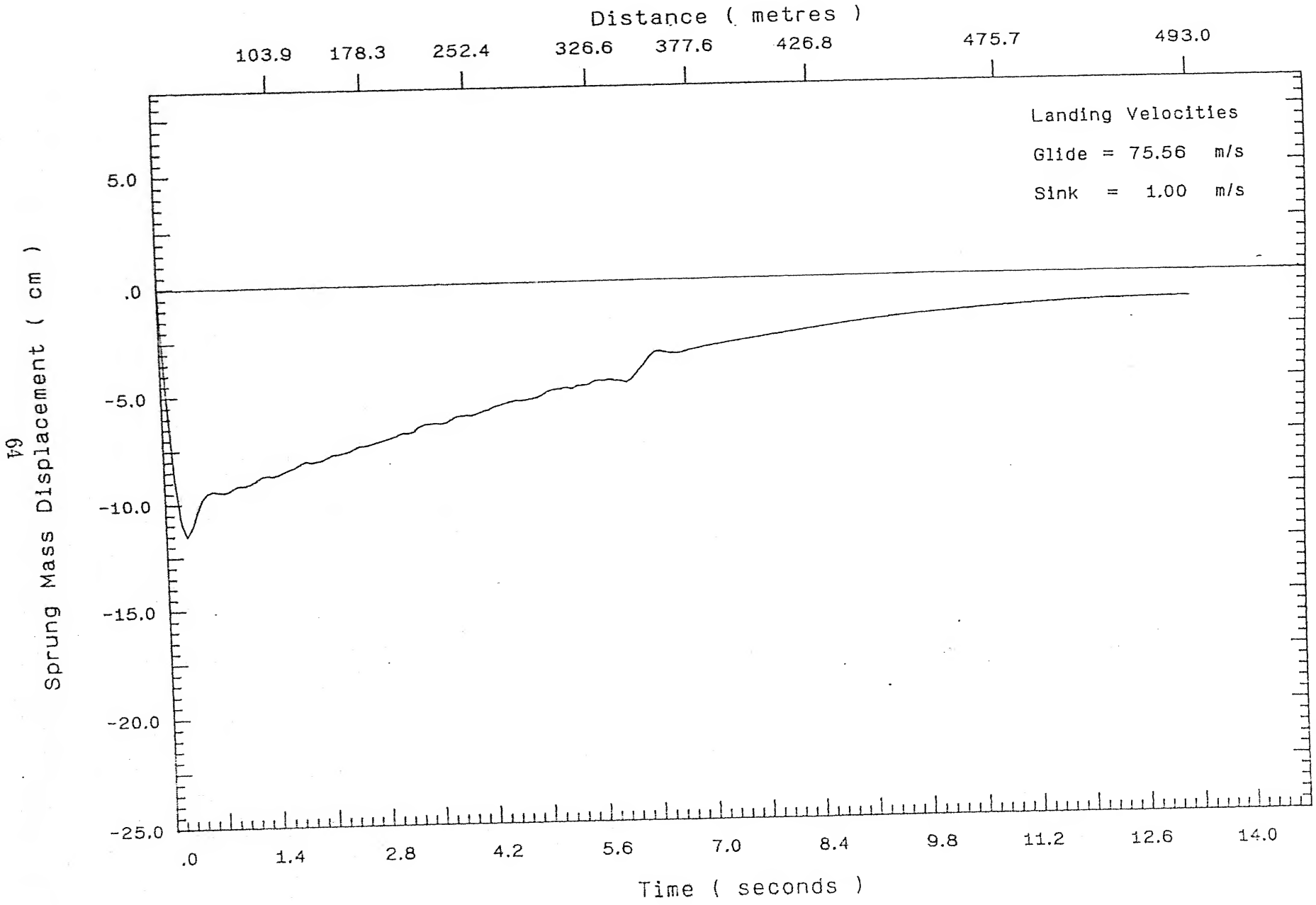

Figure 5.22: Sprung mass displacement for inclined runway , glide velocity = 75.56 $\frac{m}{s}$, sink velocity = 1.0 $\frac{m}{s}$

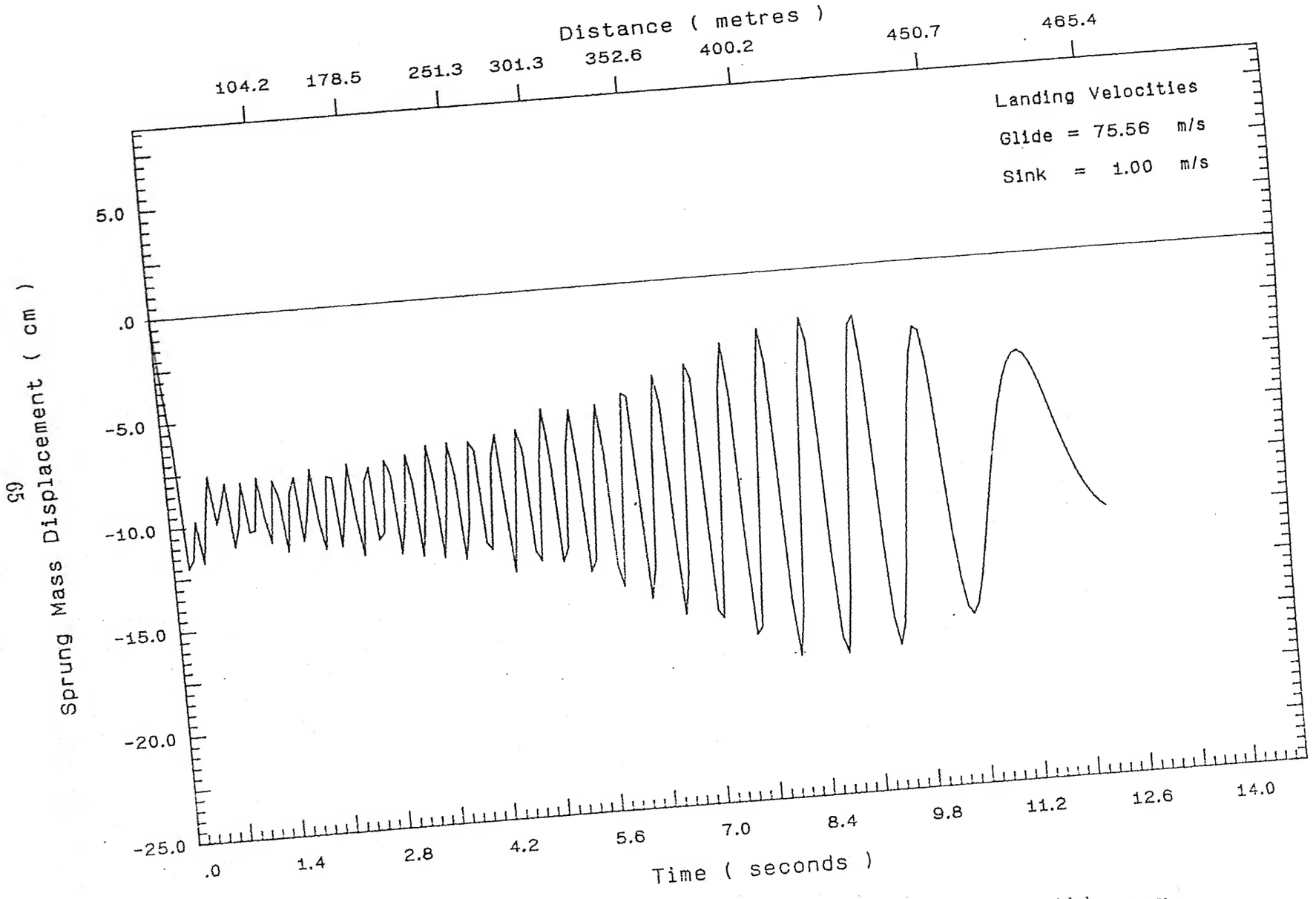

Figure 5.23: Sprung mass displacement for sinusoidal runway , glide velocity = 75.56 $\frac{m}{s}$, sink velocity = 1.0 $\frac{m}{s}$

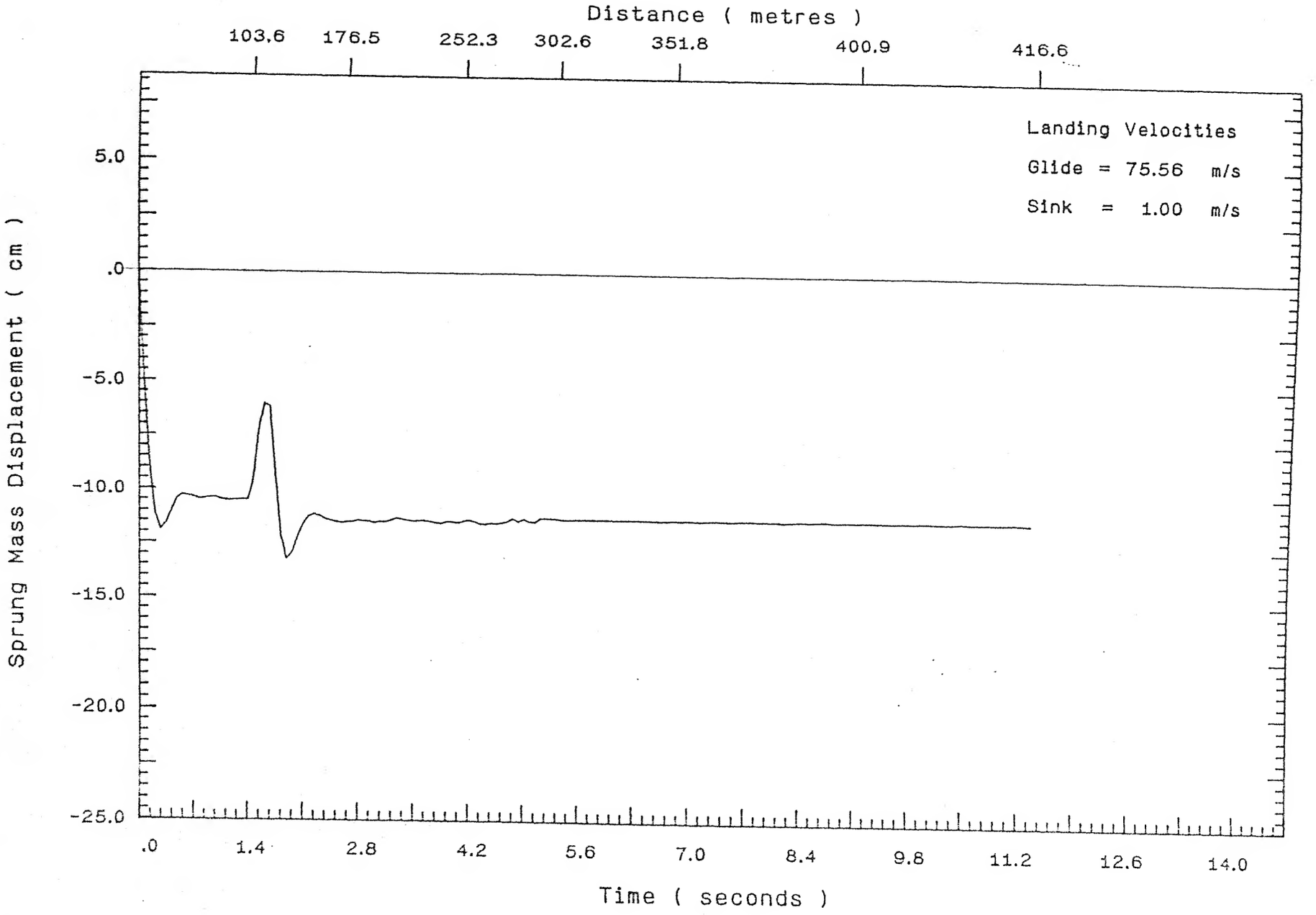

Figure 5.24: Sprung mass displacement for stepped runway , glide velocity = 75.56 $\frac{m}{s}$, sink velocity = 1.0 $\frac{m}{s}$

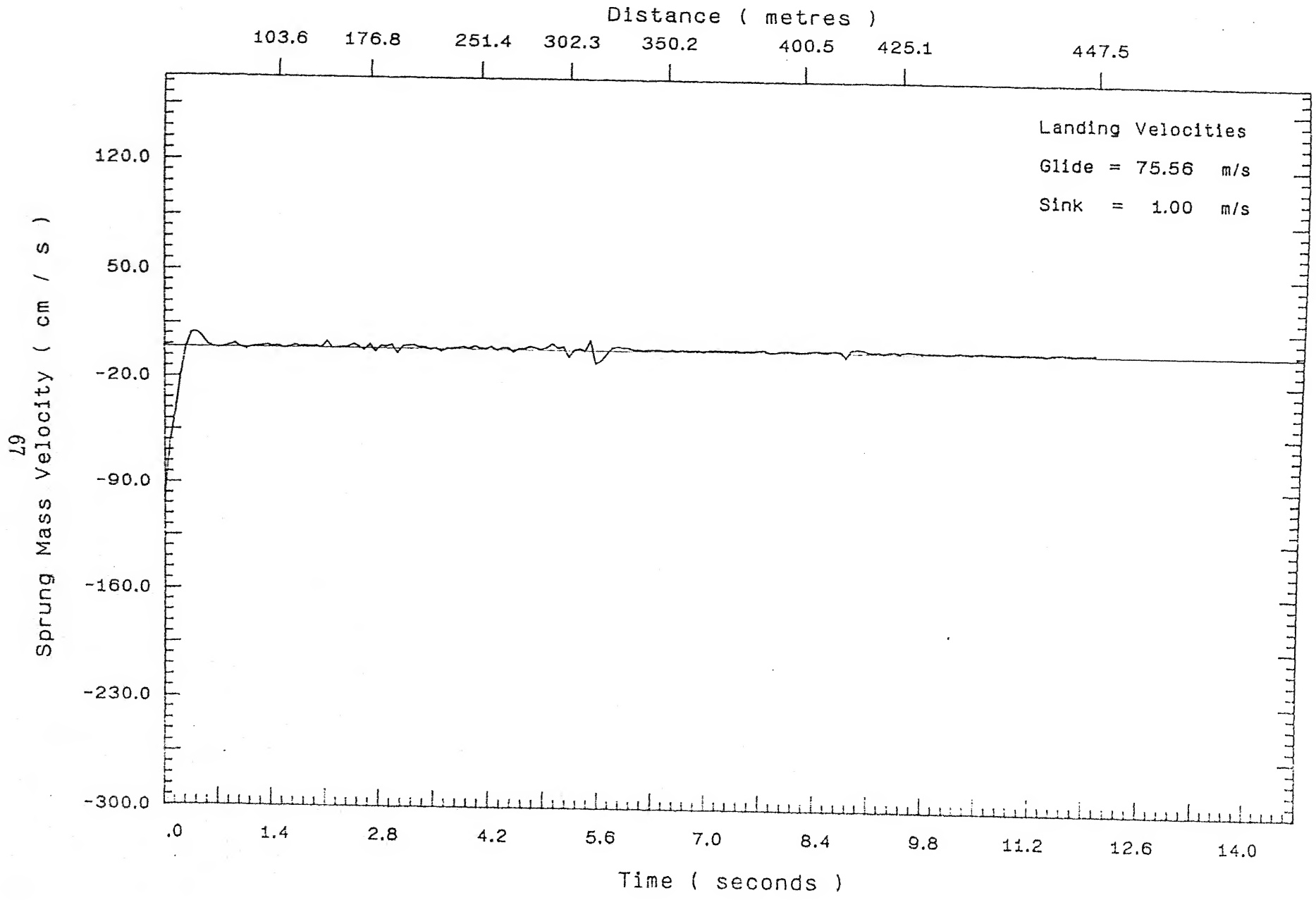

Figure 5.25: Sprung mass velocity for flat runway ,
glide velocity = 75.56 $\frac{m}{s}$, sink velocity = 1.0 $\frac{m}{s}$

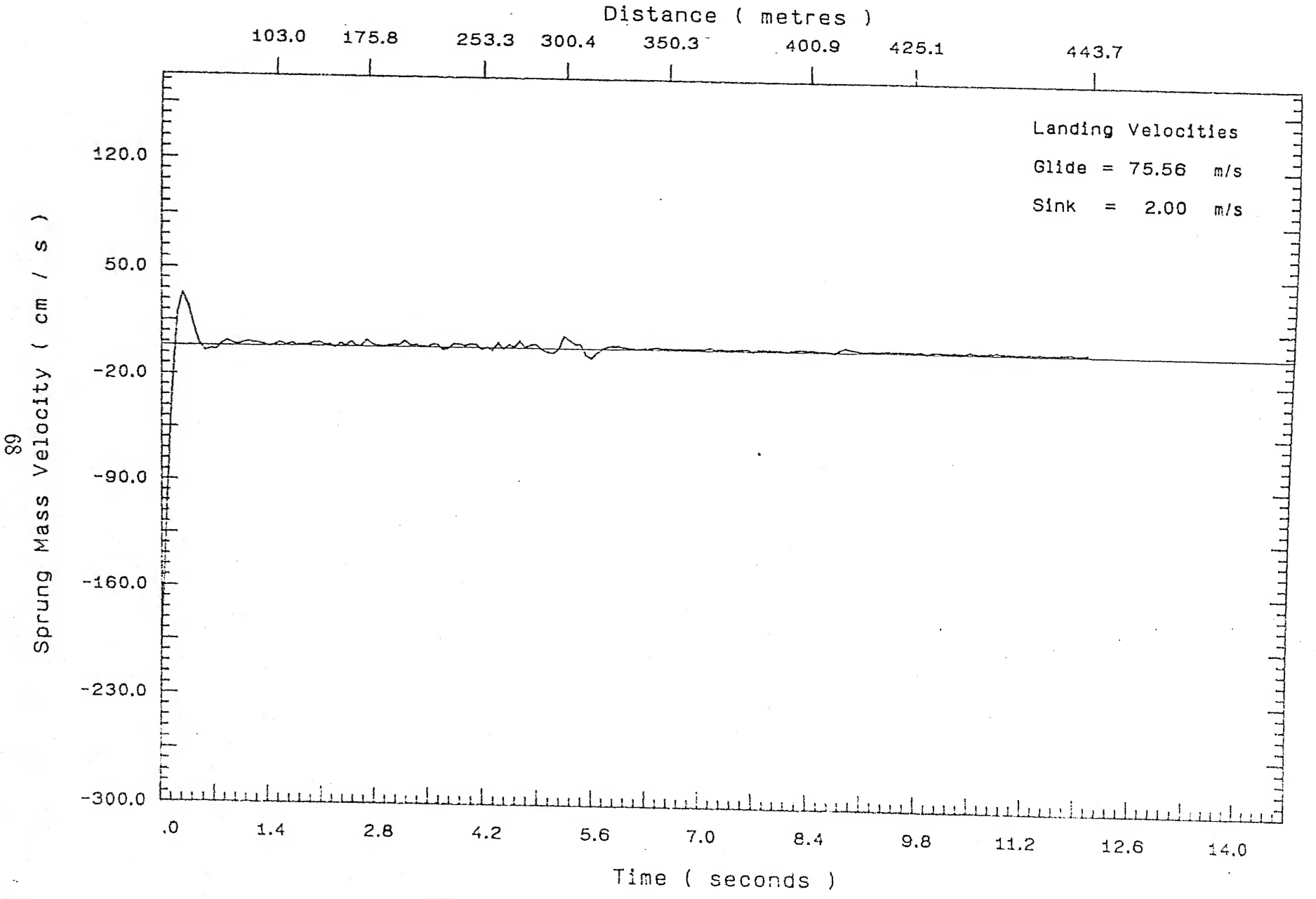

Figure 5.26: Sprung mass velocity for flat runway , glide velocity $= 75.56\ \frac{m}{s}$, sink velocity $= 2.0\ \frac{m}{s}$

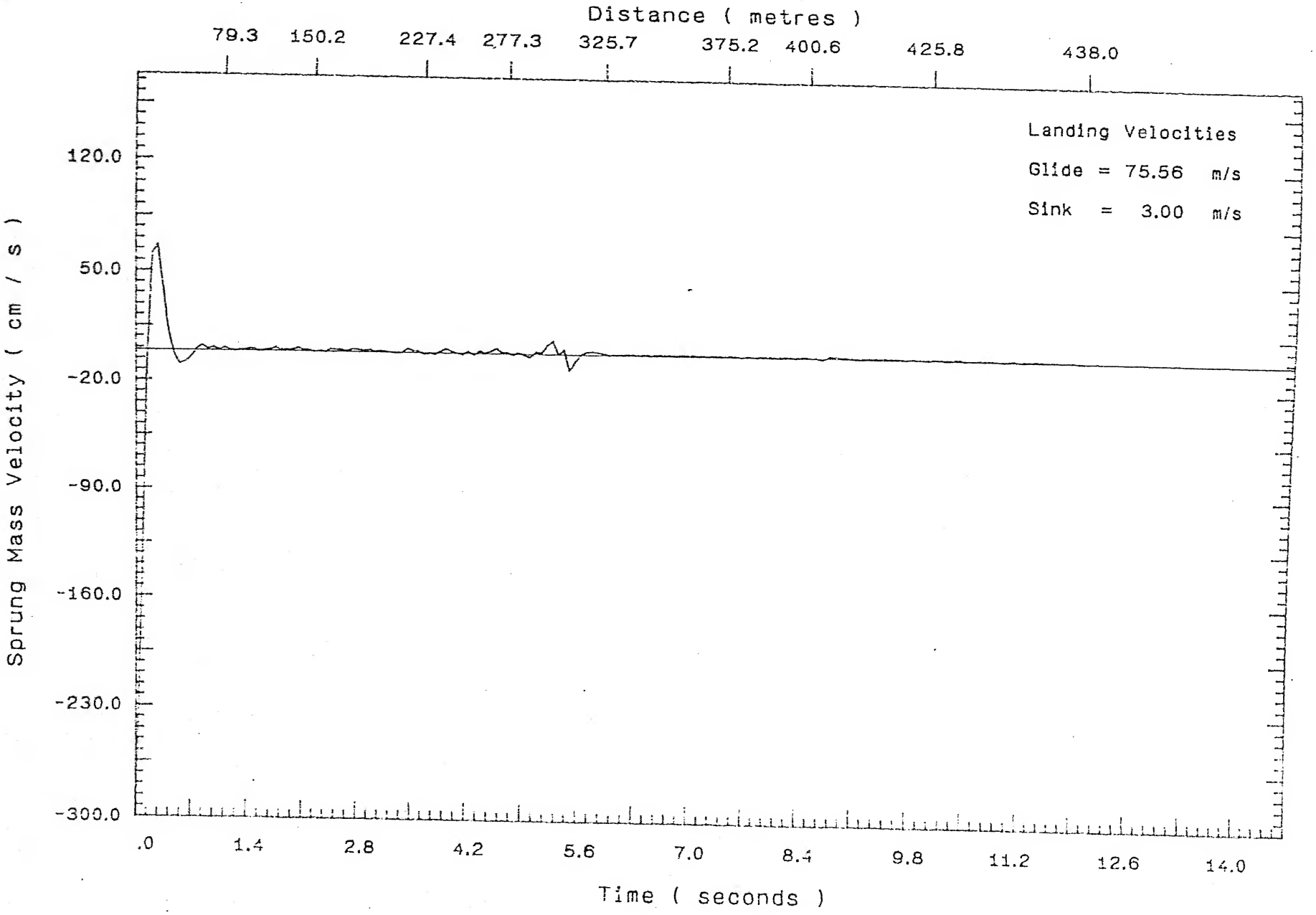

Figure 5.27: Sprung mass velocity for flat runway, glide velocity = 75.56 $\frac{m}{s}$, sink velocity = 3.0 $\frac{m}{s}$

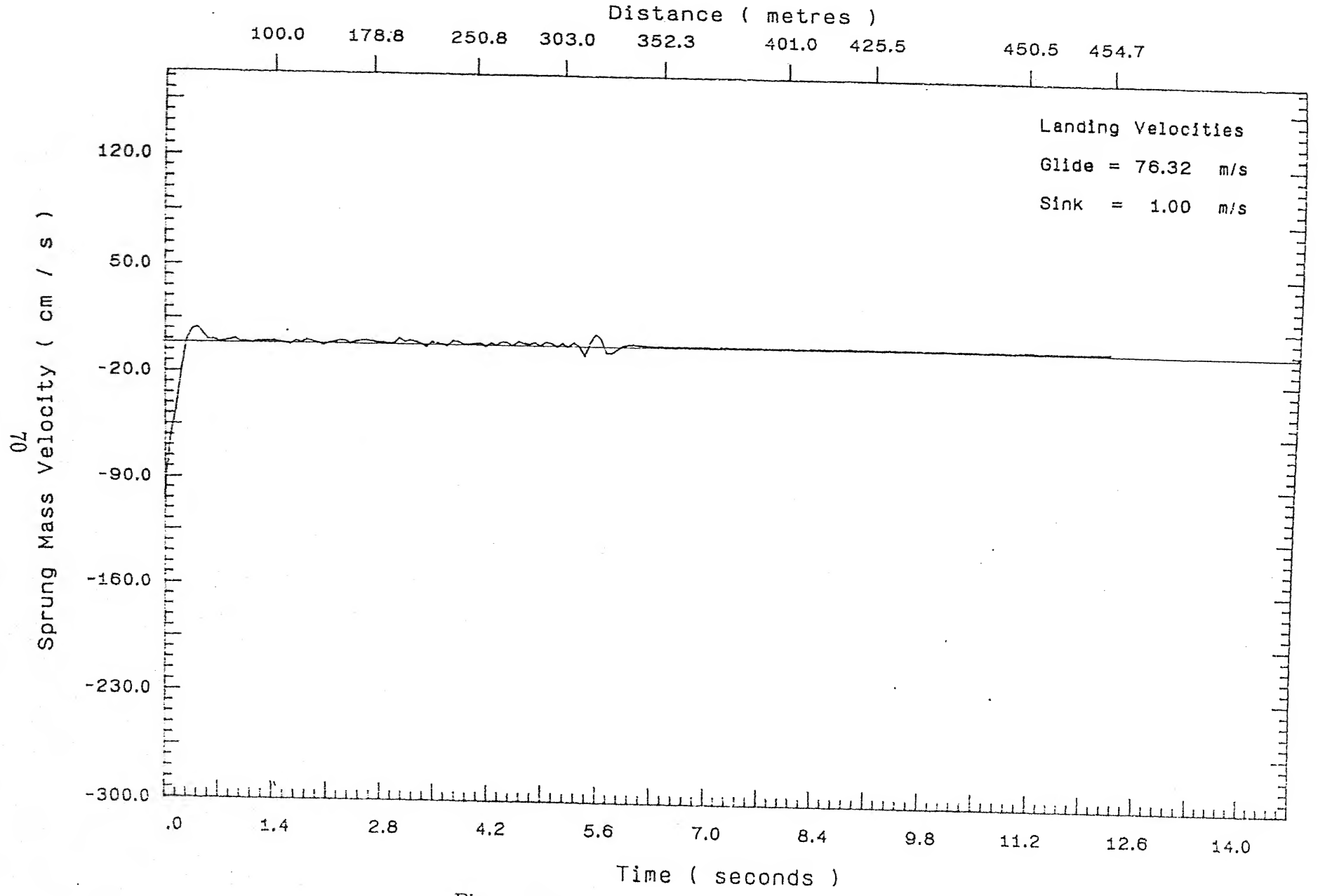

Figure 5.28: Sprung mass velocity for flat runway , glide velocity $= 76.32\ \frac{m}{s}$, sink velocity $= 1.0\ \frac{m}{s}$

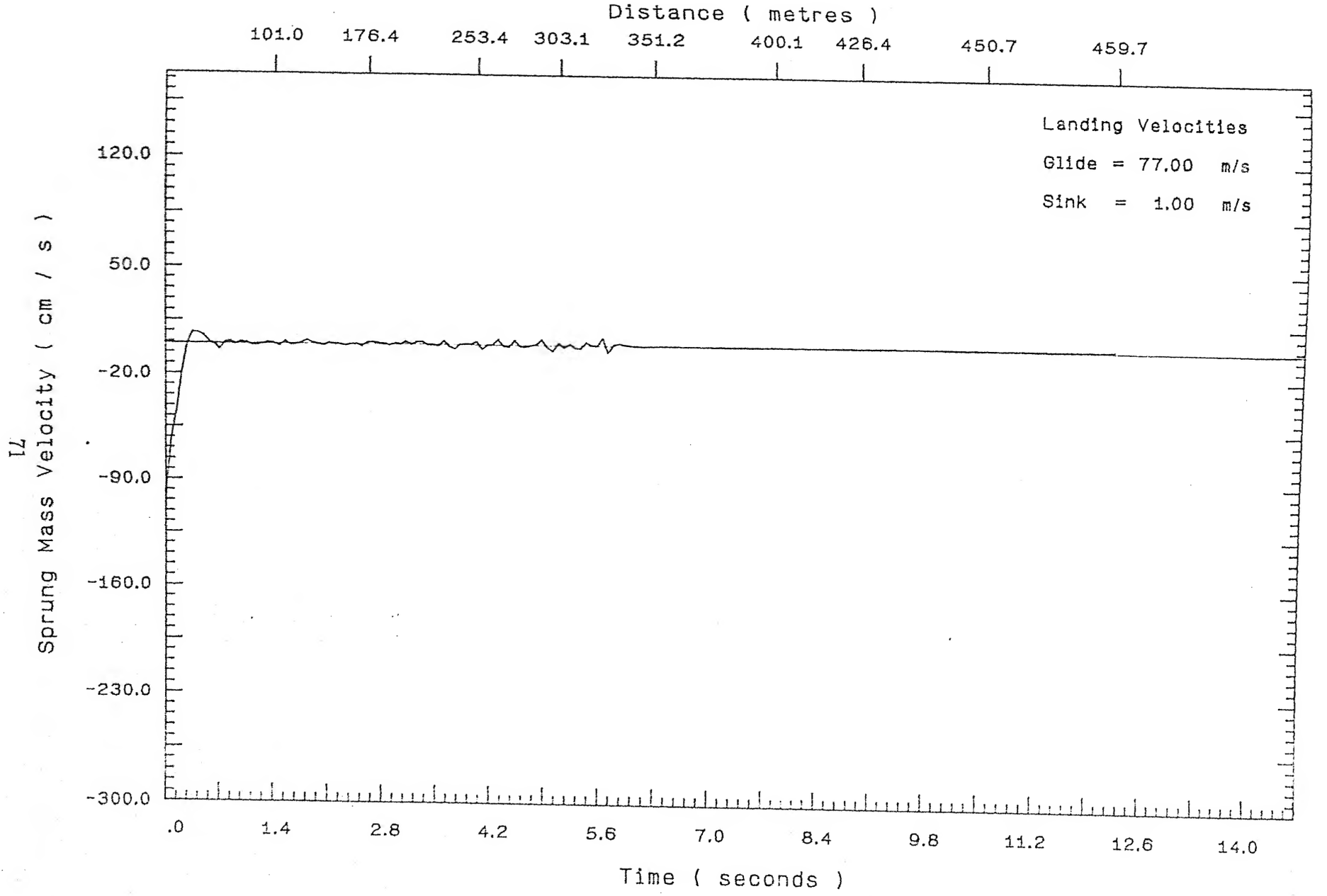

Figure 5.29: Sprung mass velocity for flat runway , glide velocity = 77.00 $\frac{m}{s}$, sink velocity = 1.0 $\frac{m}{s}$

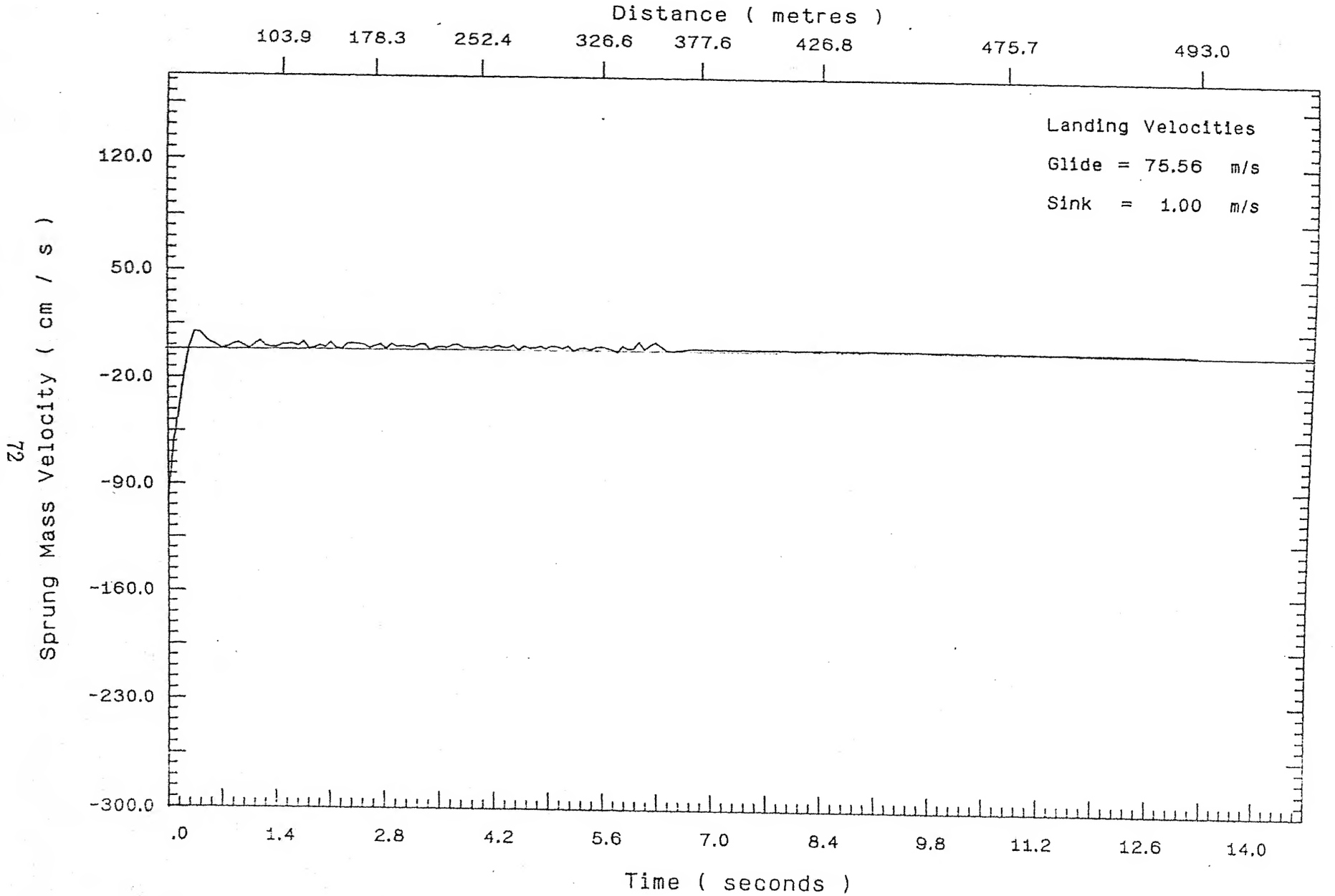

Figure 5.30: Sprung mass velocity for inclined runway , glide velocity = 75.56 $\frac{m}{s}$, sink velocity = 1.0 $\frac{m}{s}$

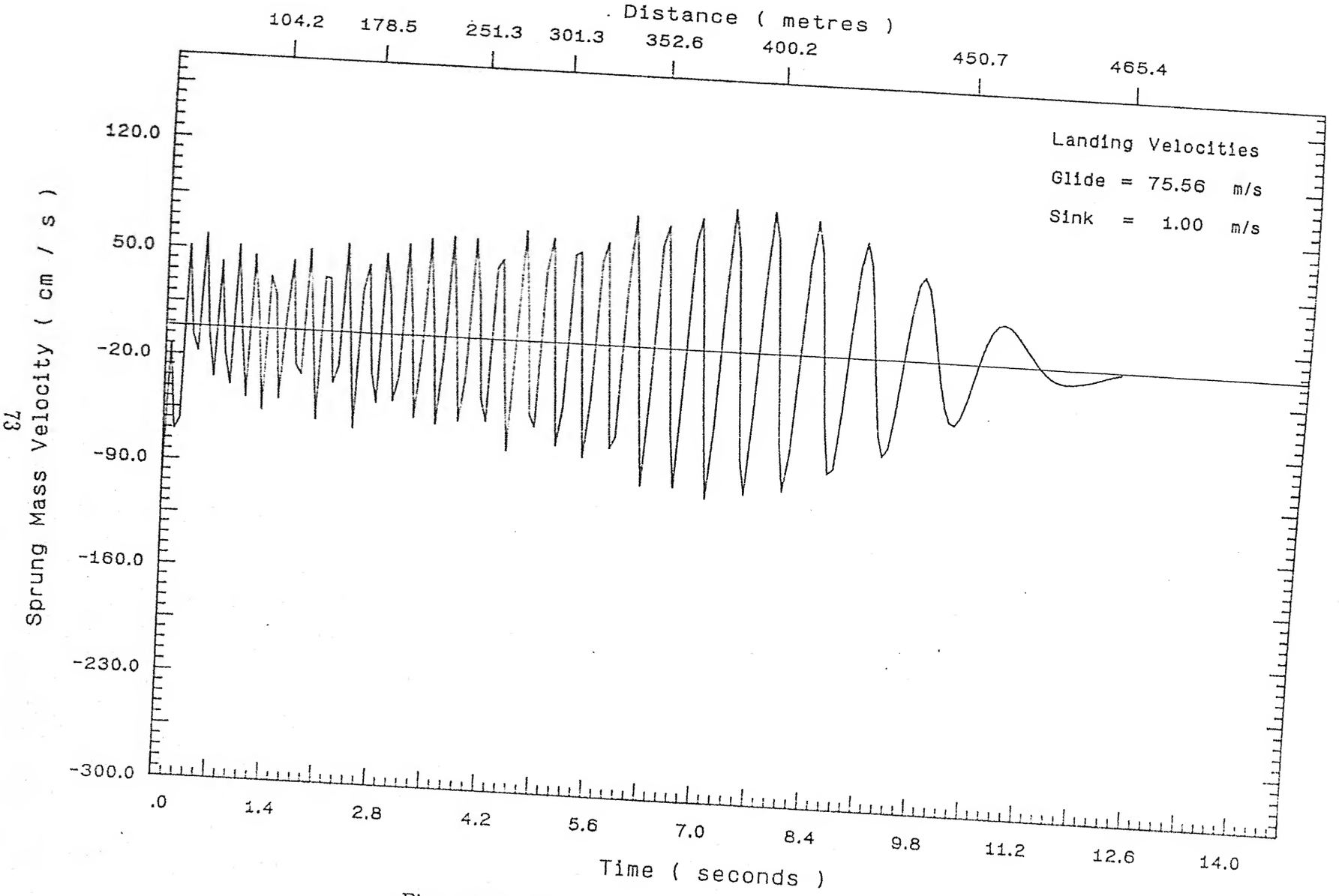

Figure 5.31: Sprung mass velocity for sinusoidal runway , glide velocity = 75.56 $\frac{m}{s}$, sink velocity = 1.0 $\frac{m}{s}$

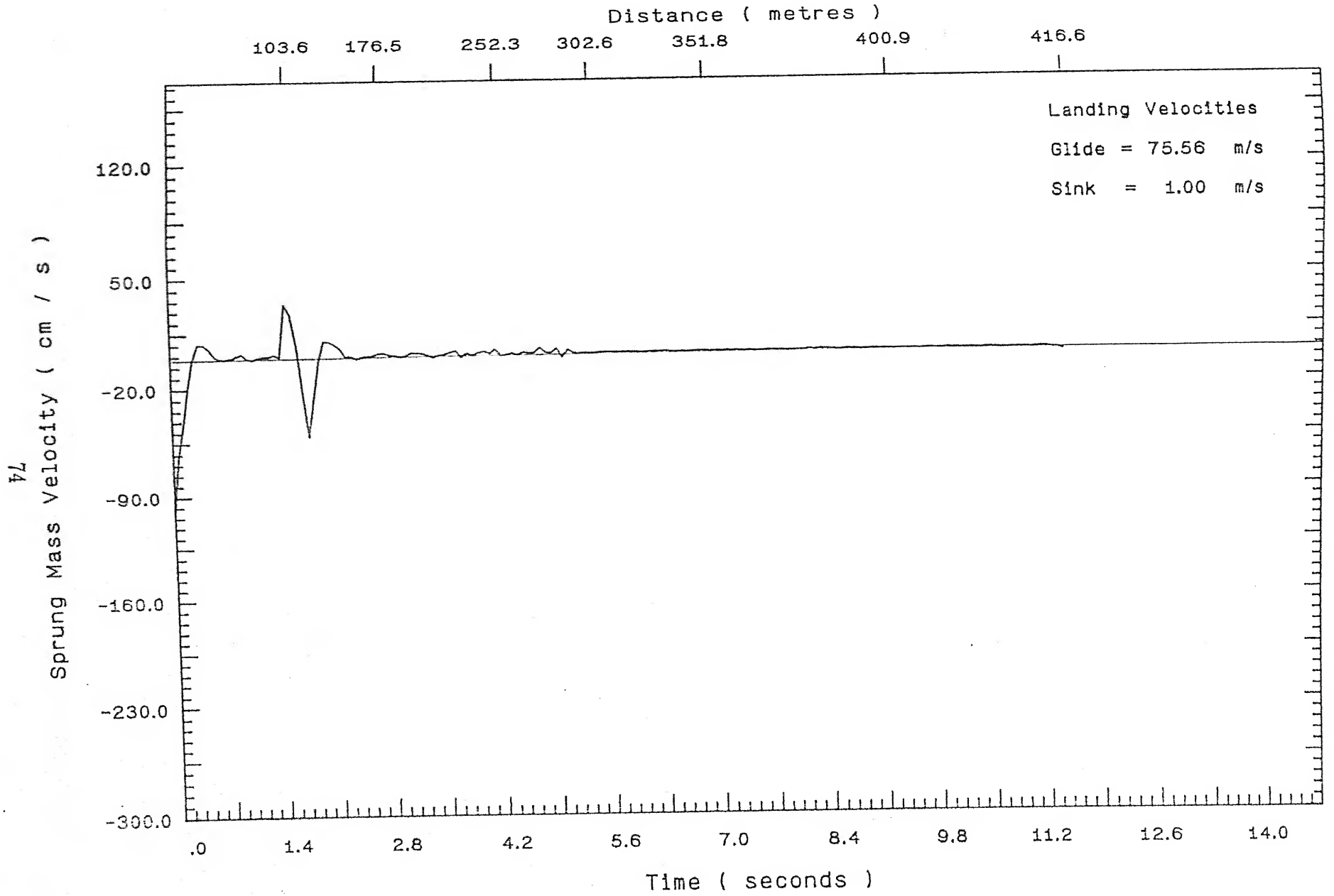

Figure 5.32: Sprung mass velocity for stepped runway ,
glide velocity = 75.56 $\frac{m}{s}$, sink velocity = 1.0 $\frac{m}{s}$

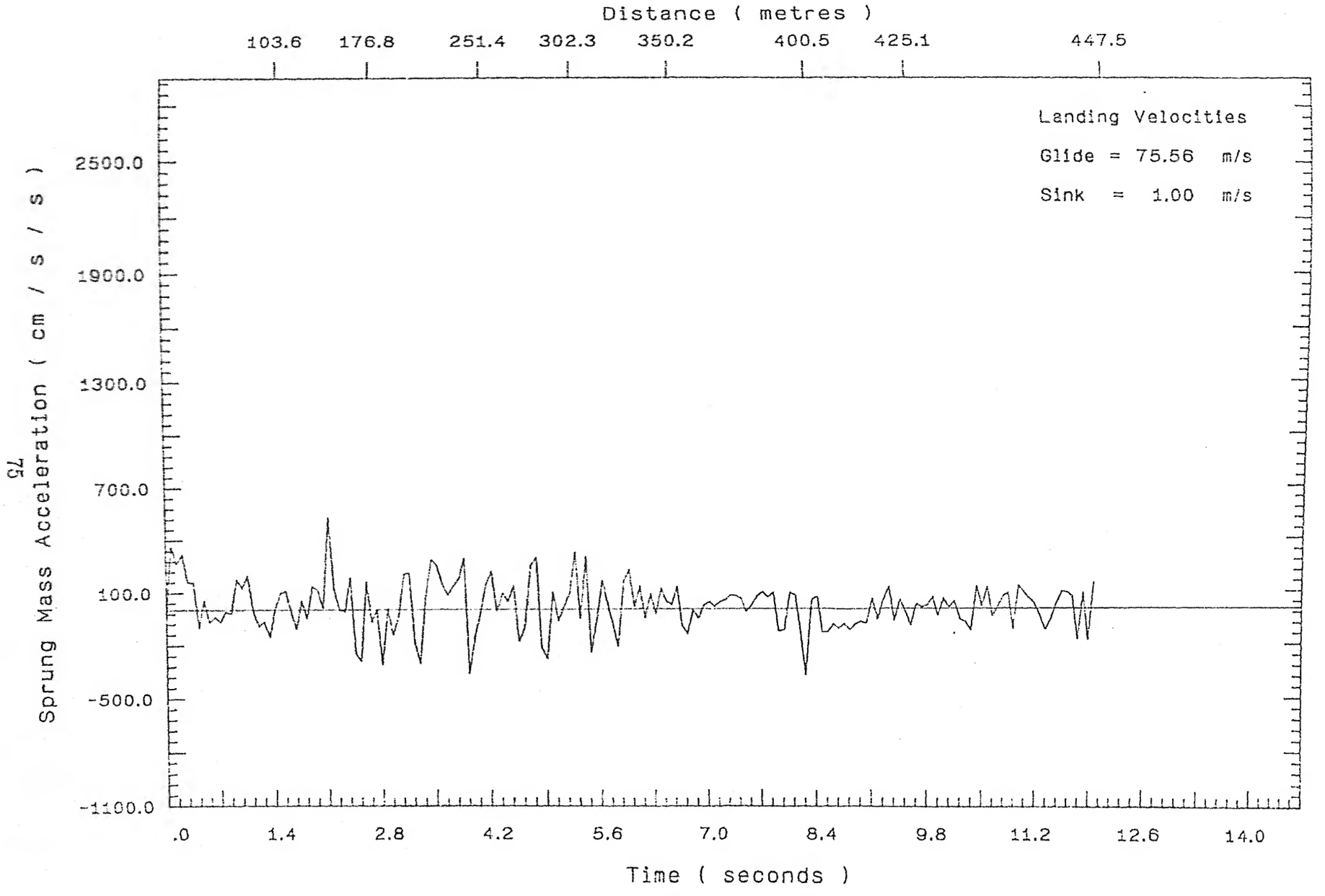

Figure 5.33: Sprung mass acceleration for flat runway , glide velocity = 75.56 $\frac{m}{s}$, sink velocity = 1.0 $\frac{m}{s}$

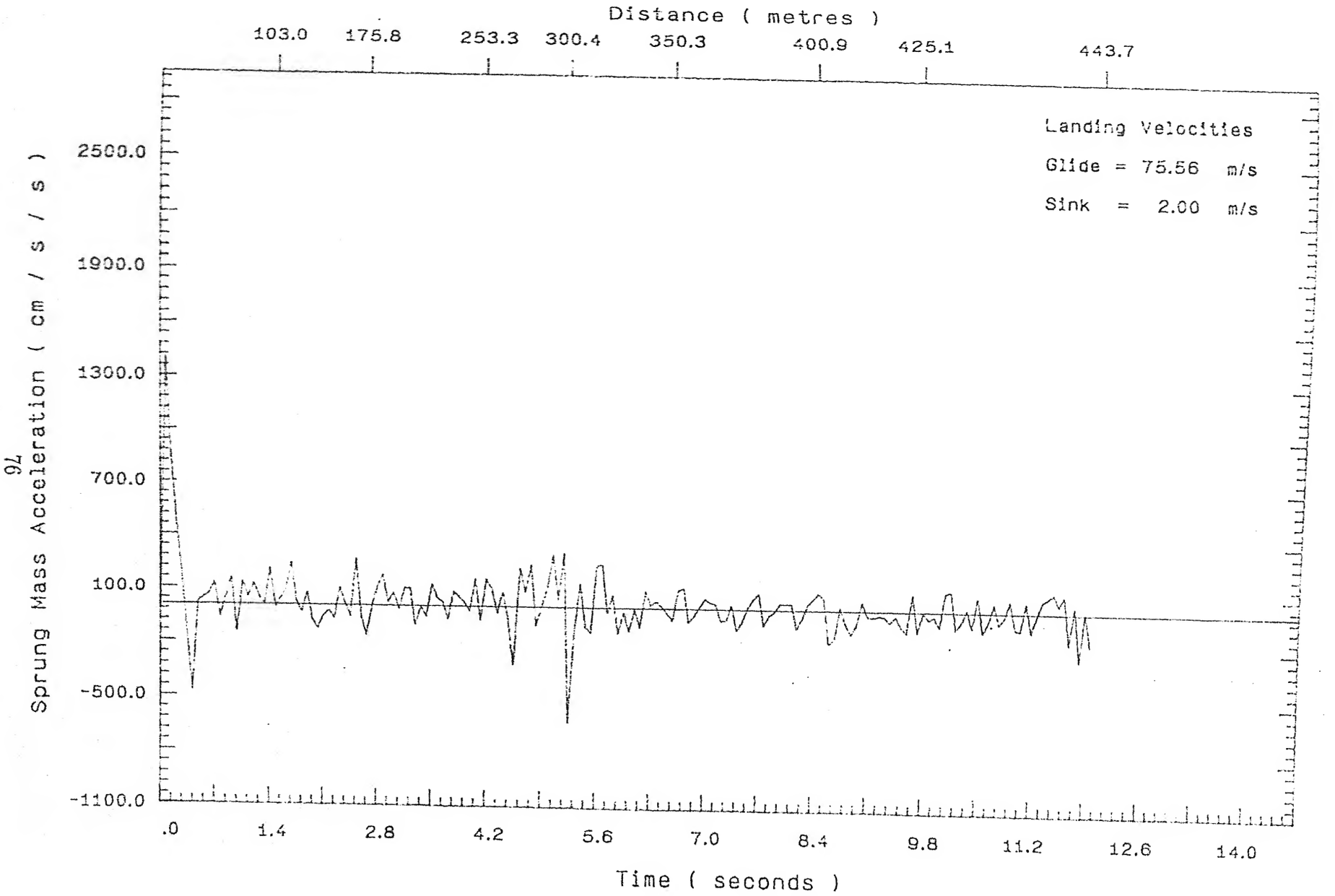

Figure 5.34: Sprung mass acceleration for flat runway , glide velocity = 75.56 $\frac{m}{s}$, sink velocity = 2.0 $\frac{m}{s}$

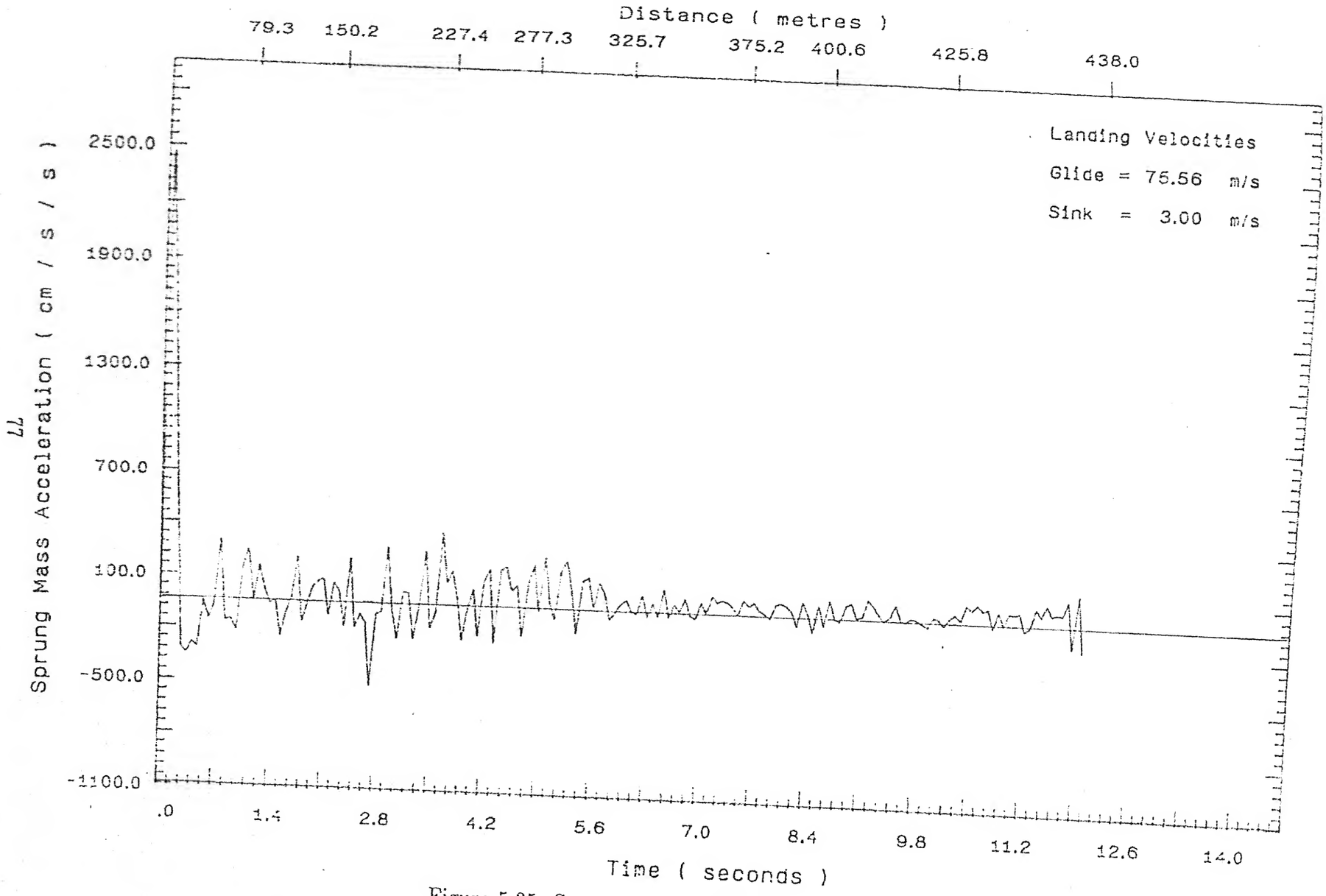

Figure 5.35: Sprung mass acceleration for flat runway , glide velocity = 75.56 $\frac{m}{s}$, sink velocity = 3.0 $\frac{m}{s}$

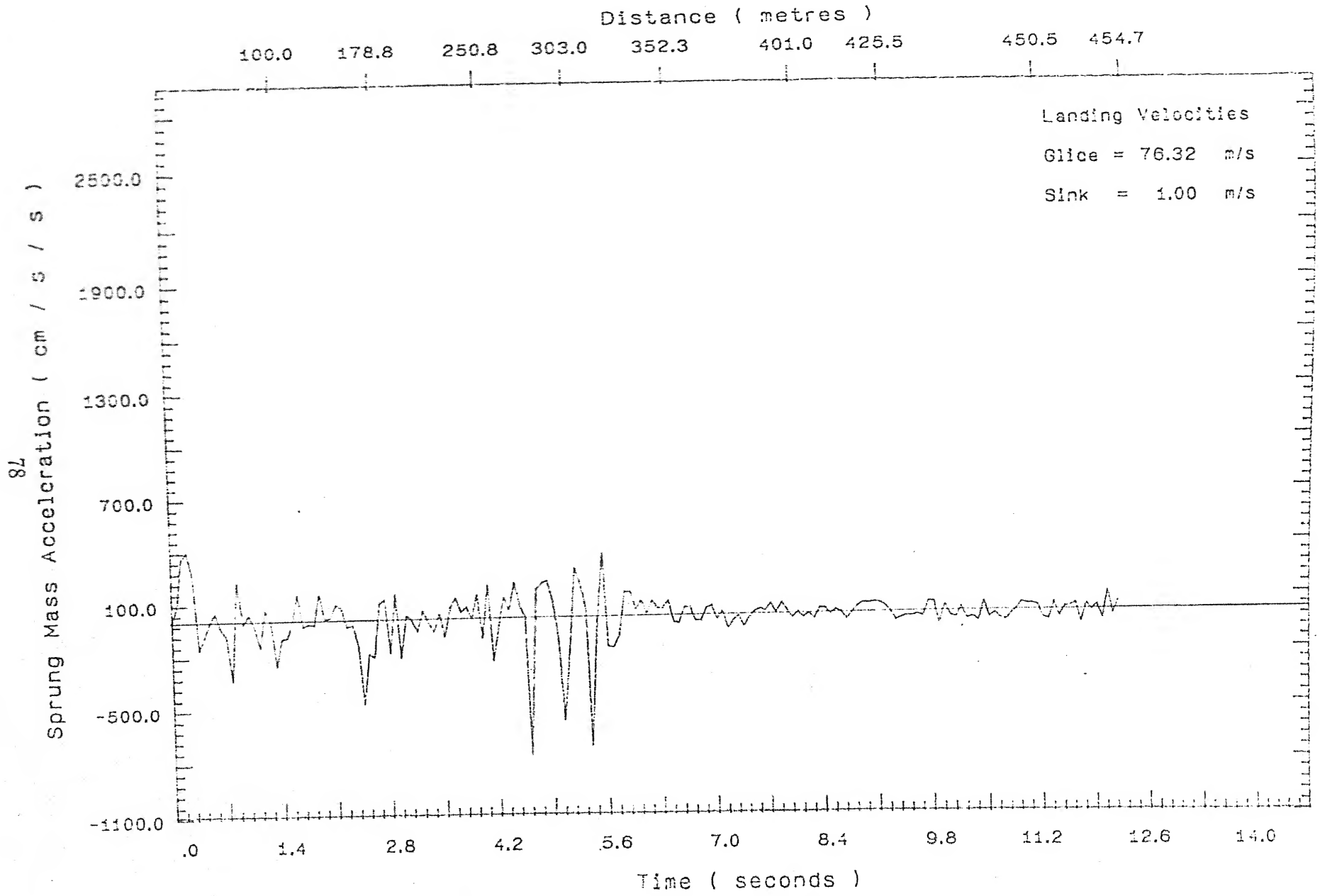

Figure 5.36: Sprung mass acceleration for flat runway ,
glide velocity = 76.32 $\frac{m}{s}$, sink velocity = 1.0 $\frac{m}{s}$

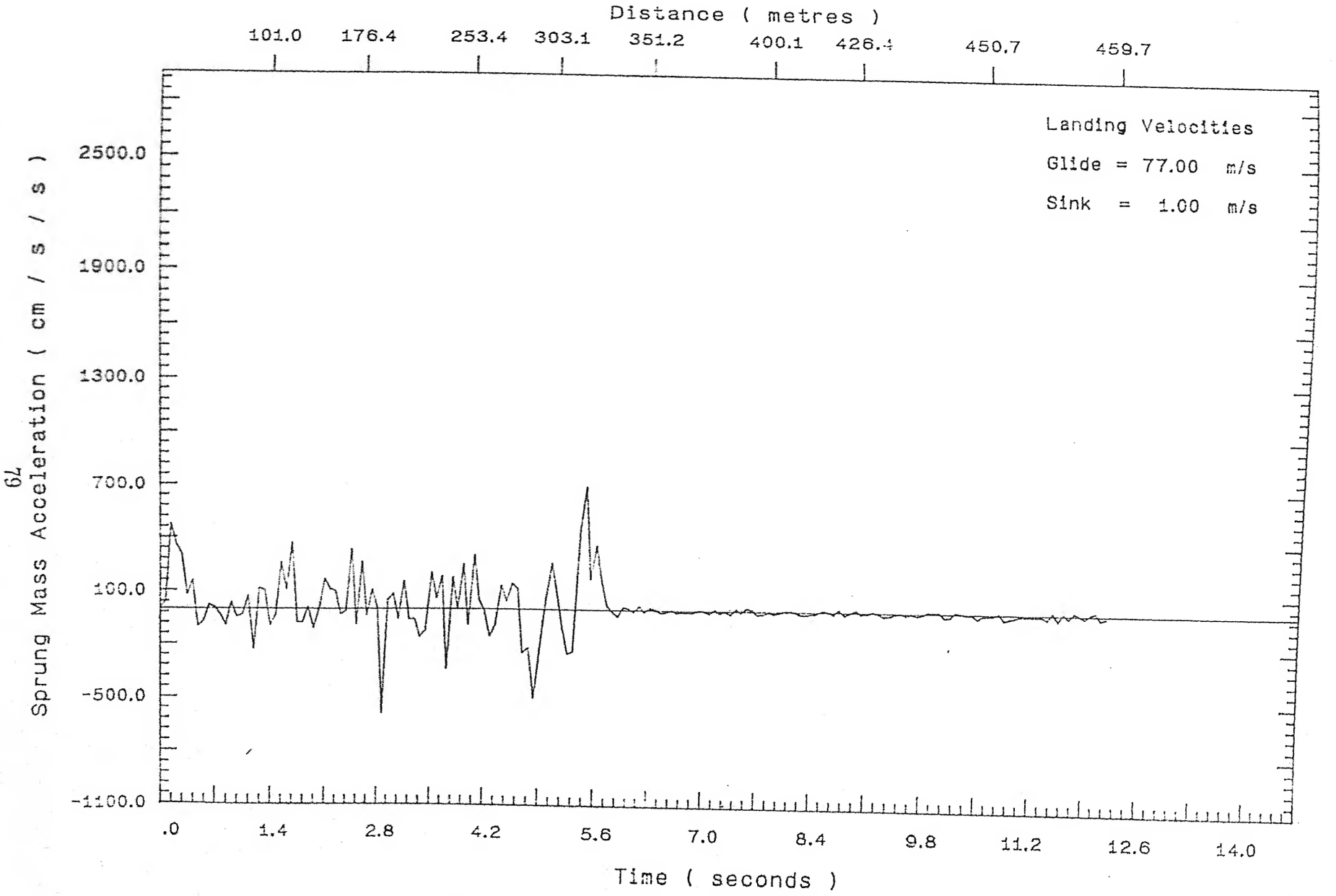

Figure 5.37: Sprung mass acceleration for flat runway ,
glide velocity = 77.00 $\frac{m}{s}$, sink velocity = 1.0 $\frac{m}{s}$

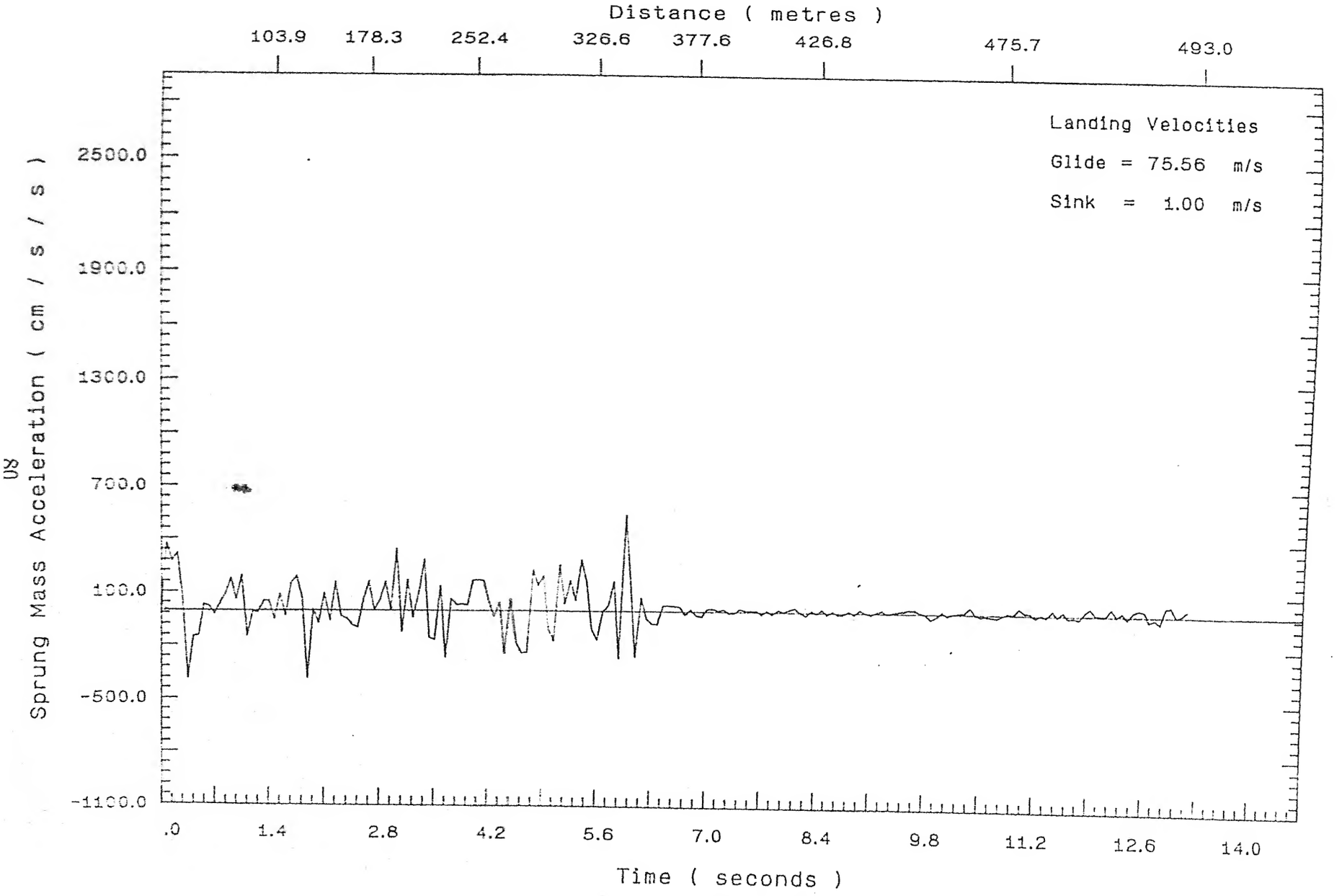

Figure 5.3S: Sprung mass acceleration for inclined runway , glide velocity = 75.56 $\frac{m}{s}$, sink velocity = 1.0 $\frac{m}{s}$

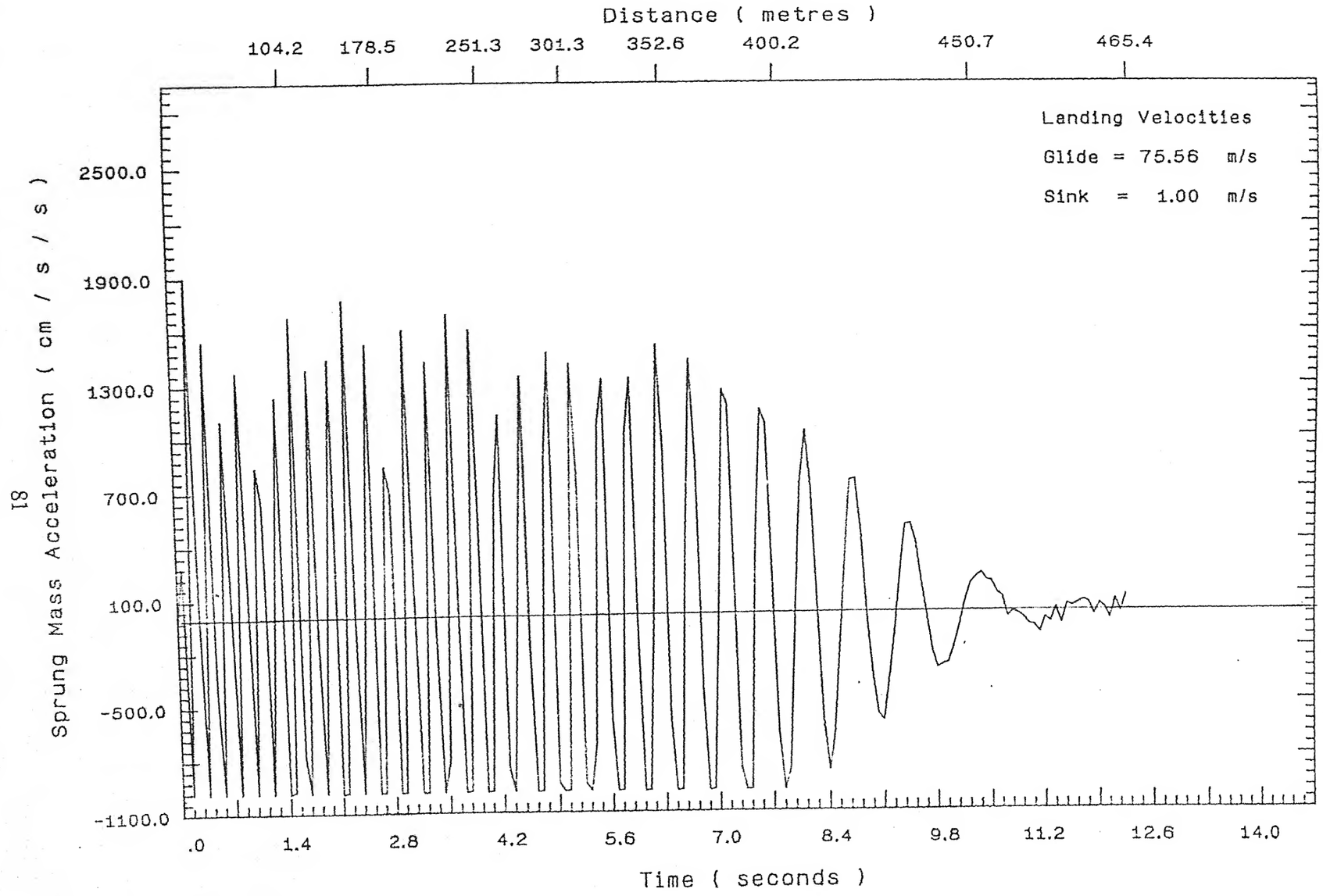

Figure 5.39: Sprung mass acceleration for sinusoidal runway , glide velocity = 75.56 $\frac{m}{s}$, sink velocity = 1.0 $\frac{m}{s}$

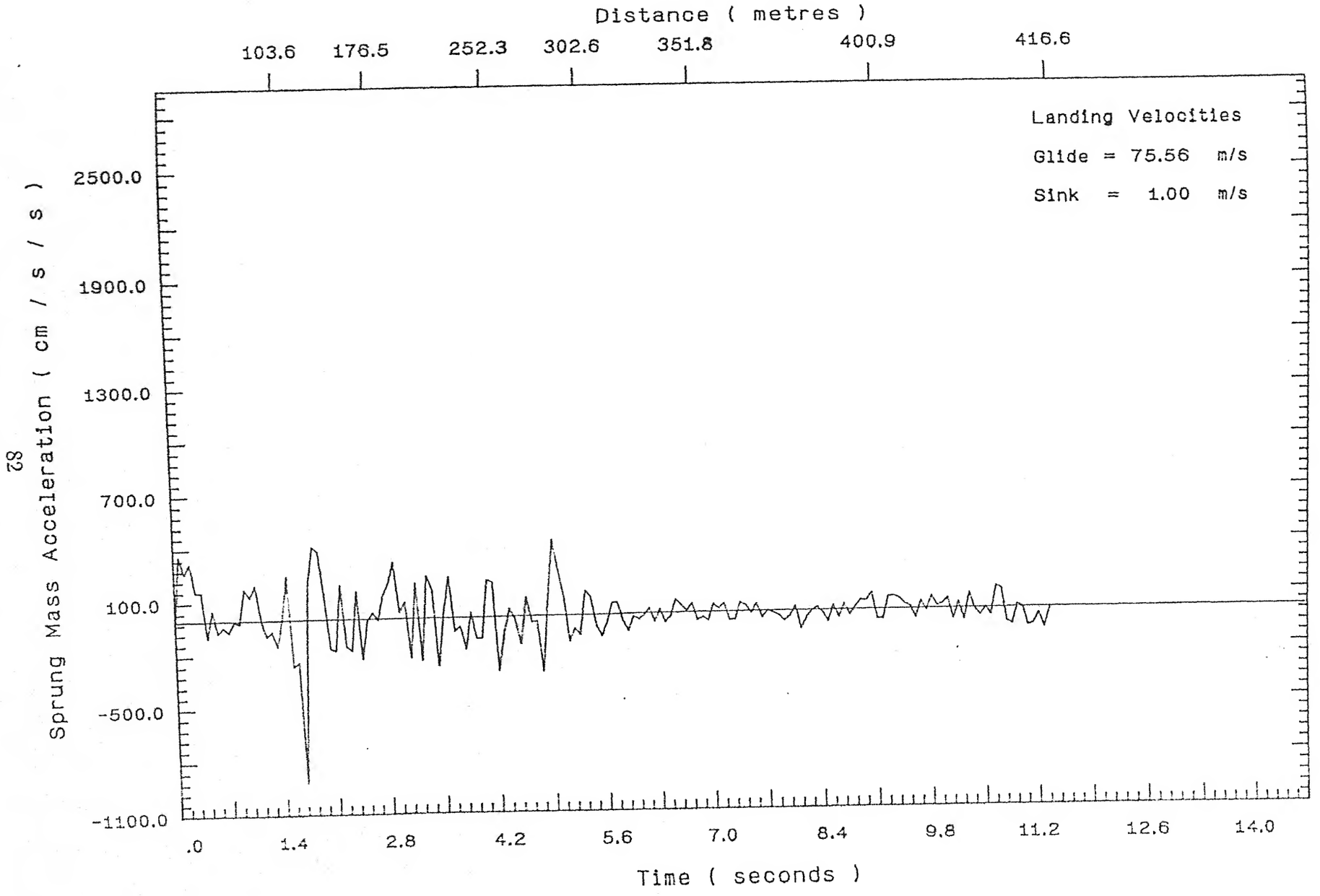

Figure 5.40: Sprung mass acceleration for stepped runway ,
glide velocity = 75.56 $\frac{m}{s}$, sink velocity = 1.0 $\frac{m}{s}$

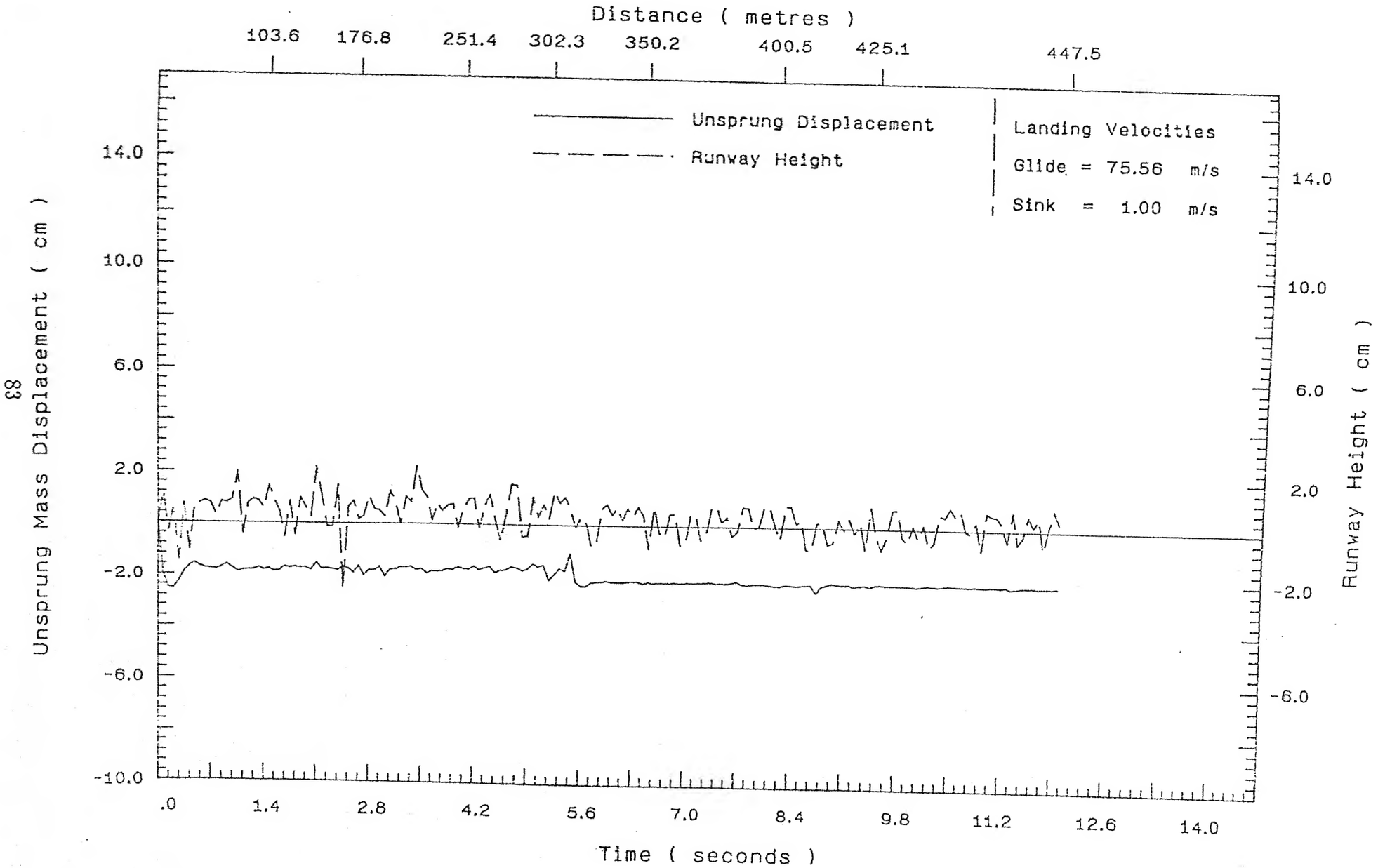

Figure 5.41: Unsprung mass displacement for flat runway , glide velocity = 75.56 $\frac{m}{s}$, sink velocity = 1.0 $\frac{m}{s}$

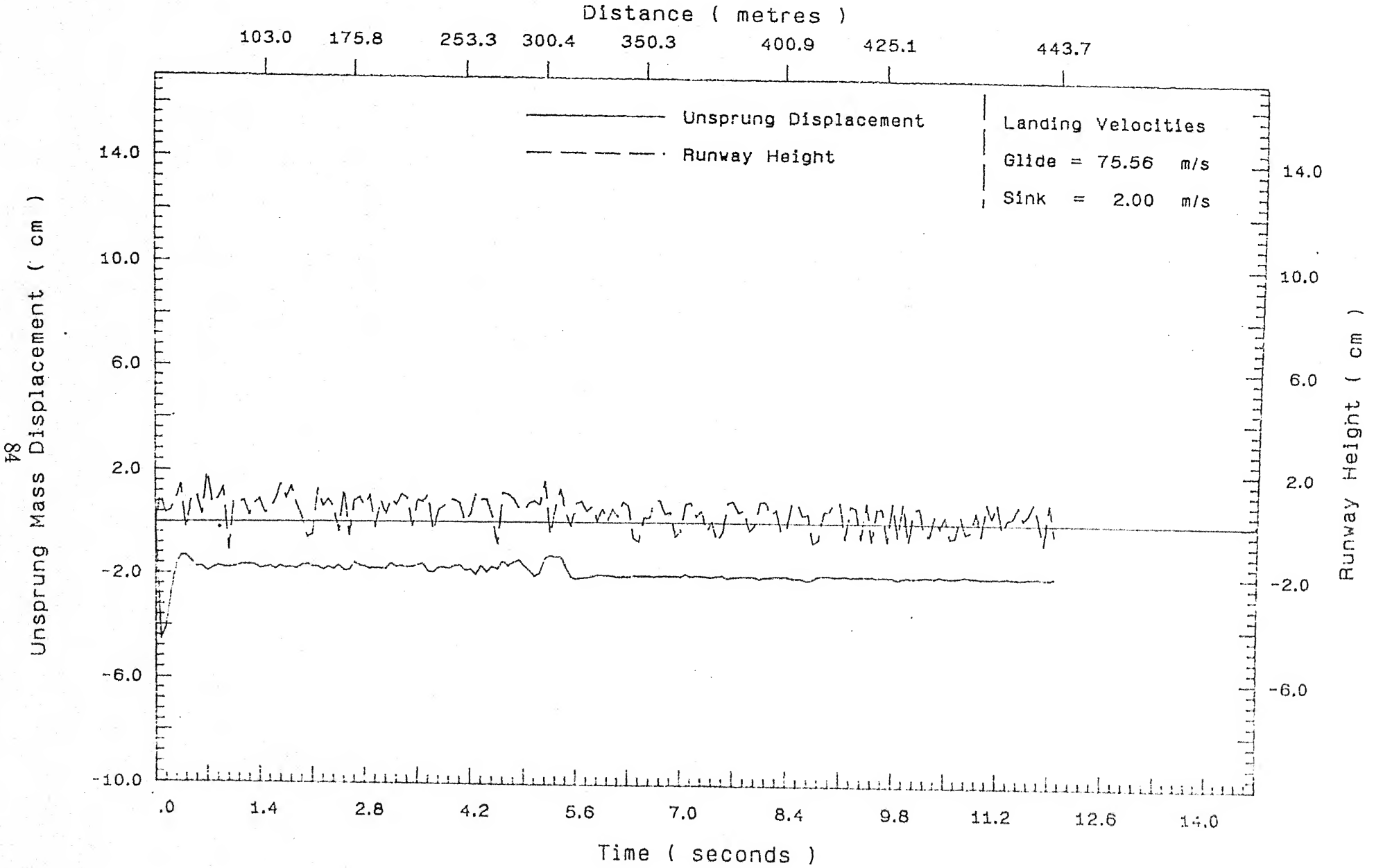

Figure 5.42: Unsprung mass displacement for flat runway , glide velocity = 75.56 $\frac{m}{s}$, sink velocity = 2.0 $\frac{m}{s}$

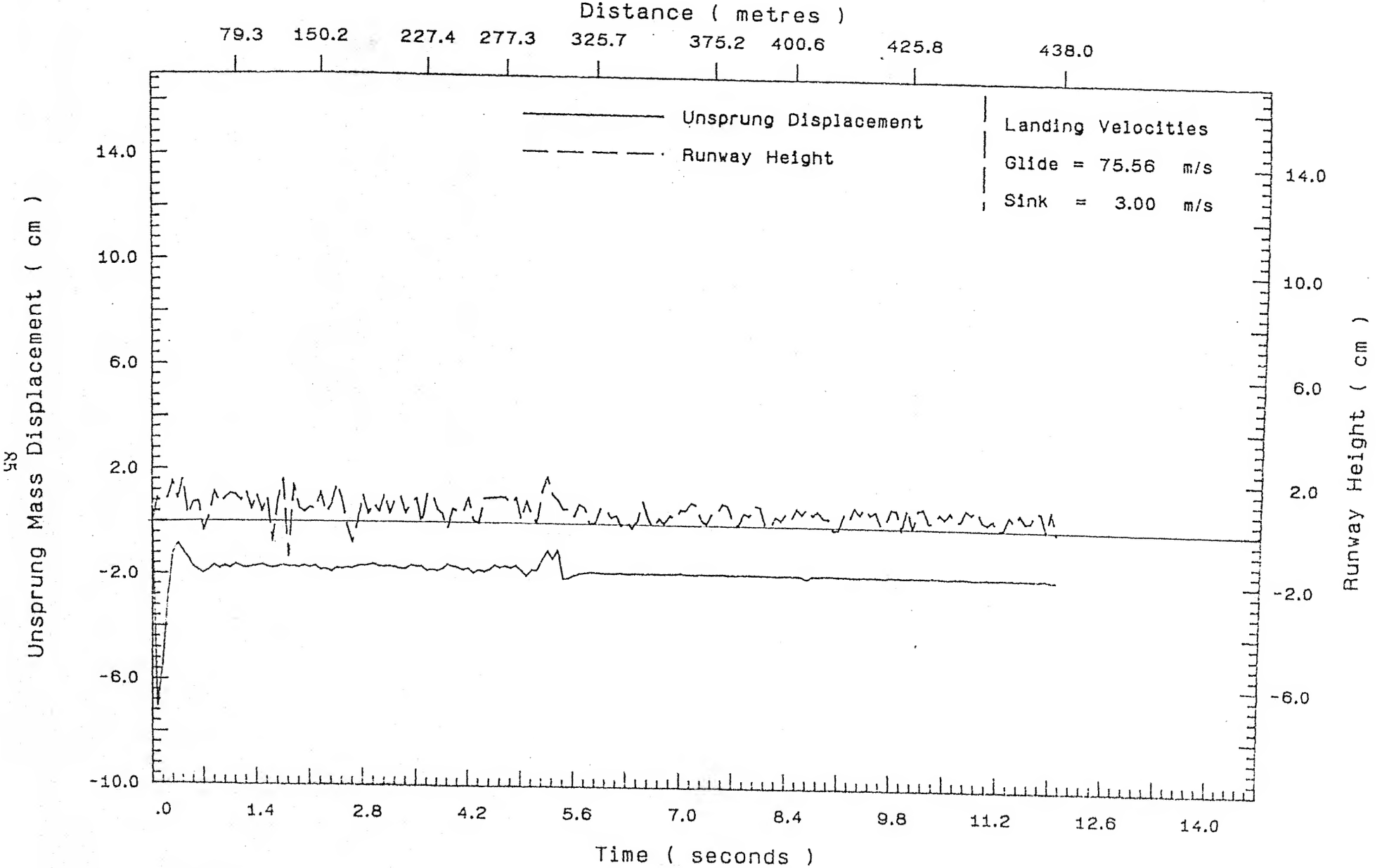

Figure 5.43: Unsprung mass displacement for flat runway , glide velocity = 75.56 $\frac{m}{s}$, sink velocity = 3.0 $\frac{m}{s}$

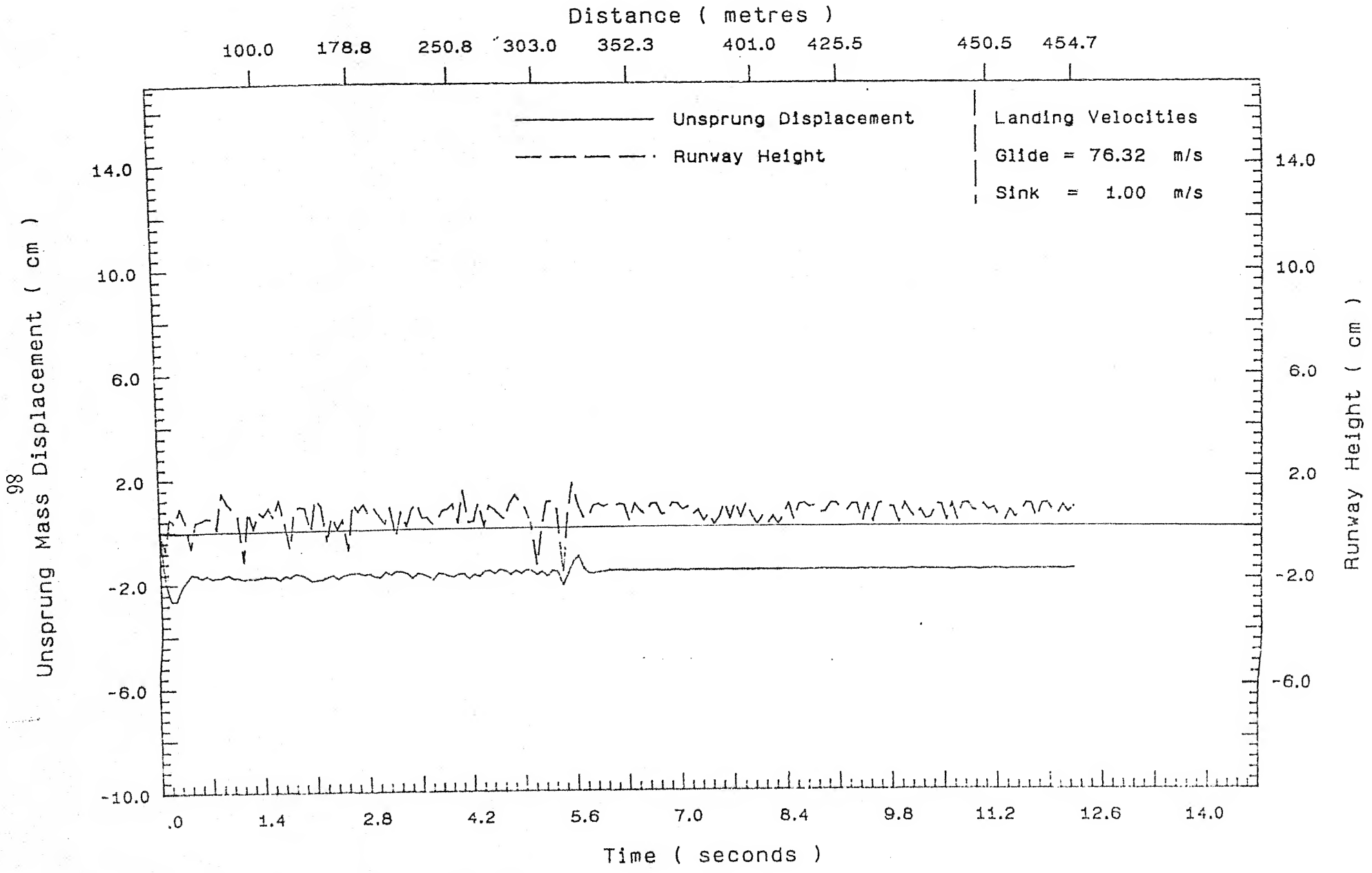

Figure 5.44: Unsprung mass displacement for flat runway ,
glide velocity = 76.32 $\frac{m}{s}$, sink velocity = 1.0 $\frac{m}{s}$

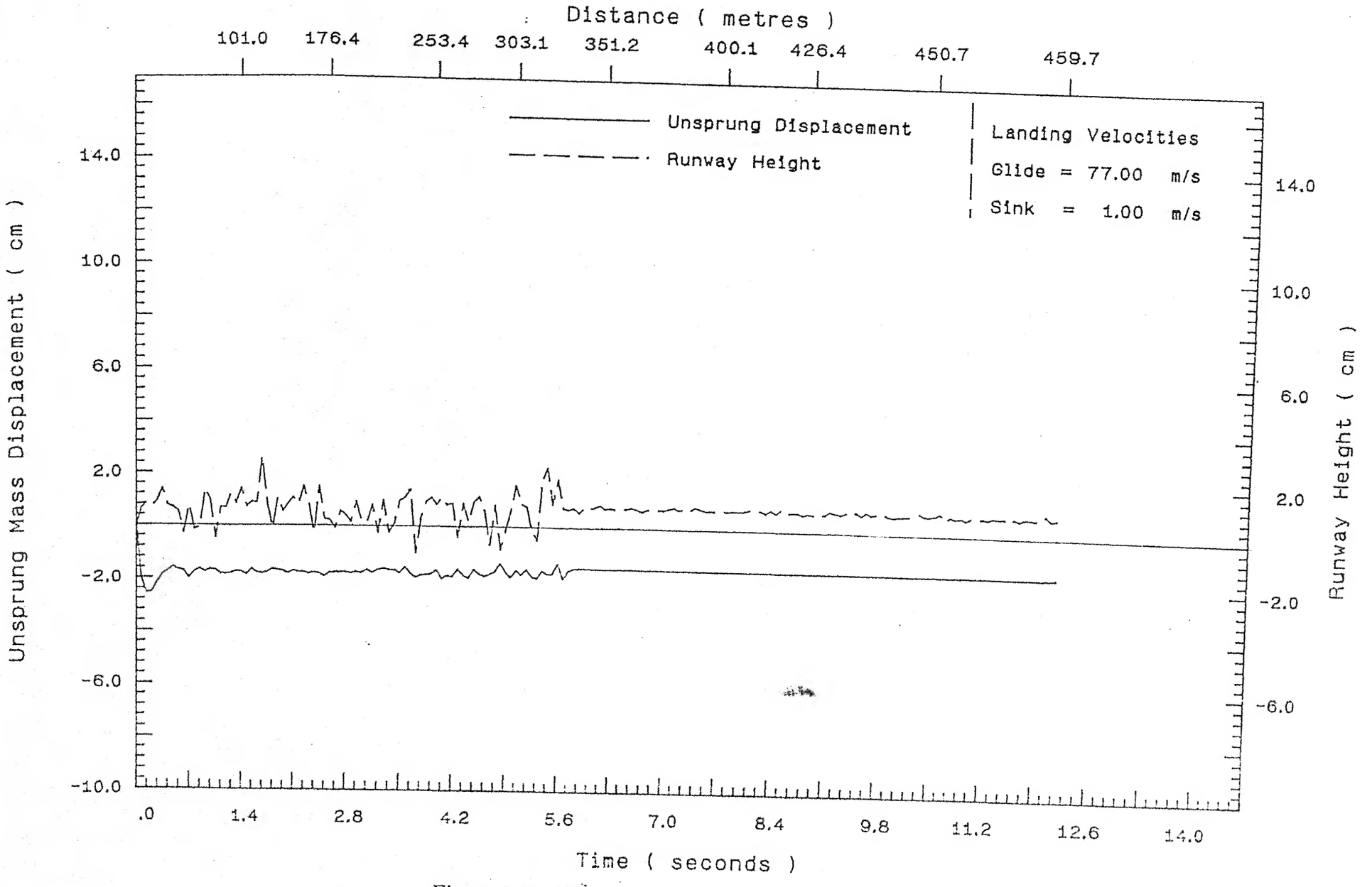

Figure 5.45: Unsprung mass displacement for flat runway , glide velocity = 77.00 $\frac{m}{s}$, sink velocity = 1.0 $\frac{m}{s}$

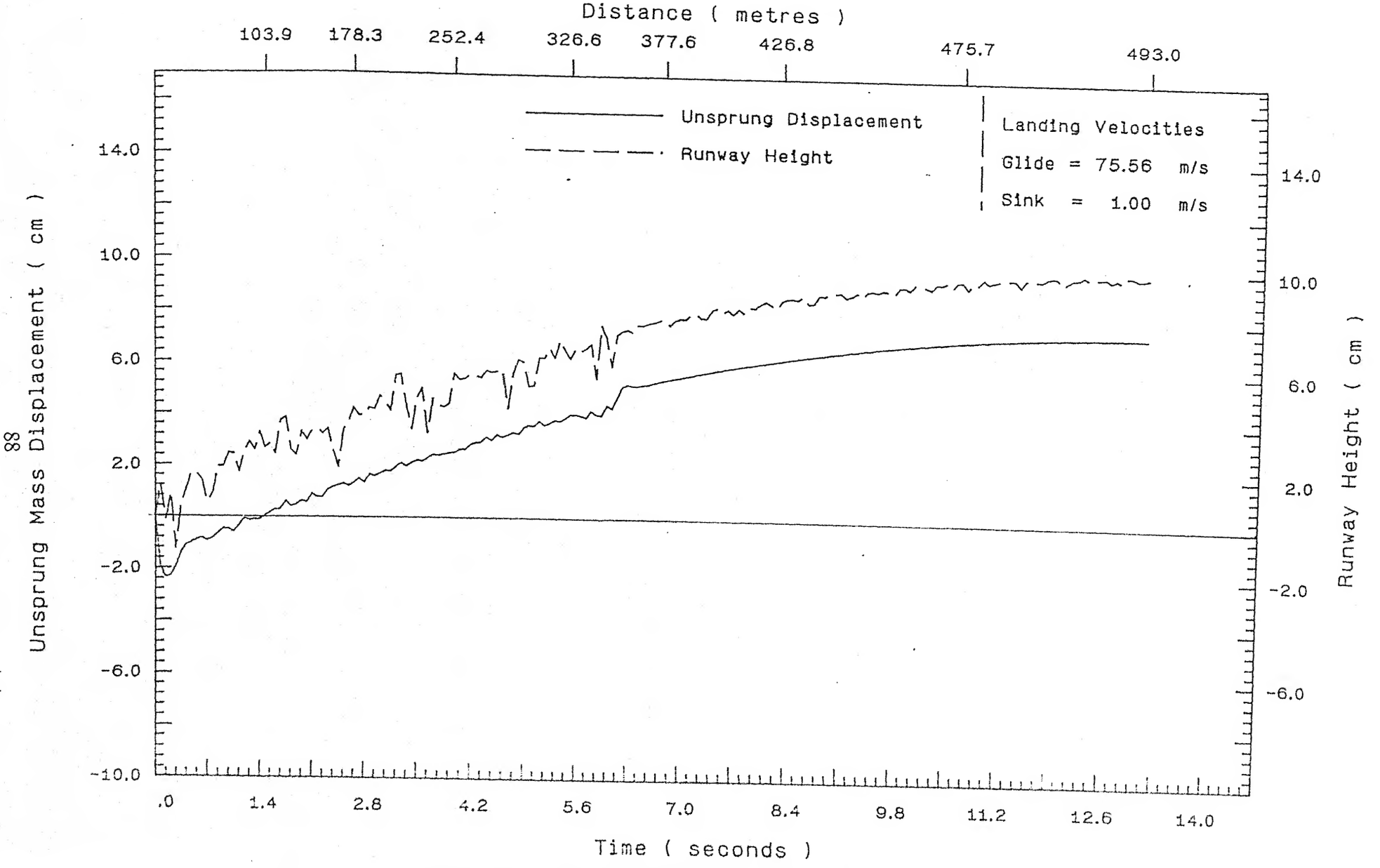

Figure 5.46: Unsprung mass displacement for inclined runway , glide velocity = 75.56 $\frac{m}{s}$, sink velocity = 1.0 $\frac{m}{s}$

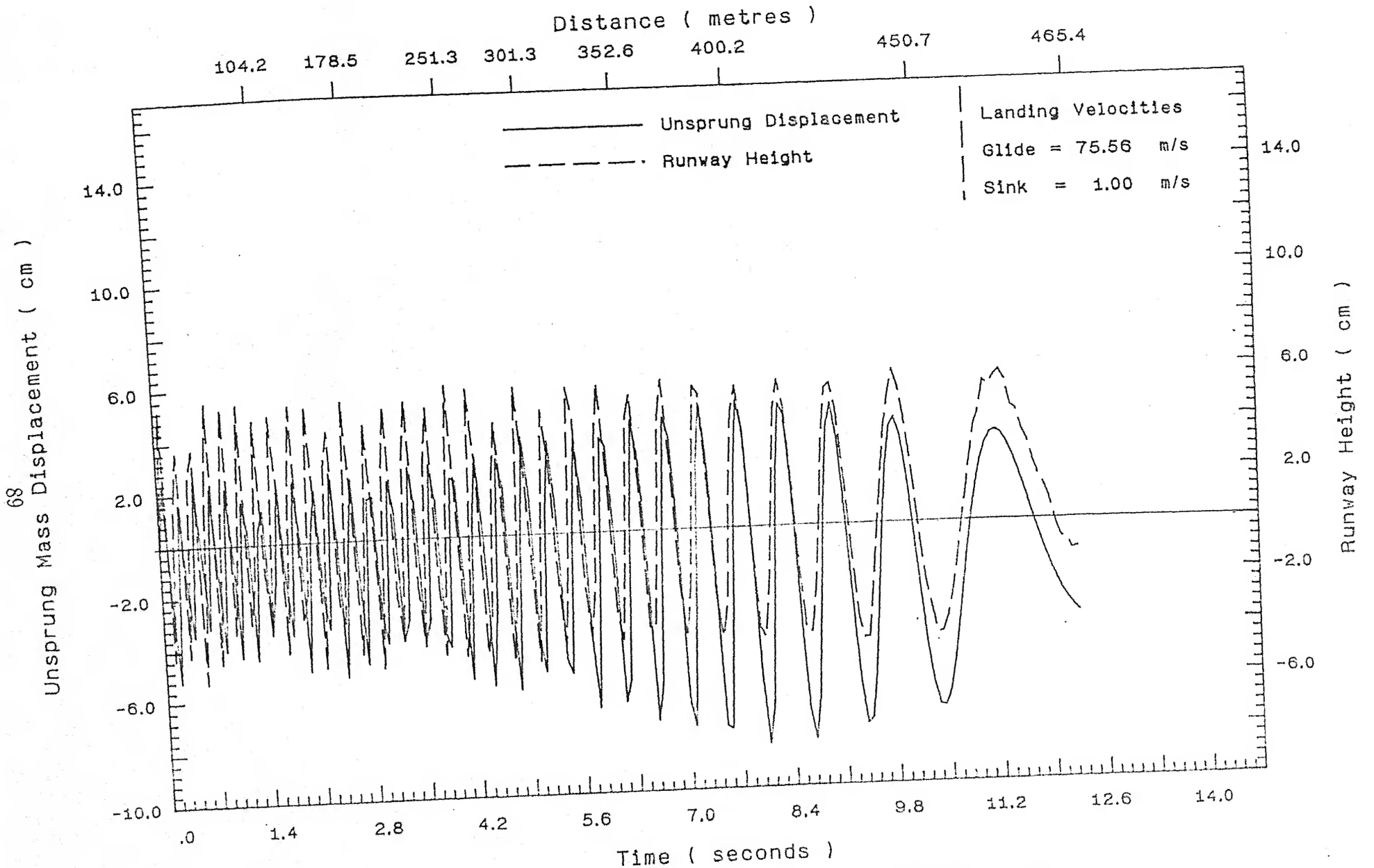

Figure 5.47: Unsprung mass displacement for sinusoidal runway , glide velocity = 75.56 $\frac{m}{s}$, sink velocity = 1.0 $\frac{m}{s}$

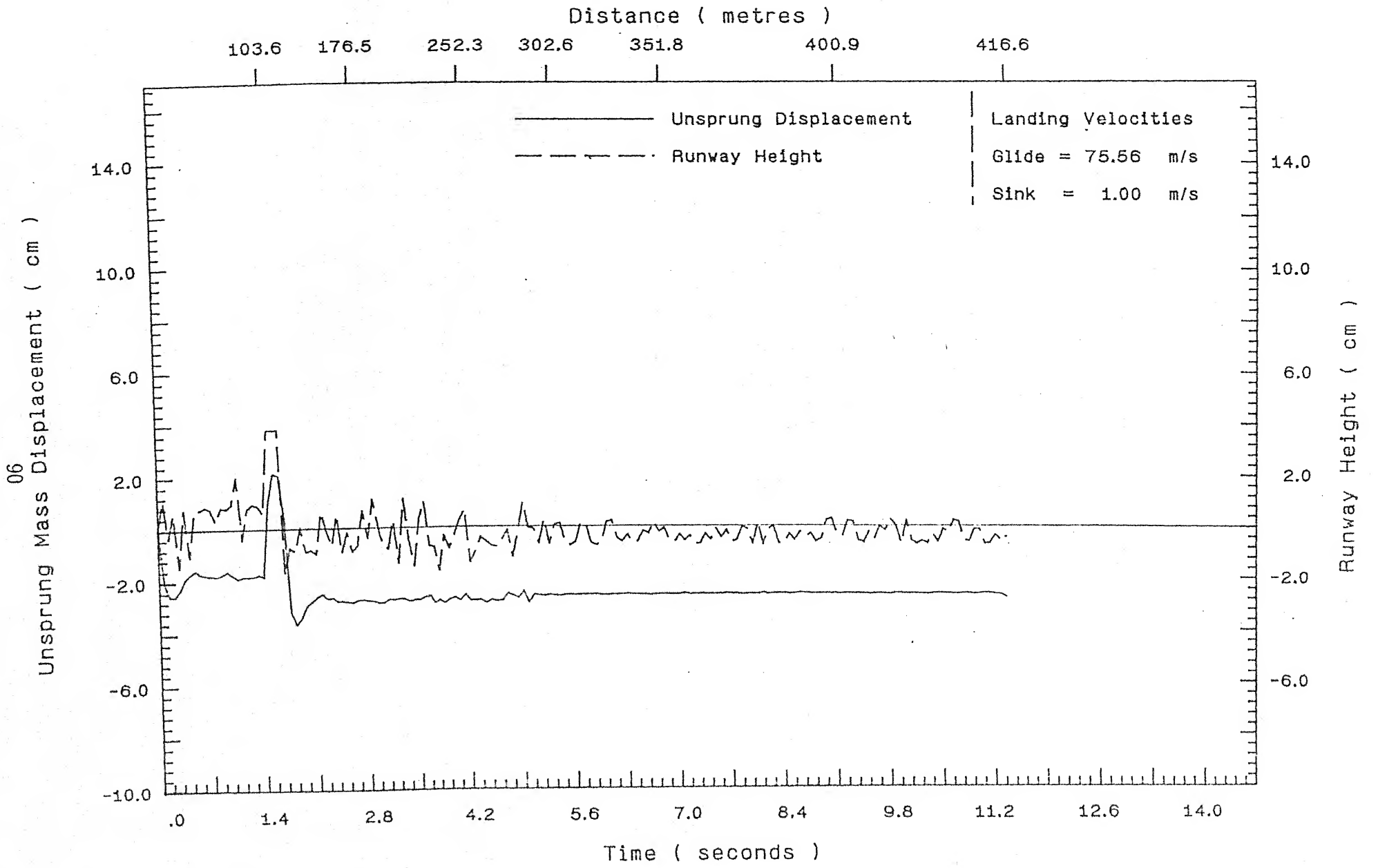

Figure 5.48: Unsprung mass displacement for stepped runway , glide velocity = 75.56 $\frac{m}{s}$, sink velocity = 1.0 $\frac{m}{s}$

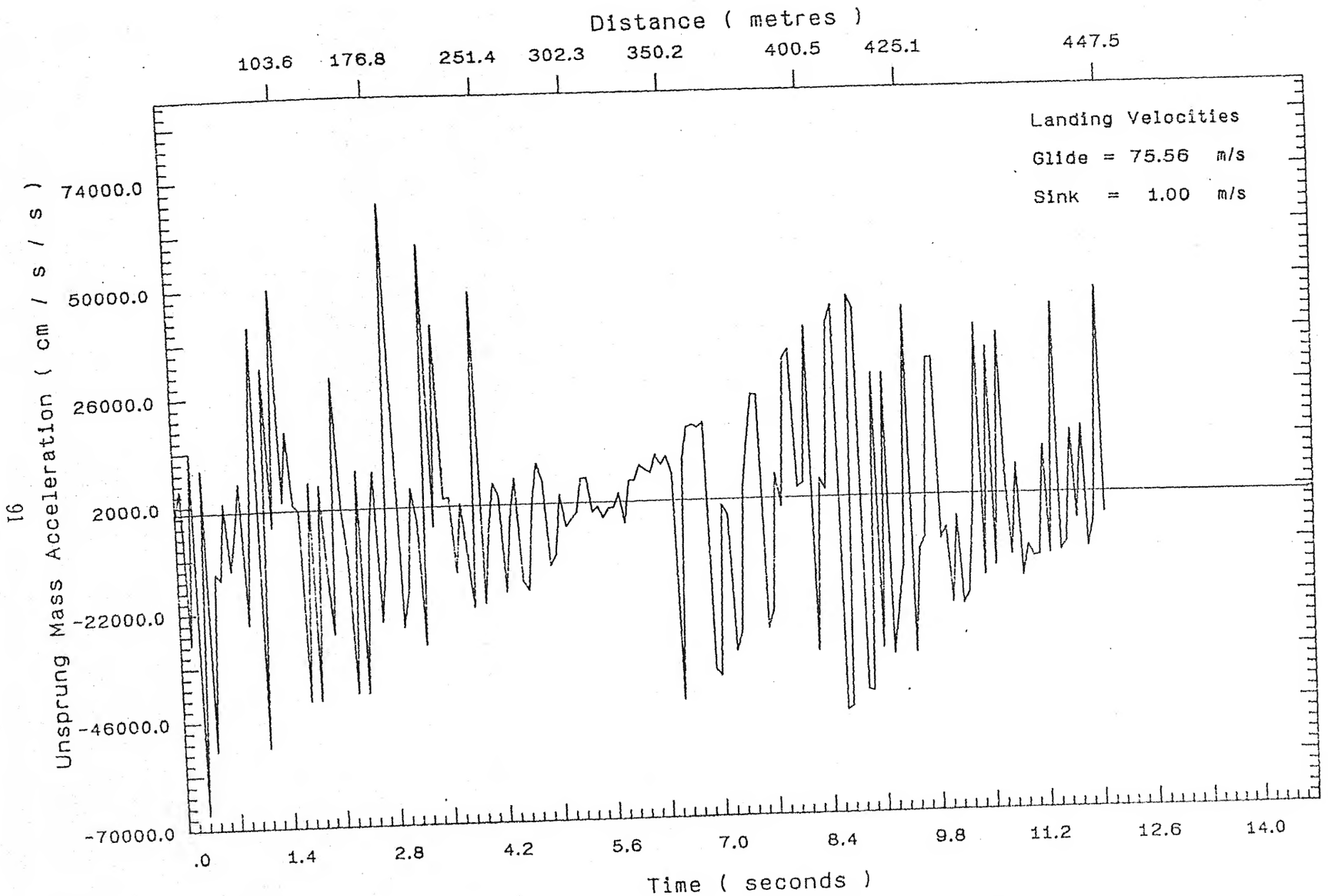

Figure 5.49: Unsprung-mass acceleration for flat runway , glide velocity = 75.56 $\frac{m}{s}$, sink velocity = 1.0 $\frac{m}{s}$

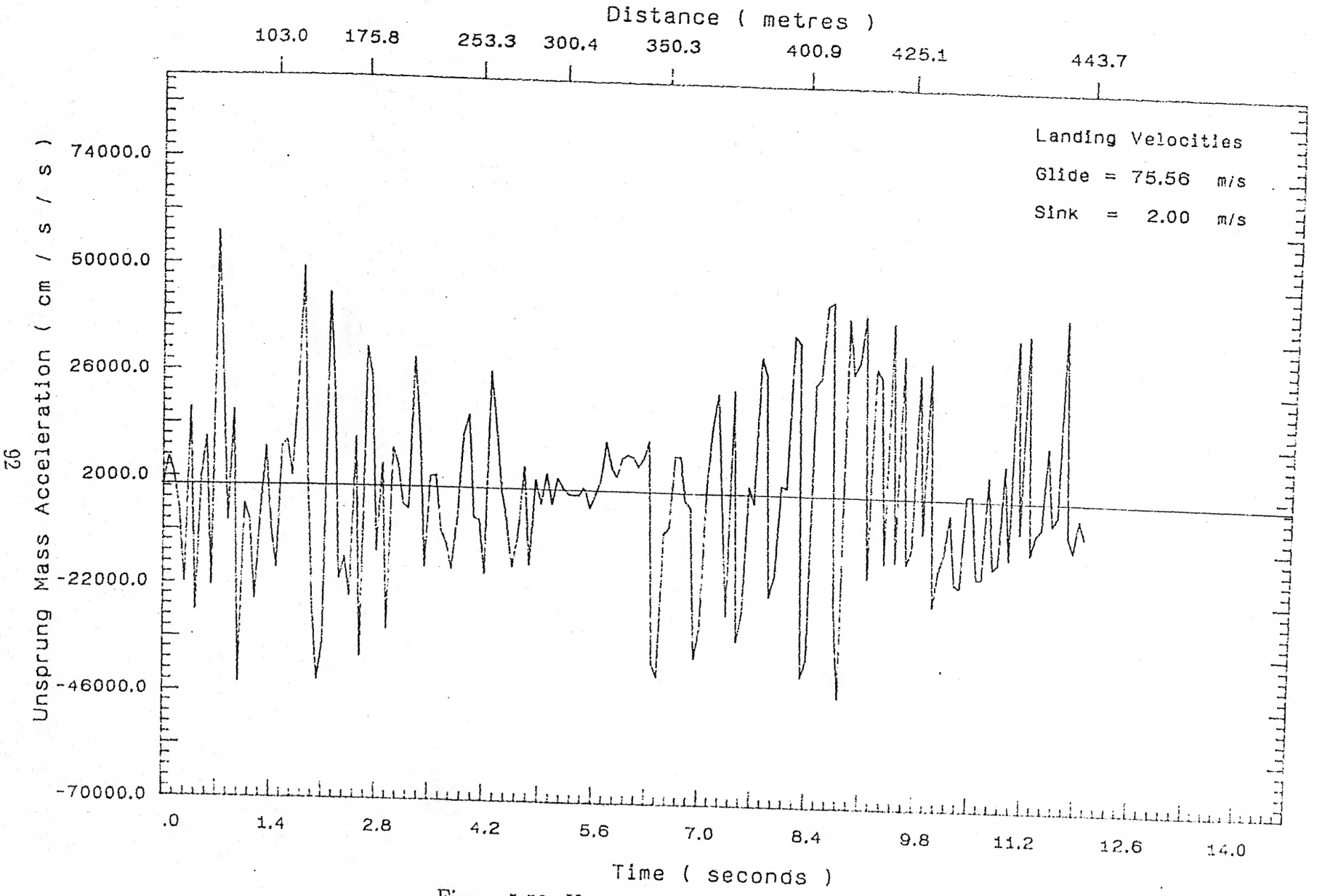

Figure 5.50: Unsprung mass acceleration for flat runway , glide velocity = 75.56 $\frac{m}{s}$, sink velocity = 2.0 $\frac{m}{s}$

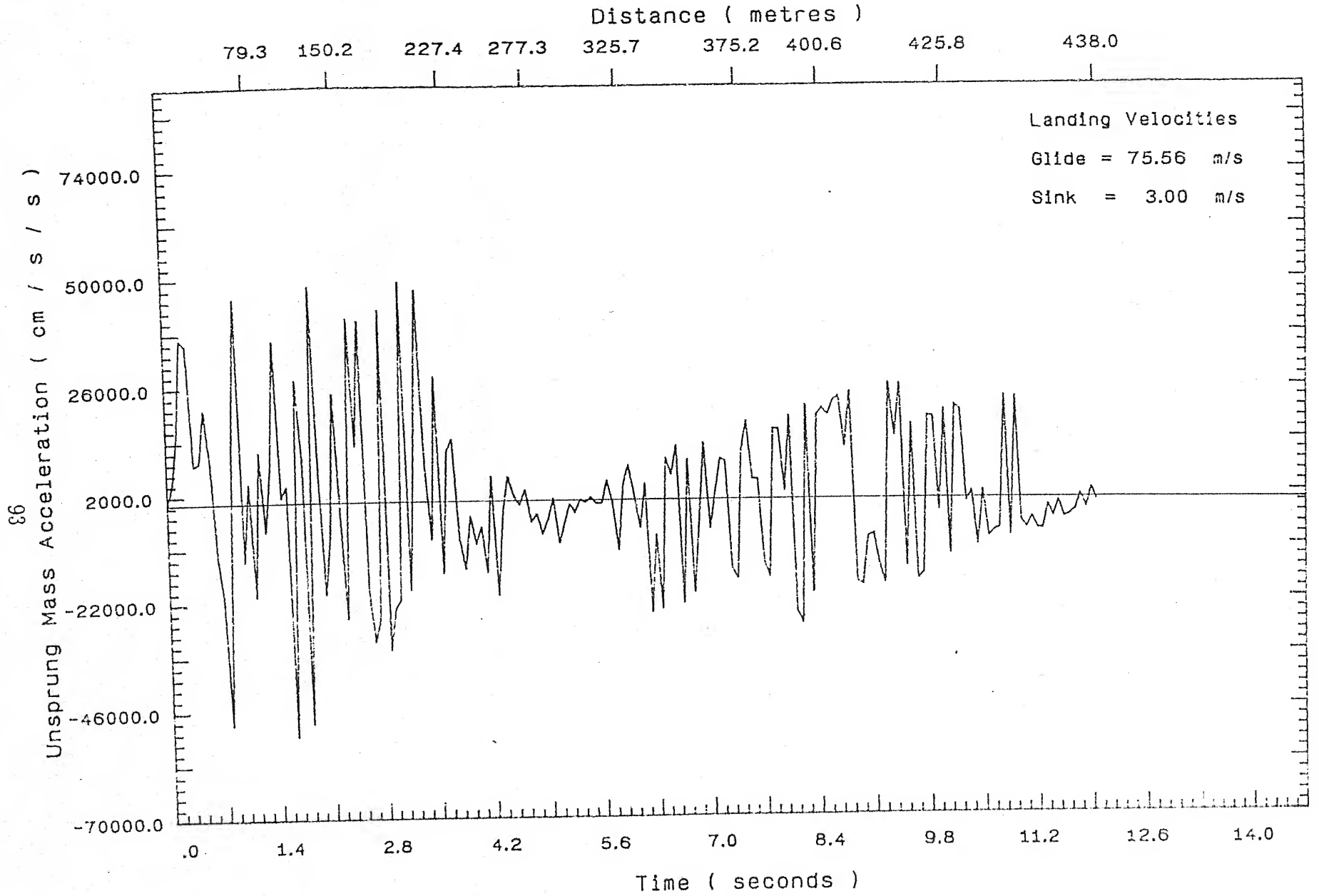

Figure 5.51: Unsprung mass acceleration for flat runway , glide velocity = 75.56 $\frac{m}{s}$, sink velocity = 3.0 $\frac{m}{s}$

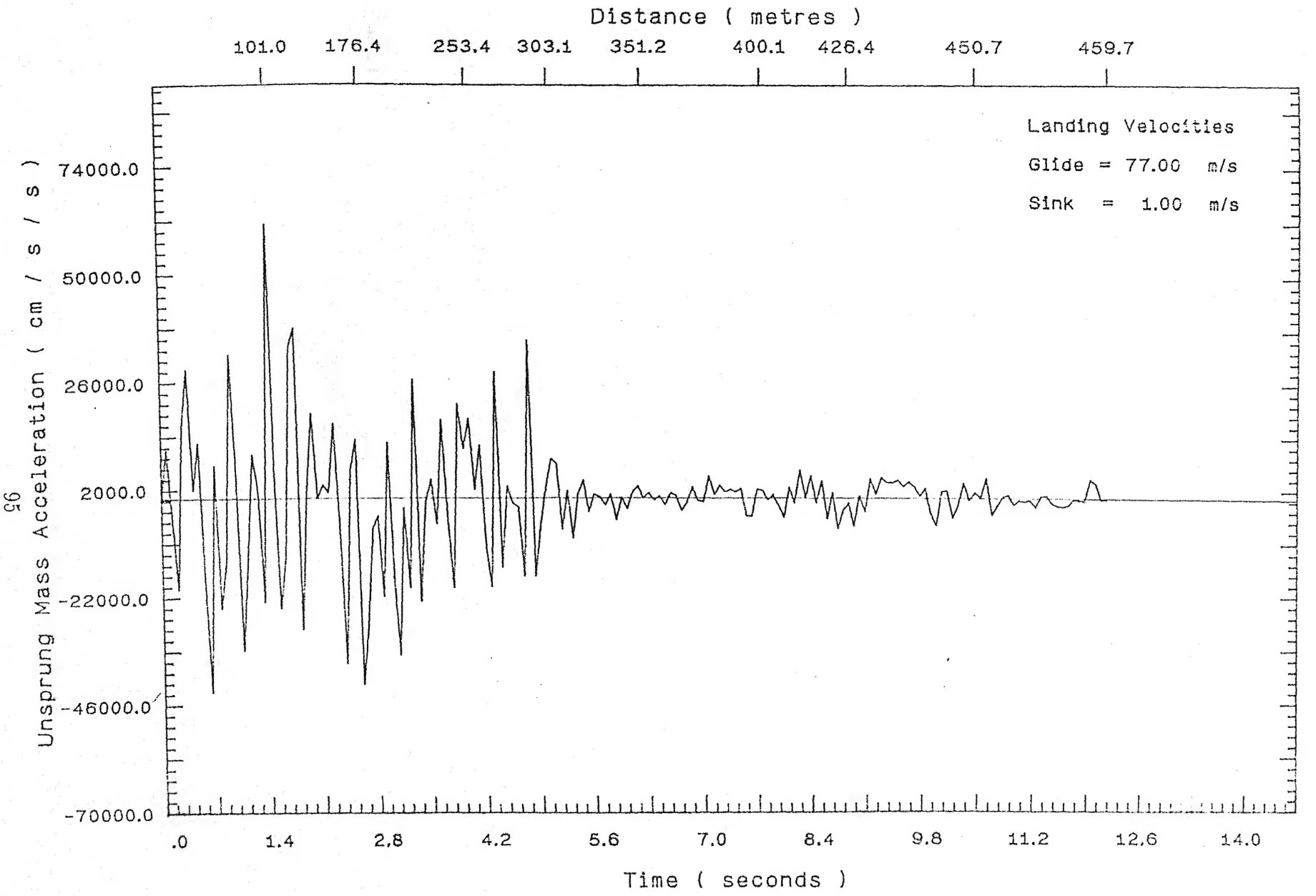

Figure 5.53: Unsprung mass acceleration for flat runway , glide velocity = 77.00 $\frac{m}{s}$, sink velocity = 1.0 $\frac{m}{s}$

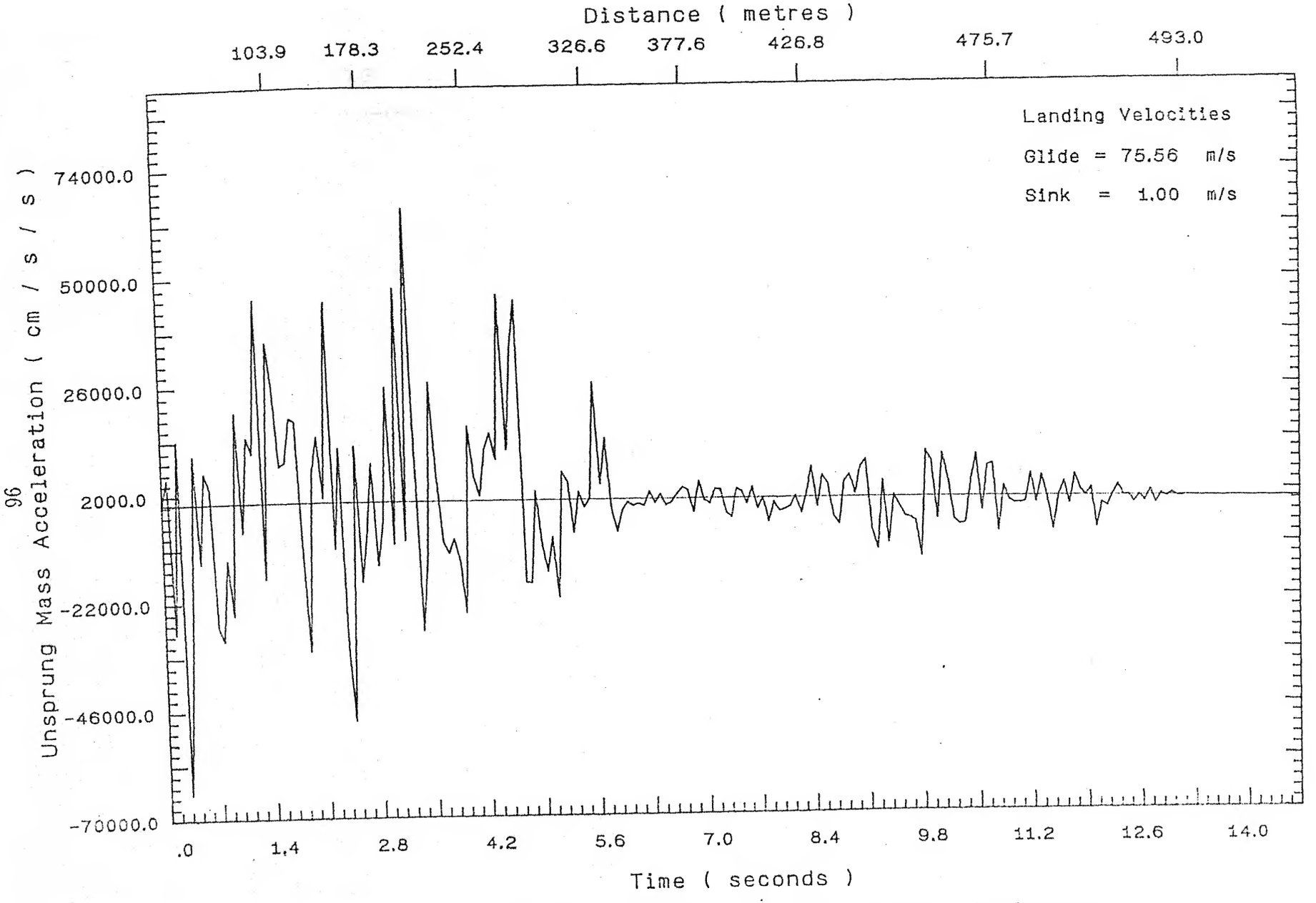

Figure 5.54: Unsprung mass acceleration for inclined runway , glide velocity = 75.56 $\frac{m}{s}$, sink velocity = 1.0 $\frac{m}{s}$.

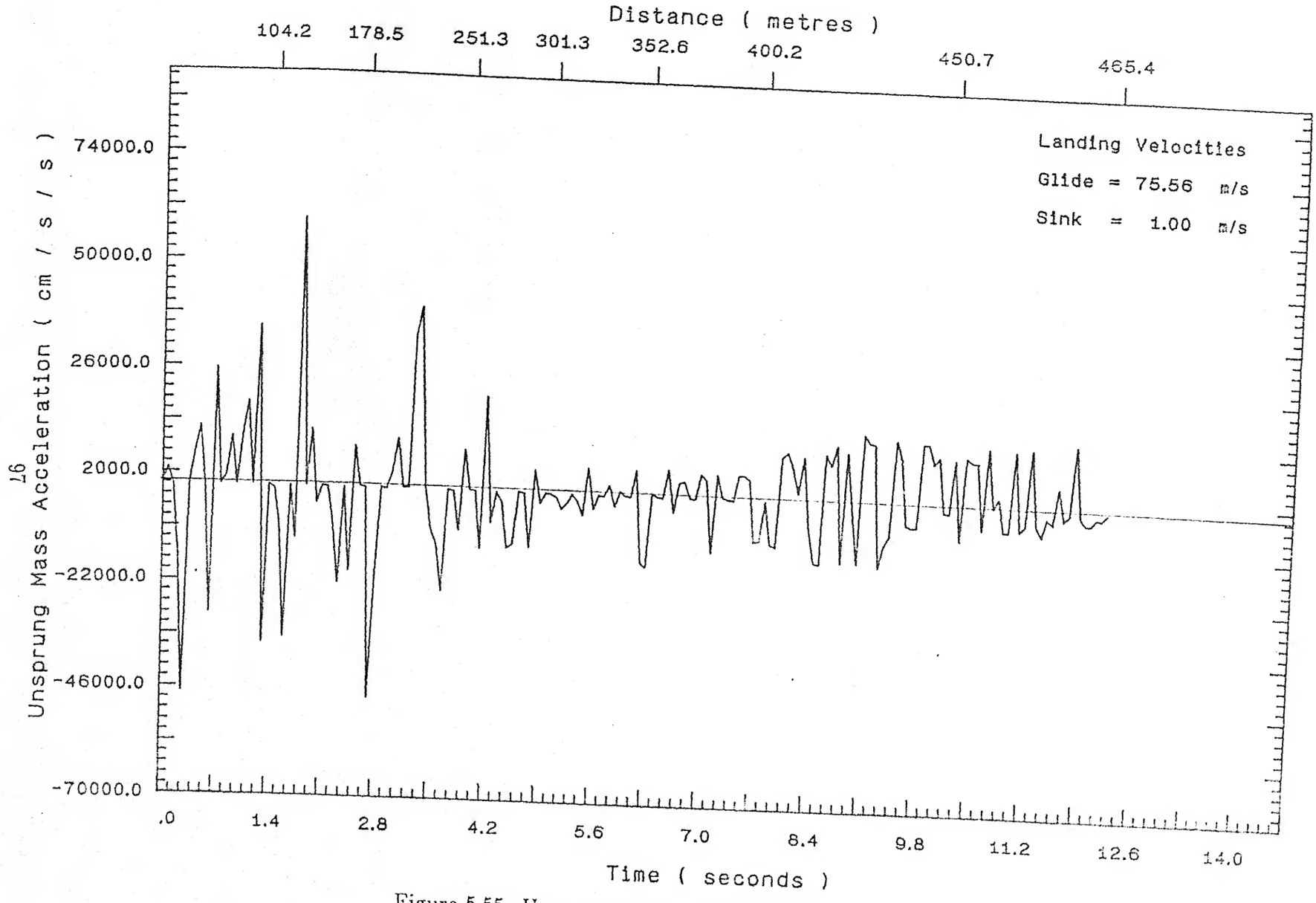

Figure 5.55: Unsprung mass acceleration for sinusoidal runway , glide velocity = 75.56 $\frac{m}{s}$, sink velocity = 1.0 $\frac{m}{s}$

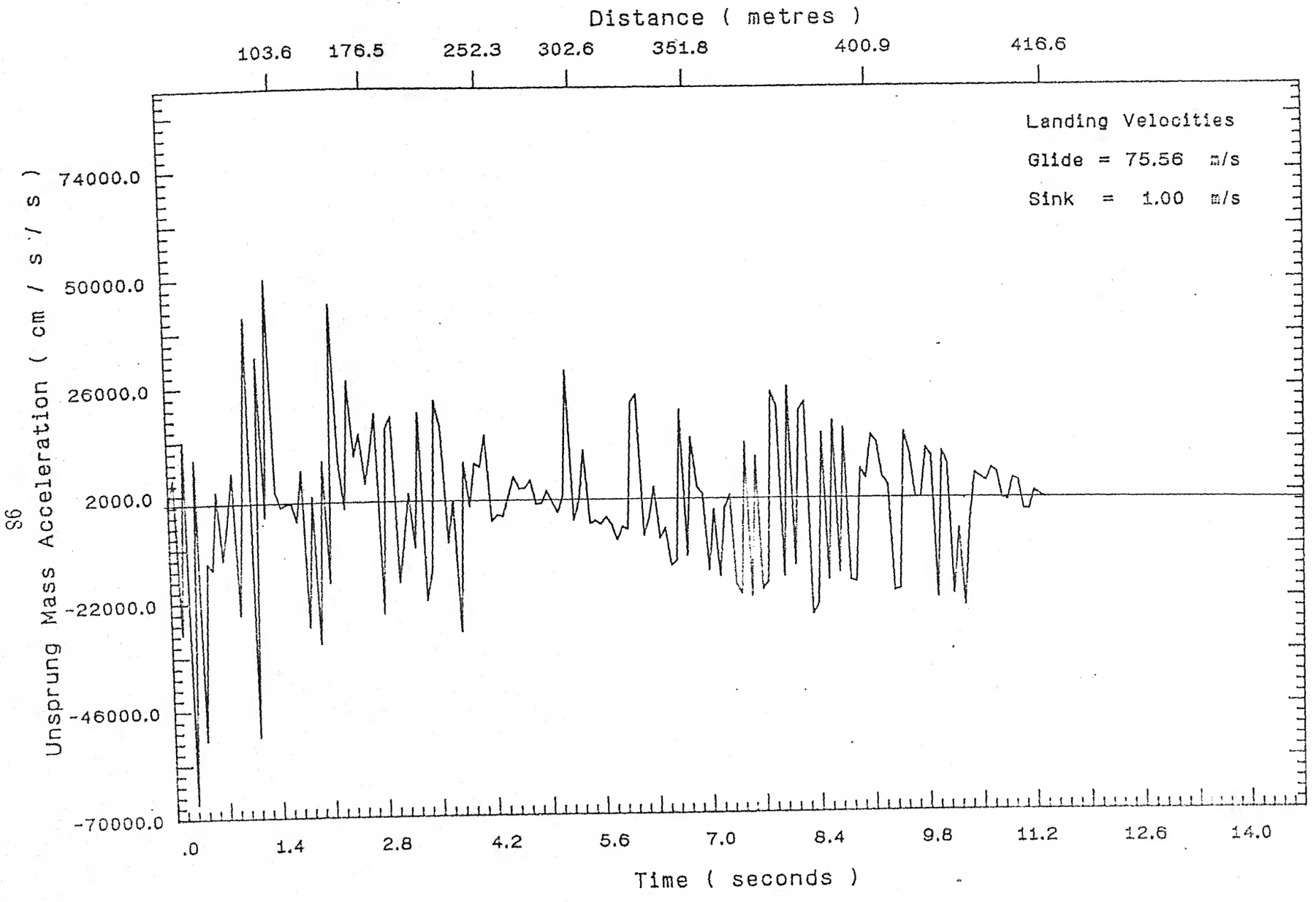

Figure 5.56: Unsprung mass acceleration for stepped runway , glide velocity = 75.56 $\frac{m}{s}$, sink velocity = 1.0 $\frac{m}{s}$

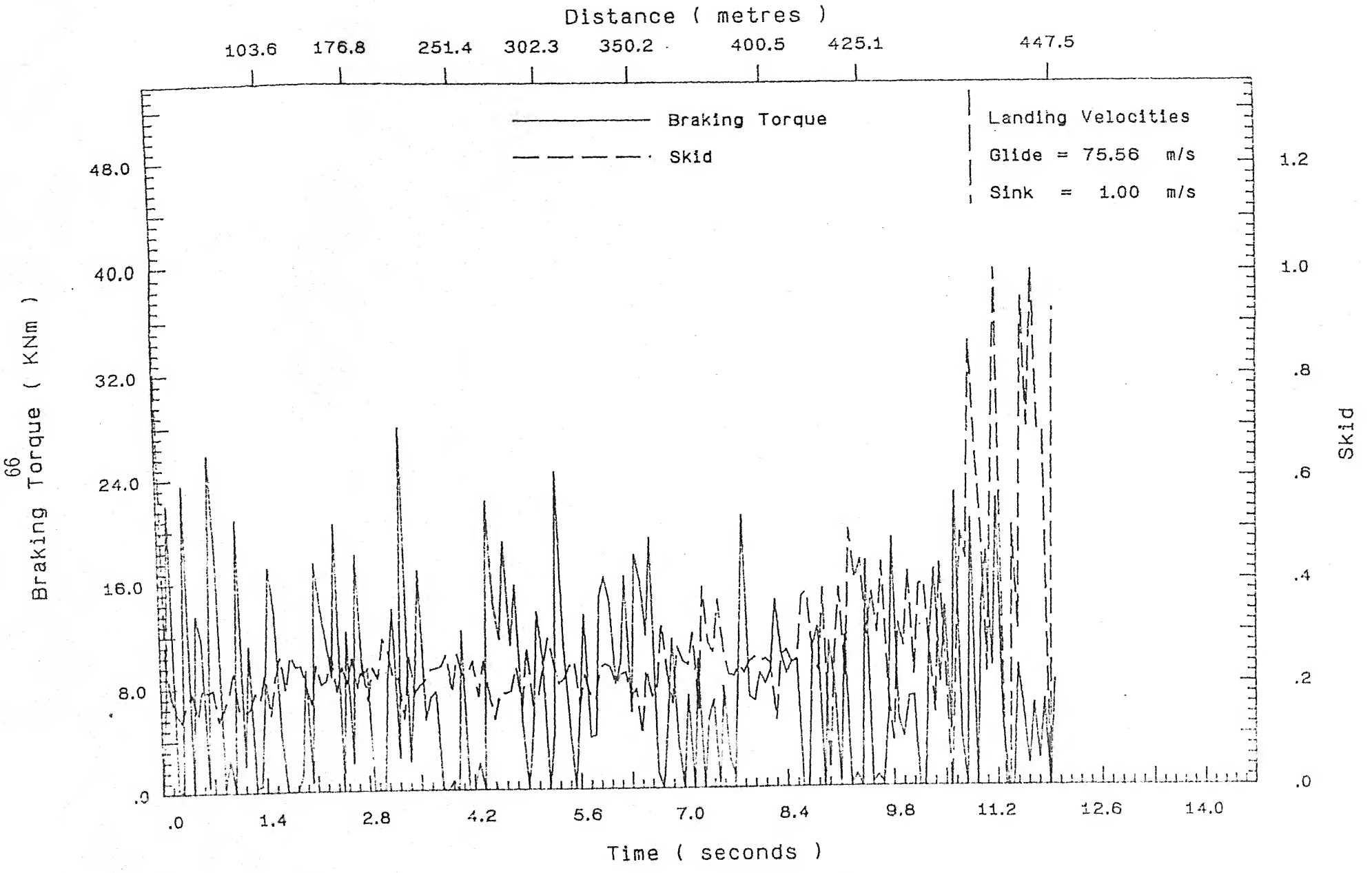

Figure 5.57: Braking torque and skid for flat runway ,
glide velocity = 75.56 $\frac{m}{s}$, sink velocity = 1.0 $\frac{m}{s}$

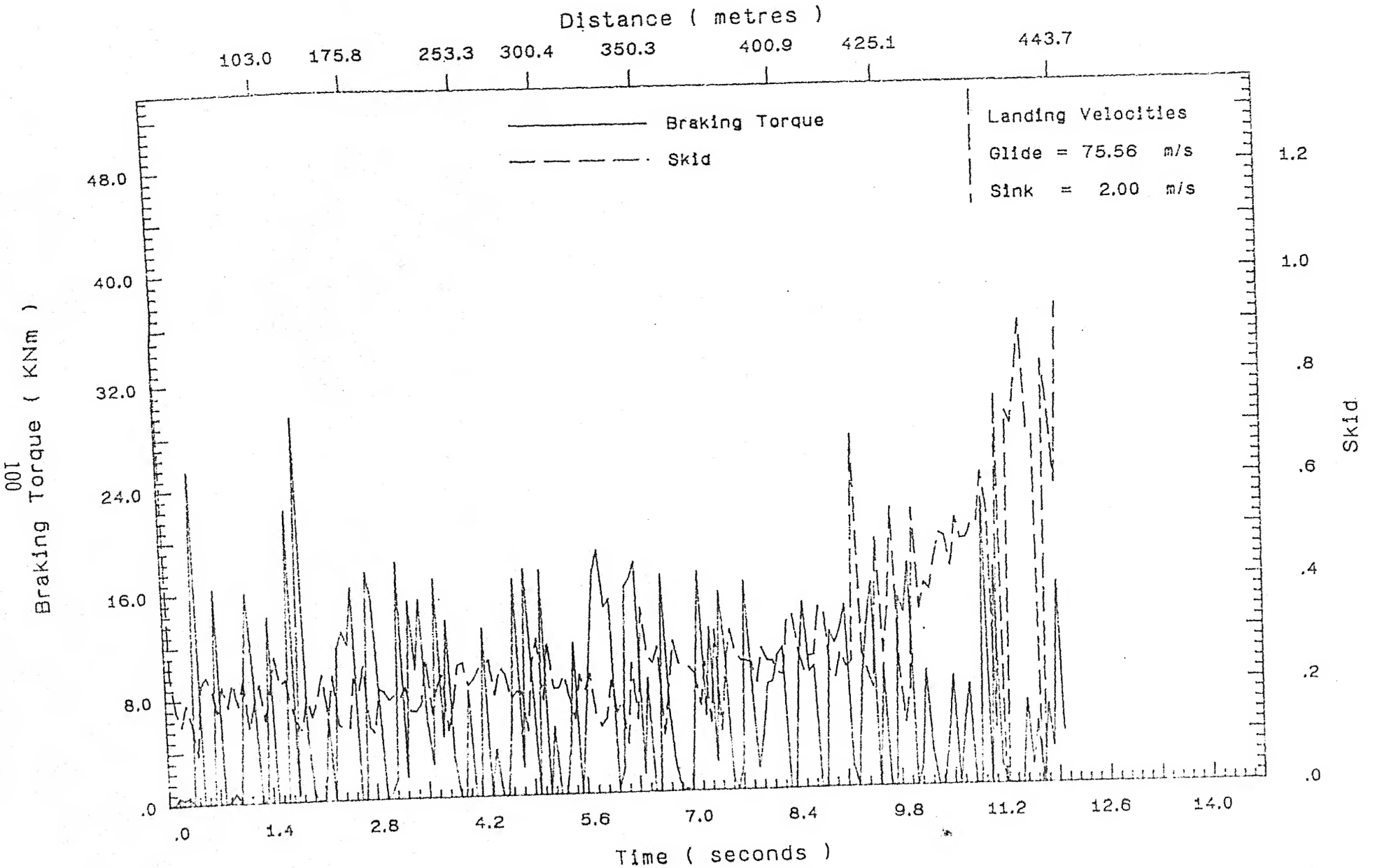

Figure 5.58: Braking torque and skid for flat runway , glide velocity = 75.56 $\frac{m}{s}$, sink velocity = 2.0 $\frac{m}{s}$

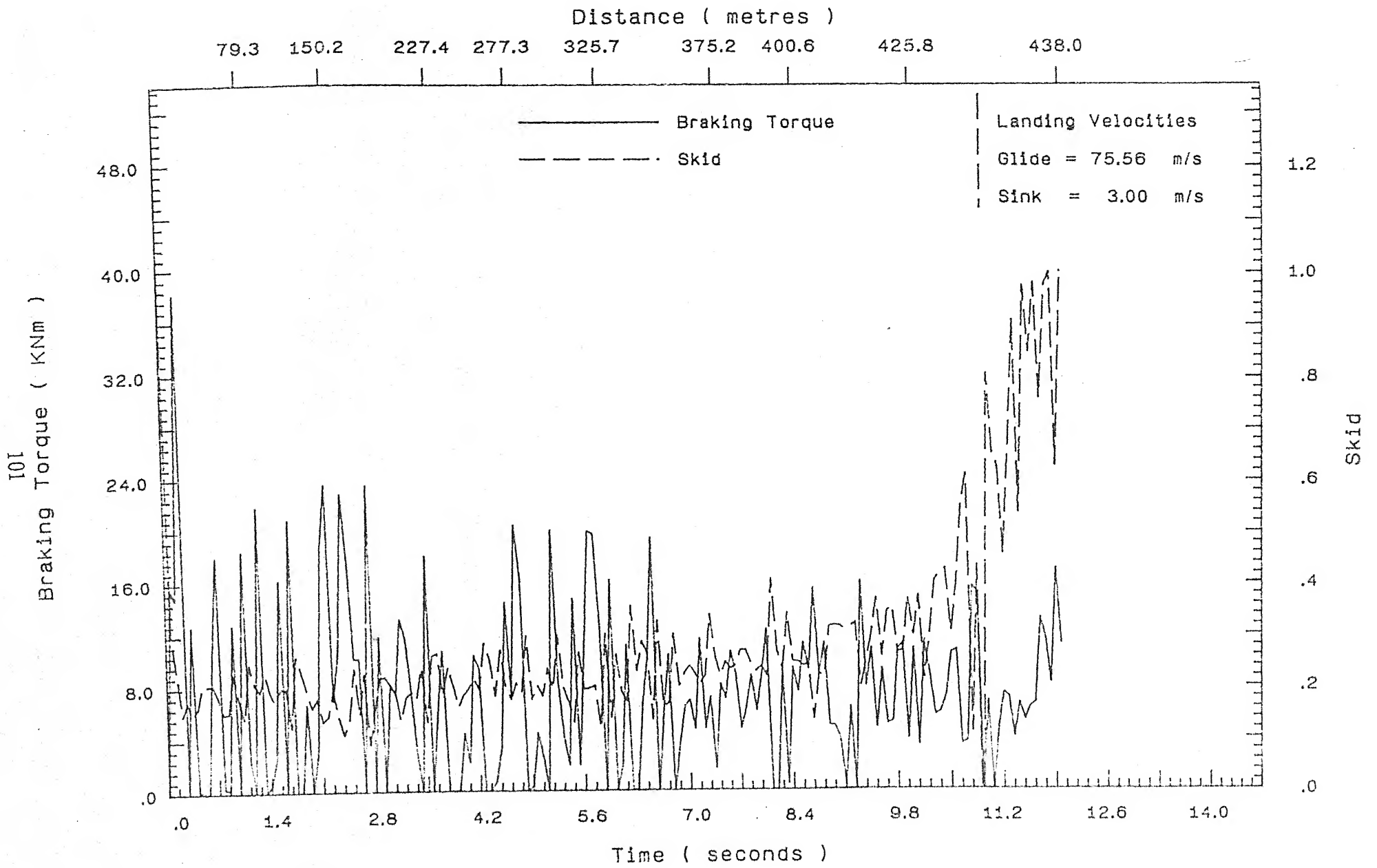

Figure 5.59: Braking torque and skid for flat runway , glide velocity = 75.56 $\frac{m}{s}$, sink velocity = 3.0 $\frac{m}{s}$

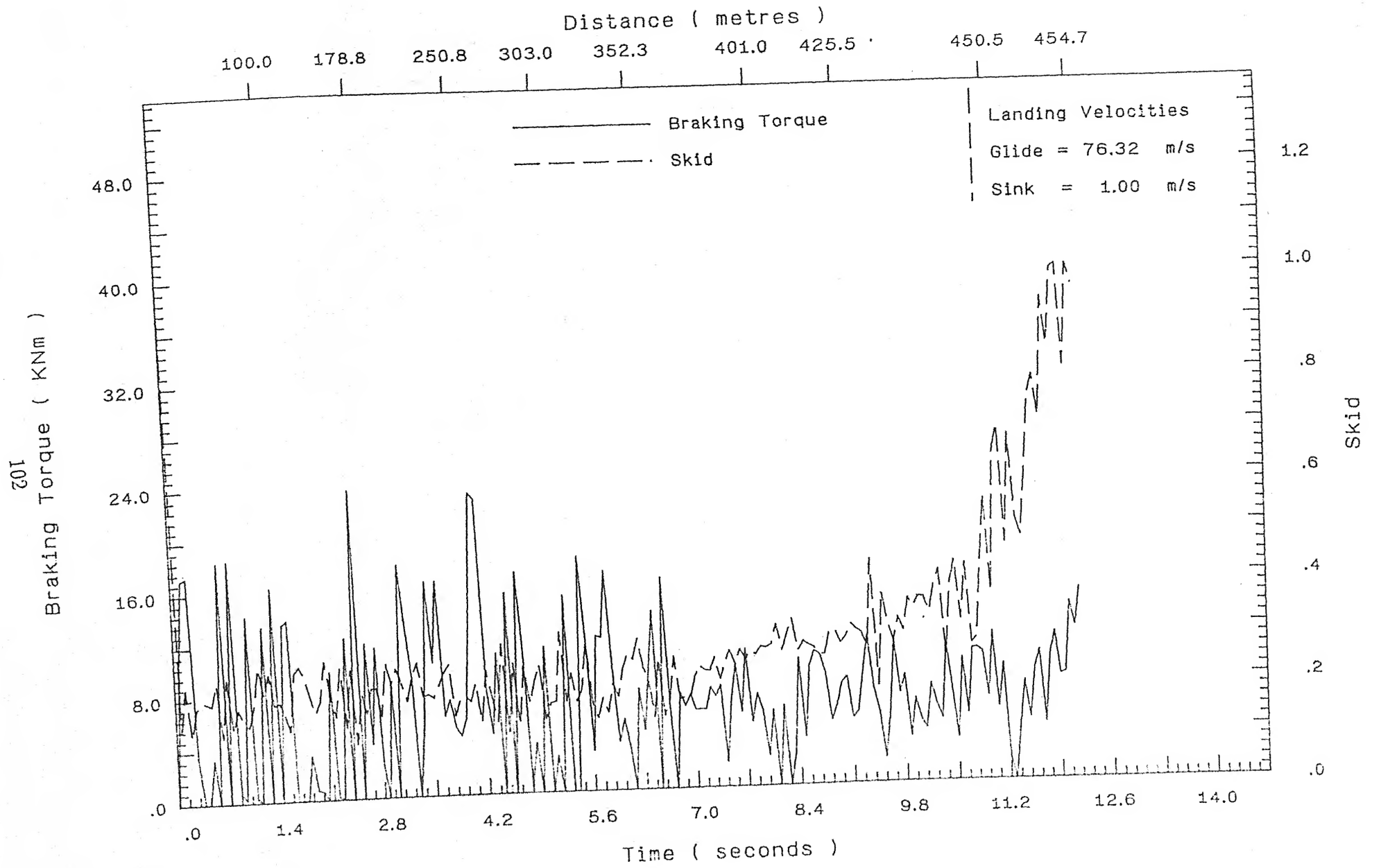

Figure 5.60: Braking torque and skid for flat runway , glide velocity = 76.32 $\frac{m}{s}$, sink velocity = 1.0 $\frac{m}{s}$

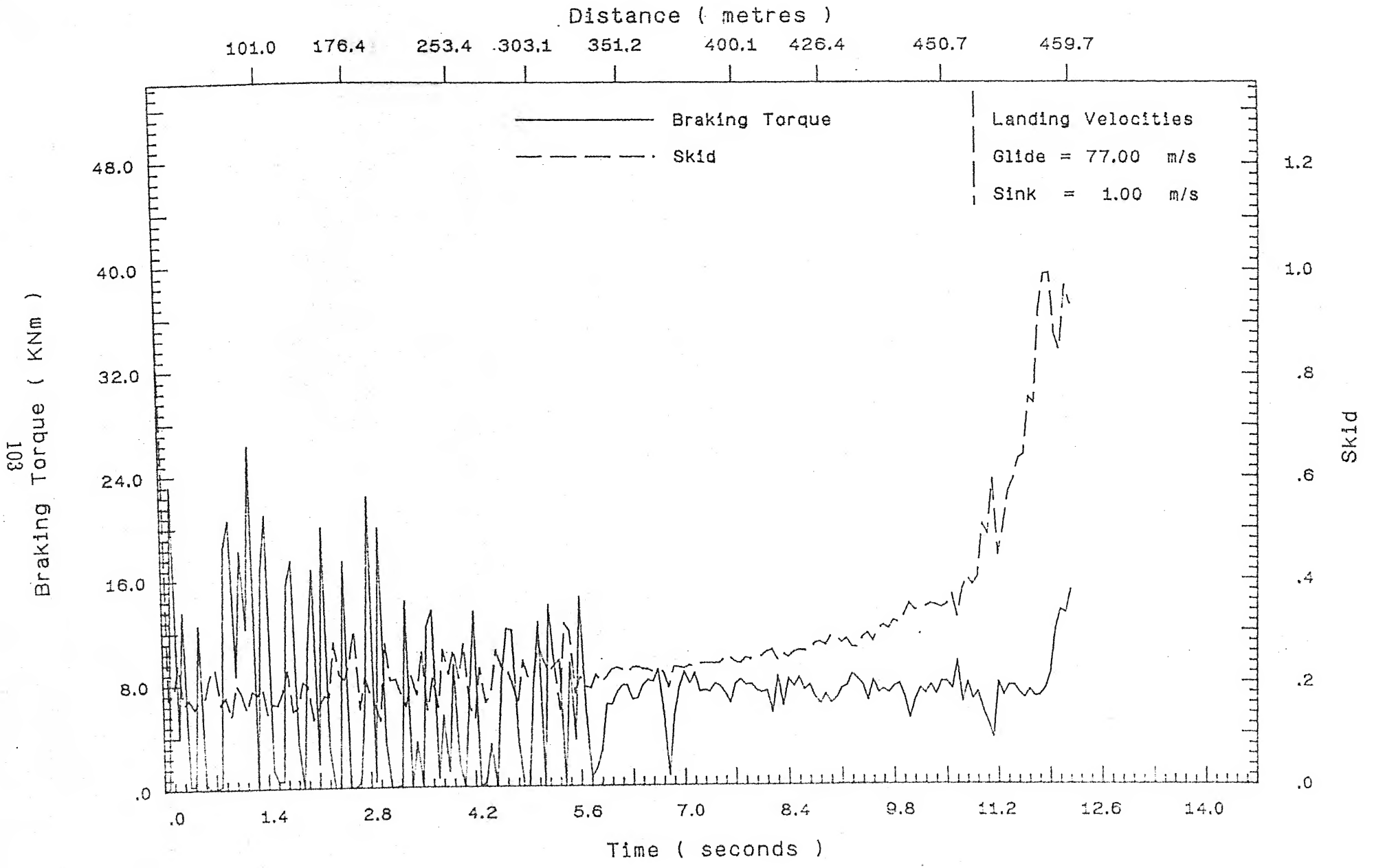

Figure 5.61: Braking torque and skid for flat runway , glide velocity = 77.00 $\frac{m}{s}$, sink velocity = 1.0 $\frac{m}{s}$

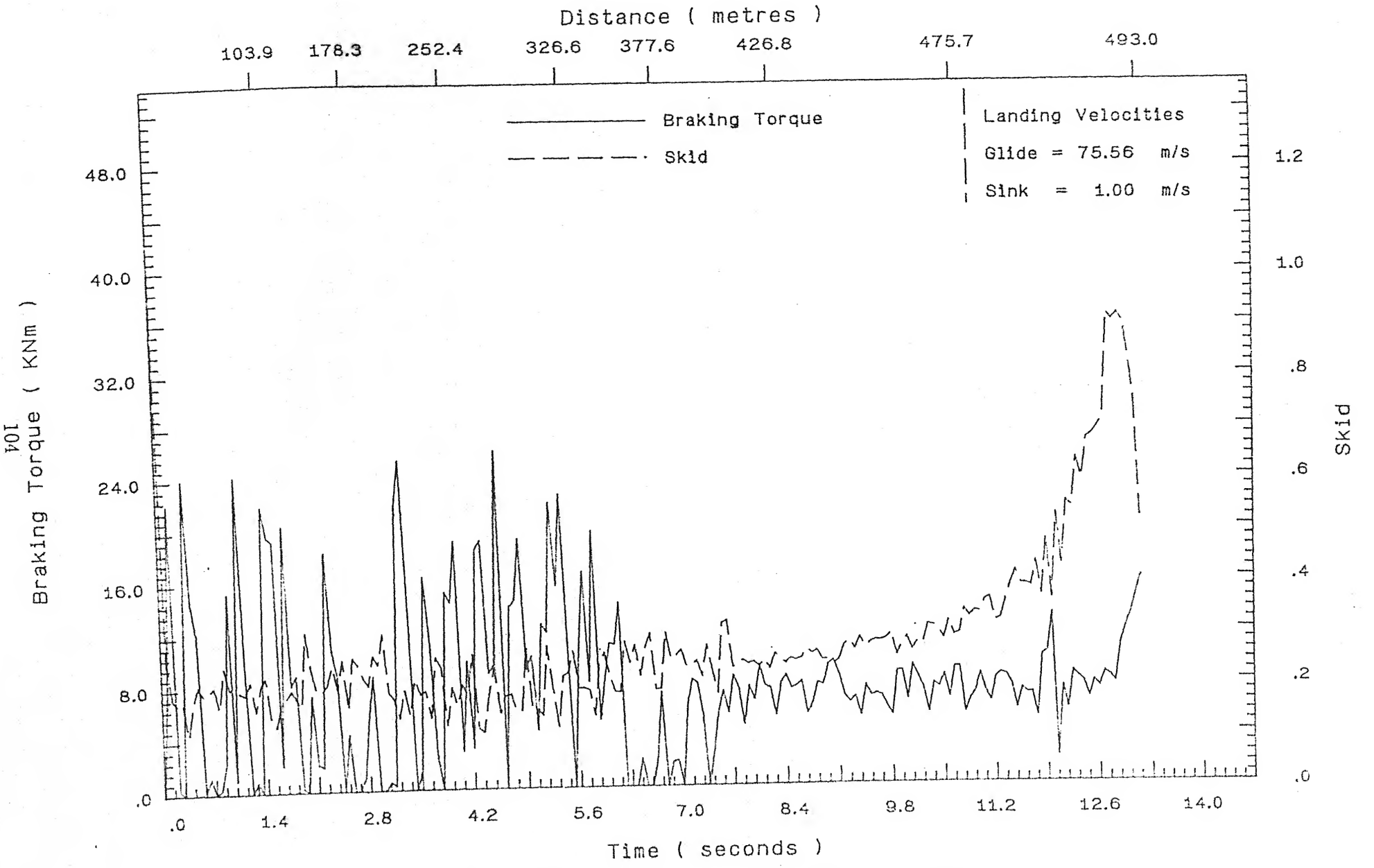

Figure 5.62: Braking torque and skid for inclined runway, glide velocity = 75.56 $\frac{m}{s}$, sink velocity = 1.0 $\frac{m}{s}$

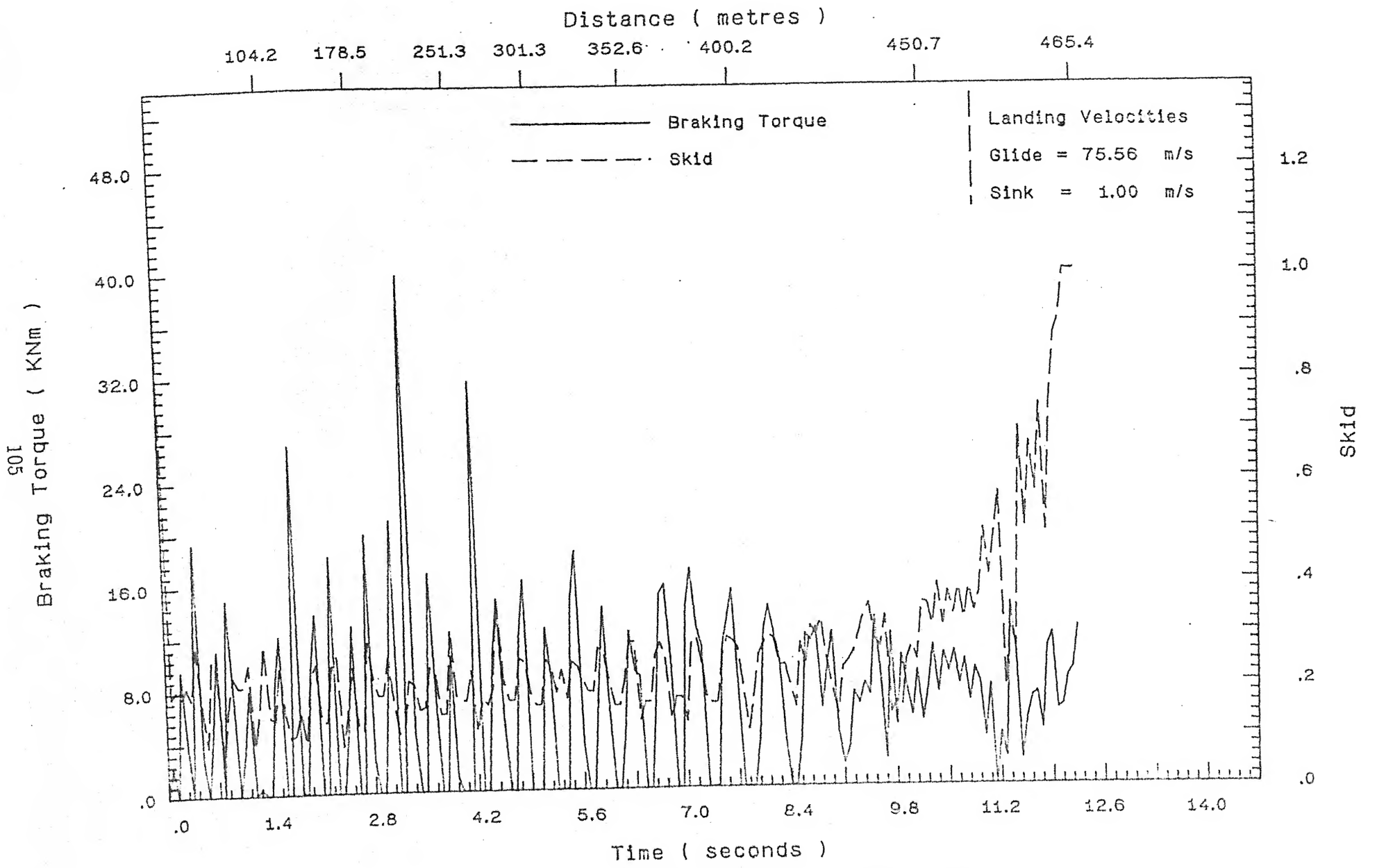

Figure 5.63: Braking torque and skid for sinusoidal runway , glide velocity = 75.56 $\frac{m}{s}$, sink velocity = 1.0 $\frac{m}{s}$

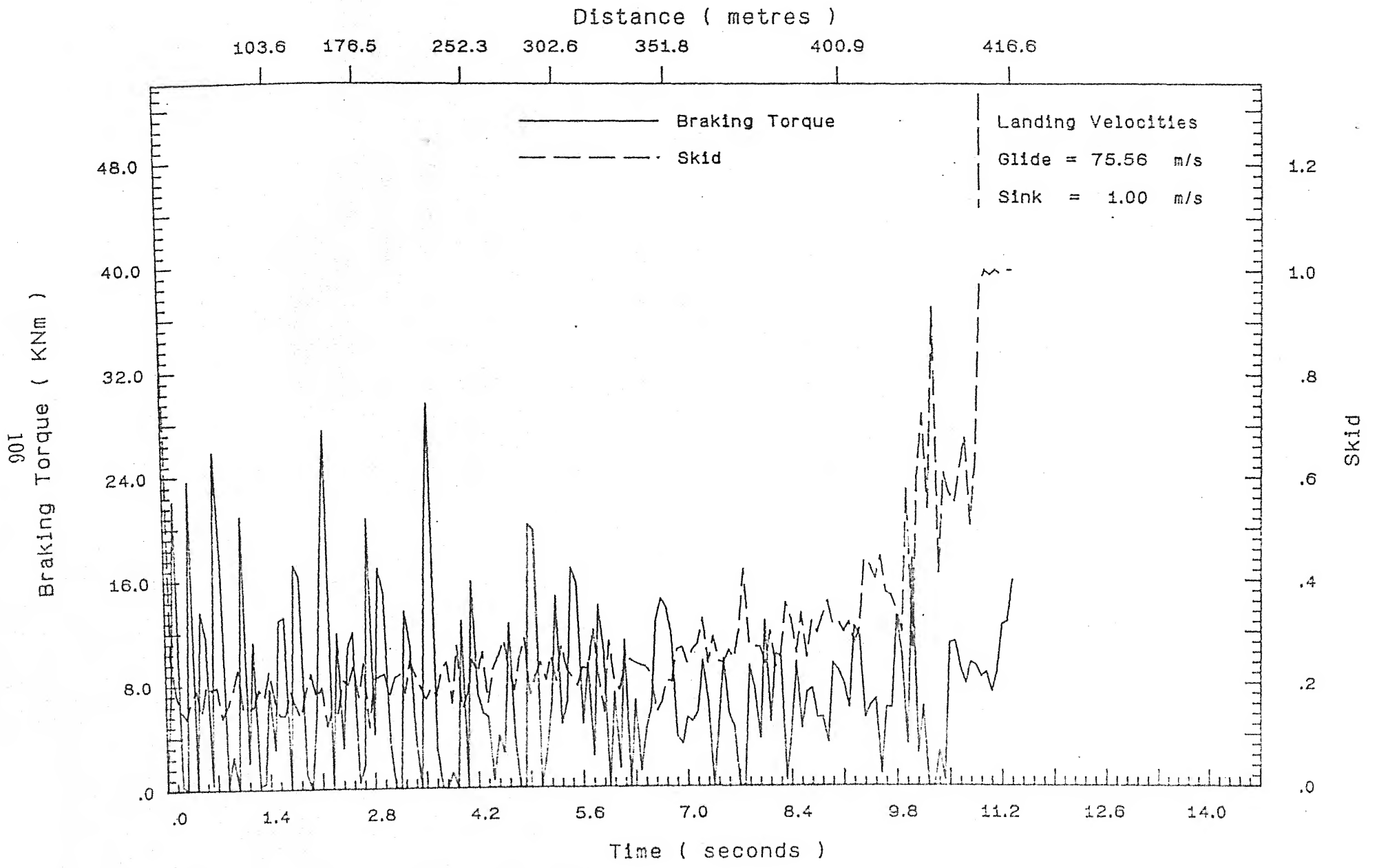

Figure 5.64: Braking torque and skid for stepped runway , . .
glide velocity = 75.56 $\frac{m}{s}$, sink velocity = 1.0 $\frac{m}{s}$

Chapter 6

Conclusions and Scope for Future Work

Some salient conclusions gleaned from the present study are presented in this chapter. The proposed scheme is very simple and a lot of work can be done by way of extension and otherwise to achieve better results. Some suggestions are made regarding the scope for such work.

6.1 Conclusions

The following conclusions are drawn from the results obtained from the various runs.

- Marked reduction in the landing run can be obtained by using the present system of anti-skid braking.
- The optimality of the proposed scheme is evident from the fact that the landing run is somewhat independent of both the sink and the glide velocities of the aircraft.
- Any dominant frequencies in the runway profile adversely effect the landing run of the aircraft, therefore care should be taken to remove such dominant frequencies from prepared runway surfaces.

- The introduction of a step early in the landing run, reduces the ground run. Concrete runways with differential settlement of slabs could therefore prove beneficial for the ground roll.

- Higher landing impact gives higher initial deceleration, therefore the lift should be spoiled as early as possible in the ground run.

- Inclined runways are not necessarily beneficial from point of view of reducing ground roll.

6.2 Scope for Future Work

The present work presents a very simple anti-skid braking system. Further work can be done by considering a more generalised system which accurately mimics the actual behaviour of the tyre and the landing gear. Systems with more degrees of freedom and with non-linear damping gears would be much nearer to the physical braking system.

Active landing gears which optimise the suspension parameters for achieving higher and more steady ground reactions would definitely improve the optimality of this scheme by far.

The track profile could be generated by using mathematically more advanced and complex methods e.g., chaos theory, for multivariate or univariate track processes . Further, simulation of the tyre's rolling effect, which has been neglected in this study, can also be pursued.

Other prediction methods which directly predict the state of the system, like the Kalman filter, instead of predicting the input as in the present study, would enhance the efficiency of the scheme.

Experimental verification of this scheme, which might produce some different results would be desirable.

References

[1] Data on various aircrafts and landing gears (communications).

[2] Brian D. O. Anderson and John B. Moore. *Optimal Filtering.* Prentice Hall Inc., Englewood Cliffs , New Jersey, 1979.

[3] John D. Anderson Jr. *Fundamentals of Aerodynamics.* McGraw Hill Book Company, Singapore, 1985.

[4] George E. P. Box and Gwilym M. Jenkins. *Time Series Analysis Forecasting and Control.* Holden Day Inc., SanFranscisco , California, 1970.

[5] S. H. Crandall and W. D. Mark. *Random Vibrations in Mechanical Systems.* Academic, New York, 1963.

[6] M. M. ElMadany. Design of an active suspension for a heavy duty truck using optimal control theory. *Computers and Structures*, 31(3):385–393, 1989.

[7] Loren D. Enochson and Robert K Otnes. *Programming and Analysis for Digital Time Series Data.* The Shock and Vibration Information Center, United States department of Defence, 1968.

[8] Joel N. Franklin. The covariance matrix of a continuous auto-regressive vector time series. *The Annals of Mathematical Statistics*, 34(4):1259–1264, December 1963.

[9] Joel N. Franklin. Numerical simulation of stationary and non-stationary gaussian random processes. *SIAM Review*, 7(1):68–80, January 1965.

[10] R. Freymann. An active control landing gear for the alleviation of aircraft taxi ground loads. *Zeitschrift fur Flugwissenschaften und Welteraumfarsschune*, 11:97–105, 1987.

[11] A. Hac. Suspension optimisation of a 2-dof vehicle model using stochastic optimal control technique. *Journal of Sound and Vibration*, 100:343–315, 1985.

[12] A. Hac. Stochastic optimal control of vehicles with elastic body and active suspension. *American Society of Mechanical Engineers Transactions, Journal of Dynamic Systems, Measurements and Control*, 108:106–110, 1986.

[13] J. K. Hammond and R. F. Harrisson. Nonstationary response of vehicles on rough ground — a state space approach. *American Society of Mechanical Engineers Transactions, Journal of Dynamic Systems, Measurements and Control*, 103:245–250, 1981.

[14] J. K. Hammond and M. Yar. Parameter estimation for hysteretic systems. *Journal of Sound and Vibration*, 117(1):161–172, 1987.

[15] R. F. Harrisson and J. K. Hammond. Approximate, time-domain, non-stationary analysis of stochastically excited, non-linear systems with particular reference to the motion of vehicles on rough ground. *Journal of Sound and Vibration*, 105:361–371, 1983.

[16] C. L. Kirk and P. J. Perry. Analysis of taxiing induced vibration by the power spectral density method. *Aeronautical Journal of the Royal Aeronautical Society*, 75:182–194, 1971.

[17] E. Kreyszig. *Advanced Engineering Mathematics*. Wiley, New York, 1962.

[18] Sandeep Kumar. Time series analysis of flicker noise. Master's thesis, IIT Kanpur, Kanpur — 208 016 , India, April 1990.

[19] Y. K. Lin. *Probabilistic Theory of Structural Dynamics.* McGraw Hill Book Company, 1967.

[20] G. Lindgren. Jumps and bumps on random roads. *Journal of Sound and Vibration*, 78(3):383–395, 1981.

[21] S. Narayanan and G. V. Raju. Stochastic optimal control theory of non-stationary response of a single degree of freedom vehicle model. *Journal of Sound and Vibration*, 141(3):449–463, 1990.

[22] N. C. Nigam. *Introduction to Random Vibrations.* MIT Press, Cambridge, Massachussetes, 1983.

[23] Athanasios Populis. *Probability, Random Variables and Stochastic Processes.* McGraw Hill Book Company, Singapore, second edition, 1984.

[24] William H. Press, Brian P. Flannery, Saul A. Teukolsky, and William T. Vetterling. *Numerical Recipes The Art of Scientific Computing.* Cambridge University Press, Cambridge, 1986.

[25] R. S. Sharp and D. A. Corolla. Road vehicle suspension system design — review. *Vehicle System Dynamics*, 16:167–192, 1984.

[26] R. S. Sharp and J. H. Hassan. Performance predictions for a pneumatic active car suspension system. *Proceedings of the Institute of Mechanical Engineers*, 202(D4):243–250, 1988.

[27] M. Shinozuka. Simulation of multivariate and multidimensional random processes. *The Journal of the Acoustical Society of America*, 49(1):357–368, 1971.

[28] K. Sobczyk and D. B. Macvean. Nonstationary random vibration of road vehicles with variable velocity. In *Symposium on Stochastic Problems in Dynamics*, pages 21.1–21.6, University of Southampton, 1976. International Union of Theoretical and Applied Mechanics.

[29] A. G. Thompson. The effect of tyre damping on the performance of vibration absorbers in an active suspension. *Journal of Sound and Vibration*, 133(3):457–465, 1989.

[30] M. Tomizuka. Optimum linear preview control with application to vehicle suspension — revisited. *American Society of Mechanical Engineers Transactions, Journal of Dynamic Systems, Measurements and Control*, 98:309–315, 1976.

[31] Francis S. Tse, Ivan E. Morse, and Rolland T. Hinkle. *Mechanical Vibrations Theory and Applications.* Alloyn and Bacon Inc, London, second edition, 1983.

[32] C. C. Tung, J. Penzien, and R. Horonjeff. The effect of runway unevenness on the dynamic response of supersonic transport. CR 119, NASA, 1964.

[33] V. J. Virchis and J. D. Robson. Response of an accelerating vehicle to random road undulation. *Journal of Sound and Vibration*, 18:423–427, 1971.

[34] I. H. Witten. Algorithms for adaptive linear prediction. *The Computer Journal*, 23(1):78–84, 1980.

[35] D. Yadav and N. C. Nigam. Ground induced non-stationary response of vehicles. *Journal of Sound and Vibration*, 61(1):117–126, 1978.

[36] T. Yoshimura, N. Ananthanarayana, and D. Deepak. An active lateral suspension to a track/vehicle system using stochastic optimal control. *Journal of Sound and Vibration*, 106(2):217–225, 1983.

[37] T. Yoshimura, N. Ananthanarayana, and D. Deepak. An active lateral suspension to a track/vehicle system using stochastic optimal control. *Journal of Sound and Vibration*, 115(3):473–482, 1987.

[38] T. Yoshimura and M. Sugimoto. An active suspension for a vehicle travelling on flexible beams with an irregular surface. *Journal of Sound and Vibration*, 138(3):433–445, 1990.